EXPERIMENTAL COMPONENT MODE SYNTHESIS OF STRUCTURES WITH JOINT FREEPLAY

by

Gary H. Blackwood

S.B., Massachusetts Institute of Technology (1986)

SUBMITTED TO
THE DEPARTMENT OF AERONAUTICS AND ASTRONAUTICS
IN PARTIAL FULFILLMENT OF THE REQUIREMENTS FOR
THE DEGREE OF

MASTER OF SCIENCE
IN AERONAUTICS AND ASTRONAUTICS

at the

MASSACHUSETTS INSTITUTE OF TECHNOLOGY
May 18, 1988

Signature of Author _____
Department of Aeronautics and Astronautics
May 18, 1988

Certified by _____
Professor Andreas H. von Flotow
Thesis Supervisor

Accepted by _____
Professor Harold Y. Wachman, Chairman
Departmental Graduate Committee

Abstract

The accuracy of component mode synthesis is investigated experimentally for substructures coupled by non-ideal joints. The work is based upon a segmented experimental beam for which the free-interface frequency response matrices are measured for each segment. These measurements are used directly in component mode synthesis to predict the behavior of the assembled structure; the segments are then physically joined and the resulting frequency response of the superstructure is compared to the prediction. Rotational freeplay is then introduced into the connecting joint and the new superstructure frequency response is compared to the original linear CMS prediction. The level of accuracy to be expected in component mode synthesis is discussed in terms of a non-dimensional parameter that reflects the degree of nonlinearity in the joints, mode number and mode shapes. Issues important to experimental component mode synthesis are reviewed in order to assess the applicability of this procedure to the analysis of more complicated structures.

Acknowledgments

I would like to dedicate this work to my parents, George and Kate Blackwood, who have literally struggled and celebrated along with me at each and every step in my MIT career. No son could feel more lucky or be more proud than I to have these two fine people as my parents. With their love and encouragement to guide me, I know that anything is possible. Thanks, Mom and Dad.

My sincere gratitude is also extended to my undergraduate laboratory assistants, Erik Saarmaa and Kelvin Scribner, for their valuable work and perseverance with this project over the past year. Their efforts have contributed a great deal to the work presented in this thesis. I wish them well.

Table of Contents

List of Figures

Chapter 1
Introduction

The ground testing of large spacecraft structures becomes more complicated as the size of the flight structures increases. For instance, air damping and the interference of suspension systems with low frequency structural modes must be considered. For those structures too large to test on the ground at full scale, scale models have been proposed[1] to validate on-orbit dynamic behavior. The accuracy of scaling could become questionable, however, particularly when nonlinear joint dynamics such as deadband or hysteresis become important. Structures that will certainly include such "sloppy" joints are deployable trusses, such as the proposed NASA COFS I MAST flight structure[2].

One alternative to testing the entire structure is to test small individual pieces--joints, truss members--and to use these static and dynamic test results to predict the behavior of the assembled structure via finite element analysis[3]. Such an approach would be at the other end of the "test spectrum" from full scale testing, and one might expect sizeable errors to accrue as hundreds or thousands of elements are assembled analytically. Ikegami et. al.[4] even found this to be the case for the prediction of the static response of a multi-bay truss, and recommended using several joints and truss members in series to account for the effects of the joints. Figure 1-1 lists options in such a "test spectrum".

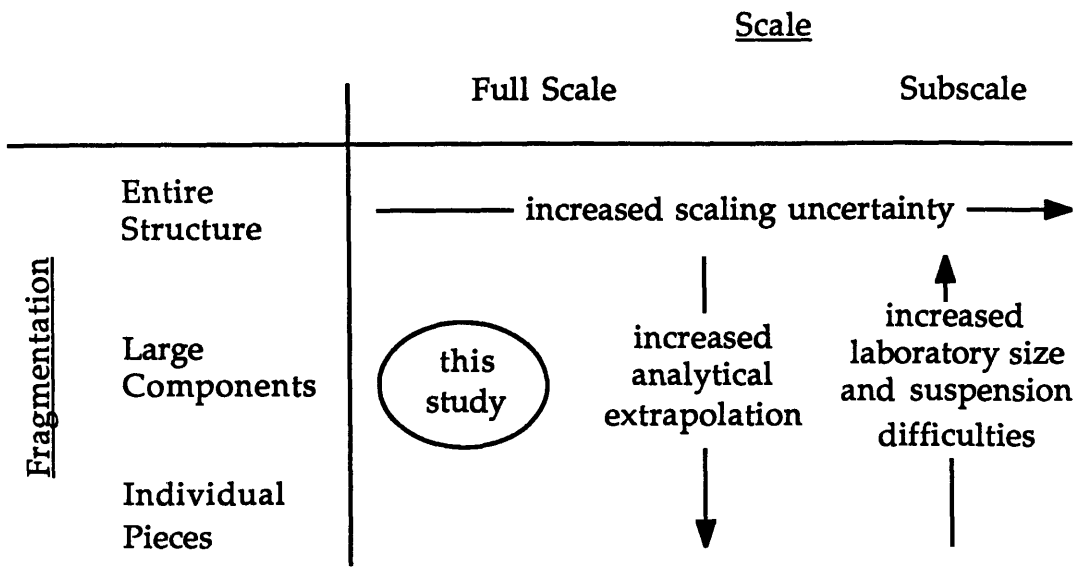

Figure 1-1: Options for Ground Testing of Spacecraft Structures

Another alternative would be to ground-test full-scale components of a size as large as possible (limited by laboratory space and by component strength requirements), and to assemble these test results analytically. Such an approach would be in the center of the "test spectrum"--in between testing the entire structure and testing small pieces. For a deployable truss structure this might mean one or several bays out of a total of dozens for the entire structure. For a spacecraft consisting of a central bus and flexible appendages, each appendage might constitute a component and be ground tested. The measured dynamic behavior of the components can then, in principle, be used to predict the dynamic response of the entire assembly. The analytical extrapolation would be minimized since the components are chosen to be as large in size, and as few in number, as possible.

A common procedure for performing analytic assembly of component dynamics is to construct a component model from spatial quantities (mass, stiffness, and damping matrices), validate this component model through experimental testing, and then perform standard matrix assembly. Other substructuring procedures based on modal models are known as component mode synthesis (CMS) and can be implemented using time domain or frequency domain methods[5,6]. Some of these procedures incorporate component dynamic measurements from the outset and are known as *experimental* component mode synthesis methods. Each of these techniques, however, assumes both linear behavior of components as well as compatibility of deflection at the interface degrees of freedom. These assumptions may be violated, to varying degrees, by deployable truss structures in which the joints exhibit some freeplay or other amplitude-dependent stiffness.

This study was motivated by the desire to predict the on-orbit dynamics of the COFS I MAST[2] deployable truss by testing components of the structure--one or more full-scale bays--in the laboratory. The measured dynamics of these components would be used to predict the dynamics of the entire truss. Structures such as the COFS I MAST will present problems for experimental modal testing and component mode synthesis. These structures may be characterized by heavy joints and light truss members, will be coupled at many degrees of freedom, have significant nonlinear joint behavior (deadband, hysteresis, nonlinear force-deflection curves), and exhibit closely-space internal resonances at frequencies will below bending or torsional modes of one or several of the

bays. Features such as these will strain the accuracy of component mode synthesis, which up to this point has been applied to analytical models and to relatively simple components and coupling.

An experimental coupled beam was constructed to simulate one of these problems--the effects that a joint with freeplay would have on the accuracy of component mode synthesis. Two beam-like components with "variable" joints are built and dynamically tested. The joints are designed to behave either rigidly or to exhibit a variable amount of rotational freeplay. The accuracy of frequency domain CMS is evaluated for this experimental structure using experimentally determined frequency response functions. In a departure from experimental CMS case studies already in the literature[6,7,8,9,10] in which component linearity and full compatibility are assumed, this study relaxes the assumption of compatibility by the introduction of freeplay in the physical joint between components. The component experimental frequency response functions (FRFs) are used with component mode synthesis to predict the behavior of the coupled structure. The beams are then physically connected and the actual frequency response of the superstructure is compared to the CMS prediction.

Results of this study indicate that reasonable levels of accuracy can be expected from component mode synthesis, given a stiff joint and correct component measurements. This result is consistent with other experimental studies conducted by Ewins and Martinez, Carne and Miller[7]. Even so, the joint does contribute some error to the linear CMS prediction; this is especially so if the joint displays any deadband nonlinearity.

Results of the frequency response measurement of a structure with varying amounts of joint deadband are also presented in terms of a non-dimensional parameter. Cases were studied in which the number of components and the level of force excitation were varied when joint deadband was present. Lastly, the issues and accuracies associated with experimental component mode synthesis for both linear and nonlinear structures are discussed.

Chapter 2
Theory and Literature Review

2.1 Overview

Component mode synthesis (CMS) is a means of determining the dynamics of coupled structures based on the analysis of individual substructures or components. Mathematical descriptions of component dynamics are developed from either analytical models, experimental measurements or both. Component dynamics are represented as a superposition of flexible modes augmented with suitable rigid body and static constraint modes. Compatibility and equilibrium are enforced at component interfaces in order to analytically assemble the global structure. CMS is also a useful means to reduce the set of coordinates that represent the components and coupled structure.

Component mode synthesis is only one form of coupled structure analysis. Ewins[6] identifies three different substructuring categories--*spatial* model analysis, *modal* model analysis, and *response* model analysis--of which the last two are referred to in the literature as component mode synthesis. A subset of component mode synthesis is *experimental* component mode synthesis, involving techniques that can directly incorporate experimental measurements. An overview of these three substructuring methods is presented in this section, followed later in the chapter by more detailed discussions of the different CMS techniques.

Spatial model analysis is a straightforward substructuring technique that combines the component mass and stiffness matrices using standard matrix assembly to arrive at the global structure. Such methods are used for static and dynamic finite element analyses. Mass and stiffness matrices are typically derived from finite element models, and are usually verified by, rather than determined from, experimental measurements. Because of this, spatial model analysis is rarely used directly in experimental modelling[6], but rather is used as a complementary analysis.

The next category, modal model analysis, is often referred to as "time domain" component mode synthesis in the literature. Work presented in the literature to date has been mostly analytical, although some methods have been explored that are based on quantities that can be experimentally determined[7,11]. In finite element studies, modal model analysis is used for the determination of coupled structure dynamics and is utilized to reduce the number of degrees of freedom in a large system model. Components are represented by state-space modal models that neglect high frequency dynamics, usually with little loss of accuracy. The effects of the higher modes are accounted for in a residual stiffness matrix for the component[12]. A number of coupling techniques presented by Craig[5] are used to augment component dynamic modes--free or fixed interface--by appropriate static deflection shapes--rigid body, constraint, attachment, or inertia-relief modes. All of these various techniques, whether analytical or experimental, require mass normalization of component eigenvectors and the solution of the eigenvalue problem for the global structure.

The third form of substructure analysis, response model analysis, is also known as frequency domain component mode synthesis. This method employs experimentally determined component frequency response functions, either raw or after curve-fitting to a modal model, in order to predict the frequency response of a coupled structure. Instead of representing components in abstract spatial form (mass or stiffness matrices), the component descriptions are left in terms of a response model (natural frequencies, damping and mode shapes). Response matrices are inverted and coupled as "impedances" to assemble the global impedance and response matrices. This method is well suited to experimental modelling, since the response models of components are immediately available and it is usually the response model of the coupled structure which is desired. There are similarities between this method and the experimental time domain CMS methods, since the same measurement information is used in both procedures. These two CMS techniques--frequency domain and time domain--will now be presented in greater detail, with particular attention given to those methods with experimental applications.

2.2 Frequency Domain Component Mode Synthesis

Ewins' frequency domain method[6,10,13] was used in this research work, and this CMS formulation is now presented. Refer to the diagram of Figure 2-1, which shows typical components and a coupled structure. The frequency response matrix of component A can be written as

$$x^a = H^a f^a \tag{2-1}$$

$$\begin{bmatrix} x_m \\ x_o \end{bmatrix}^a = \begin{bmatrix} h_{mm} & h_{mo} \\ h_{om} & h_{oo} \end{bmatrix}^a \begin{bmatrix} f_m \\ f_o \end{bmatrix}^a \tag{2-2}$$

where x_m is a displacement vector of interior degrees of freedom (DOF) and x_o is a displacement vector of boundary DOF used in coupling. Forces f_m and f_o act upon the interior and boundary DOF, respectively. Similar expressions can be written for component B. It is important to note that these frequency response function (FRF) matrices are written for free-interface components, a test configuration which enforces no constraints on any of the component degrees of freedom. This condition is approximated in the laboratory by suspending the component by very soft springs or by long cables that permit motion in the horizontal plane; suspension stiffness will then be low and suspension resonant frequencies will in most cases be well below those of the components.

When components A and B are rigidly connected at interface (o), compatibility and force equilibrium conditions can be written as

$$x_o^c = x_o^a = x_o^b \tag{2-3}$$

$$f_o^c = f_o^a + f_o^b \tag{2-4}$$

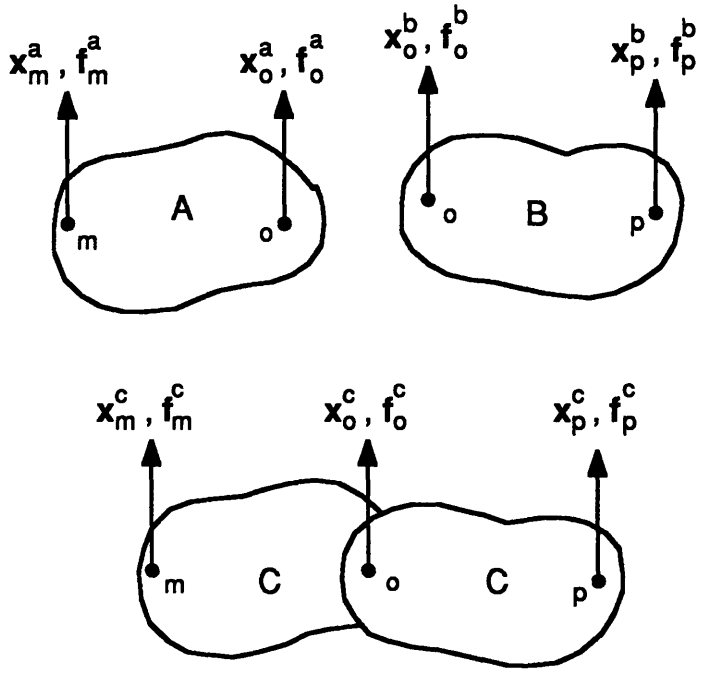

Figure 2-1: Coupling of Hypothetical Substructures.
Two hypothetical components A and B are coupled at interface (o) to form superstructure C. Points (m) and (p) are arbitrary interior degrees of freedom.

The force vectors are written in terms of the displacement vectors as

$$f^a = [H^a]^{-1} x^a = Z^a x^a \tag{2-5}$$

$$f^b = [H^b]^{-1} x^b = Z^b x^b \tag{2-6}$$

Eqs. (5) and (6) can be substituted into Eq. (4) to obtain, after matrix assembly,

$$\begin{bmatrix} f_m \\ f_o \\ f_p \end{bmatrix}^c = \begin{bmatrix} Z^a_{mm} & Z^a_{mo} & 0 \\ Z^a_{om} & Z^a_{oo} + Z^b_{oo} & Z^b_{op} \\ 0 & Z^b_{po} & Z^b_{pp} \end{bmatrix}^c \begin{bmatrix} x_m \\ x_o \\ x_p \end{bmatrix}^c \tag{2-7}$$

or

$$f^c = Z^c x^c \tag{2-8}$$

The desired FRF of the superstructure can then finally be determined by the inversion

$$H^c = [Z^c]^{-1} \tag{2-9}$$

Individual point and transfer FRFs of interest are elements of this superstructure transfer function. Since Z^c is a function of frequency it must be assembled and inverted at each frequency point of interest.

In his work Ewins[6] showed the importance of including all interface coordinates, including rotational degrees of freedom, in the compatibility conditions for coupling. Care must be taken to measure the FRFs at the exact interface points. In addition, he showed that the best assembly of the superstructure FRF occurs when "unified FRFs" for the components, derived from a consistent modal model, are used instead of individually acquired mobilities. In such a model, all the measured frequency responses for any one component have the same modal frequencies and damping. Modal residues are calculated from a consistent set of mode shapes. These "unified" quantities are still based on experimental

measurements. The effects of out-of-range modes, or residual stiffness terms, must be included for these modal models to be correct. These issues and others of importance to experimental CMS will be discussed in greater detail in Chapter 7 and in the remainder of the thesis as they arise.

2.3 Time Domain Component Mode Synthesis

Time domain component mode synthesis is used with spatial descriptions of components--mass, stiffness, and damping matrices--to assemble a system model. A set of elastic and static mode shapes is used to reduce the component physical coordinates to a set of generalized coordinates. The elastic mode shapes--either free or fixed interface--are determined either by experiment or from an analytical model. Static portions of subsystem modes are also determined by finite element model or test, when possible. As with frequency domain CMS, compatibility and equilibrium are enforced at component interfaces in order to assemble the global system matrices. The eigenvalue problem is then solved using the assembled global mass and stiffness matrices.

Hurty[14] is credited with the first work on time domain component mode synthesis in 1965. Since then his paper has been extended by several authors--Craig and Bampton[15], Rubin[16], Craig and Chang[17], Benfield and Hruda[18], MacNeal[11], among others--to include various forms of static deflection shapes. Martinez et. al.[7] have adapted Craig-Chang component mode synthesis techniques to free-interface testing of components by utilizing residual flexibility measurements to supplement dynamic mode

shapes. Kammer and Baker[19] have compared the equivalence of Craig-Bampton and residual flexibility techniques; CMS of damped structures (involving complex eigenvectors) has been studied by Craig et. al.[20], Hasselman and Kaplan[21], Geering[22], and others.

Craig[5] provides a detailed summary of these various techniques and generalizes the different methods and proposed deflection shapes. Craig derives all of these static mode shapes from the component stiffness matrix subject to the constraints for each type of mode shape. These mode shapes are combined with the flexible mode shapes to define statically and dynamically complete mode supersets, which span the full deflection space of the component. Several formulations of these supersets are possible, all of which are described by Craig to be equivalent to the residual attachment mode superset. The latter superset is attractive because it can be easily determined by experimental testing. An overview of Craig's paper is presented in order to give a framework for analytical time domain CMS; the residual attachment mode superset is later described in detail because of its application to experimental component measurements. The reader is referred to References 5 and 7 for more complete presentations of these methods.

Craig describes a hypothetical structure, in this case a beam, comprised of coupled substructures as shown in Figure 2-2. The component physical coordinates, each with two DOF in this example, are partitioned according to interior degrees of freedom I and boundary degrees of freedom B. The boundary degrees of freedom are further partitioned into the coordinates R necessary to make the substructure

statically determinate (sufficient to restrain rigid body motions) and its complement E which are "excess" boundary DOF. The total coordinate set is represented by P and has n_p elements.

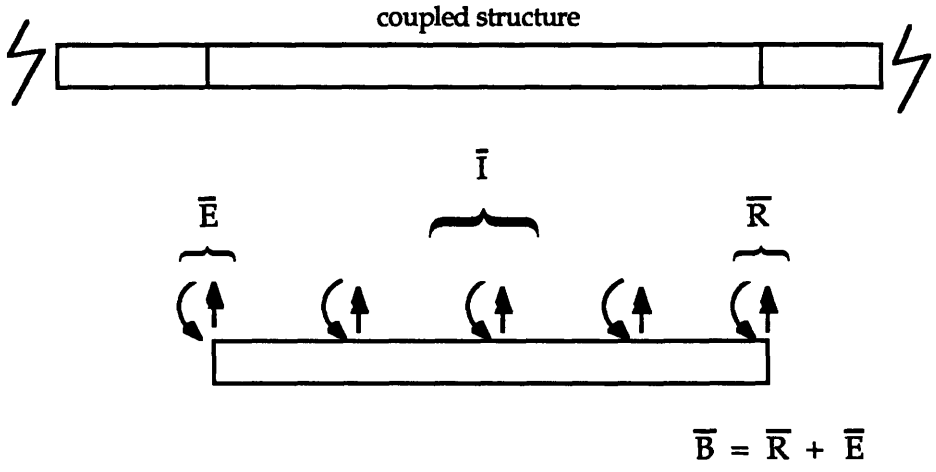

Figure 2-2: Substructure Used in Craig's Coupling Analysis.
Coordinates are divided into interior and boundary coordinates; the latter is further divided into restraint coordinates (necessary to prevent rigid body motion) and the complementary "excess" coordinates.

The standard linear equation of motion can be written for the component

$$\mathbf{M}\ddot{\mathbf{x}} + \mathbf{C}\dot{\mathbf{x}} + \mathbf{K}\mathbf{x} = \mathbf{F} \qquad (2\text{-}10)$$

where **M**, **C** and **K** are the familiar mass, stiffness, and damping matrices for the component, and **x** is the vector of physical DOF of length n_p. It is desirable to represent the physical coordinates in terms of the generalized coordinates **q** by the transformation

$$x = \Psi p \tag{2-11}$$

where the columns of Ψ are linearly independent dynamic, rigid body and static mode shapes that completely span the deflection space of the component. Craig terms this matrix a "dynamic mode superset". The mode shapes which comprise the dynamic mode superset will now be presented.

Orthogonal Dynamic Natural Modes

The free-interface dynamic modes are calculated from the eigenvalue problem

$$\left(\mathbf{K} - \omega_p^2 \mathbf{M}\right)\phi_p = 0 \tag{2-12}$$

The modes are defined to not include any rigid body modes and are normalized and assembled into a modal matrix of size $n_p x n_p$ that is partitioned according to interface and boundary degrees of freedom

$$\phi_n = \begin{bmatrix} \phi_{in} \\ \phi_{bn} \end{bmatrix} \tag{2-13}$$

Usually only a subset of these modes are retained as dynamic modes; this subset of "kept" modes is denoted Φ_k. Fixed-interface normal modes can be calculated in the same manner by solving the eigenvalue problem using **M**, **C**, and **K** matrices that are modified to reflect the fixed interface conditions.

Rigid Body Modes

Craig provided a rigorous derivation of rigid body modes given the stiffness matrix and the boundary coordinates. These modes can also be determined solely from geometrical considerations, and will be represented by Ψ_r.

Redundant Constraint Modes

A set of constraint coordinates C is set equal to the set E of redundant interface coordinates in order to define constraint modes. These mode shapes result from imposing a unit displacement on one coordinate of the C set of physical coordinates and zero displacement on the remainder of the C set. The resulting deflection shape is redundant constraint mode Ψ_c and can be determined solely from the above constraints and the stiffness matrix **K**. Experimental determination of this mode is difficult to achieve.

Attachment Modes

A similar set A of physical coordinates are also defined to be the set E of redundant interface coordinates, but the attachment modes are defined somewhat differently from the constraint modes. The attachment modes are defined by applying a unit force at one of the coordinates of an A set and zero at all others. These modes are termed Ψ_a.

Inertia Relief Modes

Two types of inertia relief modes are defined for components that undergo rigid body motion, and are necessary to define the complete static response. One form is calculated by the static displacement of a

component due to D'Alembert forces; the component is supported such that the stiffness matrix is not singular. The other form is derived by applying unit forces at all the boundary DOF and using D'Alembert forces to equilibrate the structure. These two types of inertia relief modes are termed Ψ_m and Ψ_b, respectively.

Dynamic Mode Supersets

In order to make a complete transformation between physical and generalized coordinates in Eq. (2-11), it is necessary that the columns of the transformation matrix Ψ span the full deflection space of the component. Of course, the deflection space is spanned completely and simply by Φ_n if this vector matrix contains all dynamic and rigid body modes. However, only some natural modes are retained in Φ_k and these must be supplemented with static and rigid body modes. The transformation Ψ needs to be what Craig terms a "dynamic mode superset", of which he defines four types: constraint, attachment, inertia relief, and dynamic residual attachment. These four are shown in Eqs (2-14).

$$\Psi^c = \left[\Psi_r \ \Psi_c \ \Psi_m \ \Phi_k\right] \tag{2-14a}$$

$$\Psi^a = \left[\Psi_r \ \Psi_a \ \Psi_m \ \Phi_k\right] \tag{2-14b}$$

$$\Psi^b = \left[\Psi_r \ \Psi_b \ \Phi_k\right] \tag{2-14c}$$

$$\Psi^d = \left[\Psi_r \ \Psi_d \ \Phi_k\right] \tag{2-14d}$$

One important requirement of these mode supersets is that the columns be linearly independent. This requirement may be violated if most or all of the dynamic modes are contained in Φ_k; Ψ_m and Ψ_a would then be linearly dependent on Φ_k. This can be circumvented by removing the contributions of the dynamic modes from Ψ_m and Ψ_a. The residual attachment mode superset of Eq. (2-14d) is equivalent to the other dynamic supersets since it spans the same deflection space as the others. This superset and the residual flexibility matrix Ψ_d will now be presented in greater detail because of their relevance to experimental component mode synthesis.

2.4 CMS Using Measured Residual Flexibility

The definition of a dynamic mode superset is that it spans the full deflection space of the component and can therefor serve as a complete transformation between generalized and physical coordinates. This deflection space would be completely spanned by the rigid body modes and the dynamic modes if all the dynamic modes were contained in Φ_n. Usually the modelled dynamic modes are only a subset of the total; the remaining higher modes will contribute stiffness-like terms at frequencies well below their resonance. Their collective influence is called the residual flexibility, and is defined by the matrix **G**

$$G = \sum_{i=n_k+1}^{N} \left[\frac{\Phi_i \Phi_i^T}{\Omega_i^2} \right] \tag{2-15}$$

The static deflection mode shapes Ψ_d are columns G_B of the residual flexibility matrix corresponding to the boundary degrees of freedom, and are effectively "residual flexibility attachment modes" at the interface DOF. G is partitioned consistent with the defined interior and boundary degrees of freedom

$$G = \left[G_I \;\; G_B \right] = \left[G_I \;\; \Psi_d \right] = \begin{bmatrix} G_{II} & G_{IB} \\ G_{BI} & G_{BB} \end{bmatrix} \tag{2-16}$$

The notation G_B will be retained from here so that the residual term will "stand out" from the other mode shapes in the generalized mass and stiffness equations. Note that the requirement of linear independence of static and dynamic basis vectors is satisfied by the definition of G, which is determined from a superposition of orthogonal dynamic modes. Thus G is orthogonal to both Φ_k and Ψ_r.

Eq. (2-10) will now be transformed to generalized coordinates by the dynamic residual mode superset

$$x = \left[\Psi_r \;\; \Phi_k \;\; G_B \right] q = T_1 q \tag{2-17}$$

$$x = \begin{bmatrix} x_I \\ x_B \end{bmatrix} = \begin{bmatrix} \Psi_{Ir} & \Phi_{Ik} & G_{IB} \\ \Psi_{Br} & \Phi_{Bk} & G_{BB} \end{bmatrix} \begin{bmatrix} q_r \\ q_k \\ q_B \end{bmatrix} \tag{2-18}$$

With this transformation the undamped component equations become

$$M^R \ddot{q} + K^R q = F^R \tag{2-20}$$

where

$$K^R = \begin{bmatrix} 0 & 0 & 0 \\ 0 & \Omega^2_{kk} & 0 \\ 0 & 0 & G_{BB} \end{bmatrix} \tag{2-20}$$

$$M^R = \begin{bmatrix} \mu_{rr} & 0 & 0 \\ 0 & I_{kk} & 0 \\ 0 & 0 & \mu_{BB} \end{bmatrix} \tag{2-21}$$

$$\Omega^2_{kk} = \Phi_k^T K \Phi_k \qquad I_{kk} = \Phi_k^T M \Phi_k$$

$$G_{BB} = G_B^T K G_B \qquad \mu_{BB} = G_B^T M G_B$$

$$\mu_{rr} = \Psi_r^T M \Psi_r$$

One interesting result is that the residual stiffness at the boundary degrees of freedom, G_{BB}, is retained in the generalized stiffness matrix. These are the "residual stiffness" terms associated with the static deflection shapes due to residual flexibility, and include diagonal and off-diagonal terms.

The residual mass term is traditionally neglected at this point, since it is difficult to measure experimentally and its omission greatly simplifies the analysis. Martinez et. al. have shown that the error incurred in this step is very small[7]. The residual stiffness term is important however, and can be determined from modal tests.

At this point the system equations are almost ready for coupling--but first the physical degrees of freedom of the boundary coordinates must be recovered to permit the enforcement of compatibility. Eq. (2-19) can be solved for

$$q_B = G_{BB}^{-1}\left[x_B - \Phi_{Bk}q_k - \Psi_{Br}q_r\right] \tag{2-22}$$

A second, and final, set of generalized coordinates is then introduced as

$$\eta = \begin{bmatrix} q_r \\ q_k \\ x_B \end{bmatrix} \tag{2-23}$$

The generalized coordinates are given by the transformation

$$q = T_2\eta = \begin{bmatrix} I_{rr} & 0 & 0 \\ 0 & I_{kk} & 0 \\ -G_{BB}^{-1}\Psi_{Br} & -G_{BB}^{-1}\Phi_{B\kappa} & G_{BB}^{-1} \end{bmatrix} \begin{bmatrix} q_r \\ q_k \\ x_B \end{bmatrix} \tag{2-24}$$

This transformation is substituted into Eq. (2-20) to obtain new generalized mass and stiffness matrices that are suitable for coupling. The new component dynamic equation and generalized matrices are

$$M_2^R \ddot{\eta} + K_2^R \eta = F_2^R \tag{2-25}$$

$$K_2^R = \begin{bmatrix} \Psi_{Br}^T G_{bb}^{-1} \Psi_{Br} & \Psi_{Br}^T G_{BB}^{-1} \Phi_{Bk} & -\Psi_{Br}^T G_{BB}^{-1} \\ \Phi_{Bk}^T G_{BB}^{-1} \Psi_{Br} & \Omega_{kk}^2 + \Phi_{Bk}^T G_{BB}^{-1} \Phi_{Bk} & -\Phi_{Bk}^T G_{BB}^{-1} \\ -G_{BB}^{-1} \Psi_{Br} & -G_{BB}^{-1} \Phi_{Bk} & G_{BB}^{-1} \end{bmatrix} \tag{2-26}$$

$$M_2^R = \begin{bmatrix} \mu_{rr} & 0 & 0 \\ 0 & I_{kk} & 0 \\ 0 & 0 & 0 \end{bmatrix} \tag{2-27}$$

The coupled system equations may now be assembled by standard matrix assembly. The eigenvalue problem is solved for the system mass and stiffness matrices; the physical coordinates can be recovered from the generalized coordinates by the appropriate transformations presented above.

The elements of the matrices of Eqs. (2-26) and (2-27) can be determined from measurements, or by measurements and analysis. The necessary quantities are component rigid body modes, natural frequencies of k retained dynamic modes, and the residual flexibility at the interface degrees of freedom. Each of these can be determined from frequency response measurements of the components[7]; rigid body terms and

residual flexibility are determined from the residual terms in the FRF measurement. While the work in this thesis is based upon frequency domain CMS, the procedures just outlined could easily be implemented using the measurements taken in this study.

2.5 Experimental Work in the Literature

As was pointed out earlier, there are three general categories of substructure analysis--spatial model, modal model, and response model analysis, of which the latter two are commonly referred to as component mode synthesis. Little experimental work has been done in component mode synthesis, although a significant amount of experimental work can be found in the literature regarding spatial model substructuring. These studies have mostly entailed updating component mass and stiffness matrices to reflect static and dynamic test results, and it is not the purpose of this thesis to review the body of work in spatial model analysis.

Studies in time domain CMS have been almost exclusively analytical, and rightly so--the problem of experimentally measuring attachment, constraint, inertia-relief or fixed interface modes is difficult if not impossible for most structures. However, Martinez et. al.[7] have conducted an experimental study in which they determine static deflection shapes from experimentally measured residual flexibilities. The "coupled" structure that was used was a continuous beam with point masses; two components were later "created" by cutting the superstructure in two. Modal tests using impact hammer were conducted to measure

natural modes and residual terms. Three superstructure modes were accurately predicted; experimental results were also coupled to a finite element model. A sensitivity analysis was performed that showed that acceptably small errors are introduced by neglecting residual mass and off-diagonal residual flexibility terms from the component generalized mass and stiffness matrices.

Ewins has done a number of experimental studies[6,9,23] in frequency domain component mode synthesis, most of which involved two components of beam-like behavior, and were conducted in frequency ranges above 30-50 Hertz. One study involved a helicopter carriage assembly with multiple components. Brassard and Massoud[8] coupled two beam structures by frequency domain CMS but apparently failed to include rotational coupling in their analysis, leading to poor predictions of superstructure modes.

Other relevant experimental work in spatial substructuring has been conducted by Crawley and O'Donnell[3], in which a linearized joint model was developed from experimental force-state mapping and used in a finite element analysis of a truss structure with joints. This procedure was used by the authors to predict the contribution of the joints to the damping in the truss structure. Bohlen and Gaul[24] identify the parameters of a nonlinear joint model by experiment, and use this model in finite element analysis to predict the dynamics of two and three member beam structures connected by pinned joints. Accuracies between 1% and 4% were achieved between predicted and measured superstructure modal frequencies.

Chapter 3
Experimental Work

3.1 Experimental Design

A set of experimental beam structures was constructed in order to investigate the effect of nonlinear joint dynamics on the accuracy of component mode synthesis. This section will give an overview of the experimental structures, followed by a discussion of the criteria used to select this design. Presented later in the chapter will be the experimental results of static and dynamic tests of components, joints, and linearly coupled structures. Chapters 5 and 6 cover the dynamic tests of structures that are coupled with a nonlinear joint.

Four identical beam components were built, with lengths of 25.4 inches and tip masses that serve as joint connections to other members. One of these components is pictured in Figure 3-1. The component dynamics are dominated by bending modes; there are five below 1000 Hertz, the lowest of which is at 55 Hertz. Figure 3-2 is a photograph of superstructure C, which is formed when two identical components A and B are coupled. Relevant dimensions of the structures are presented in Figure 3-3.

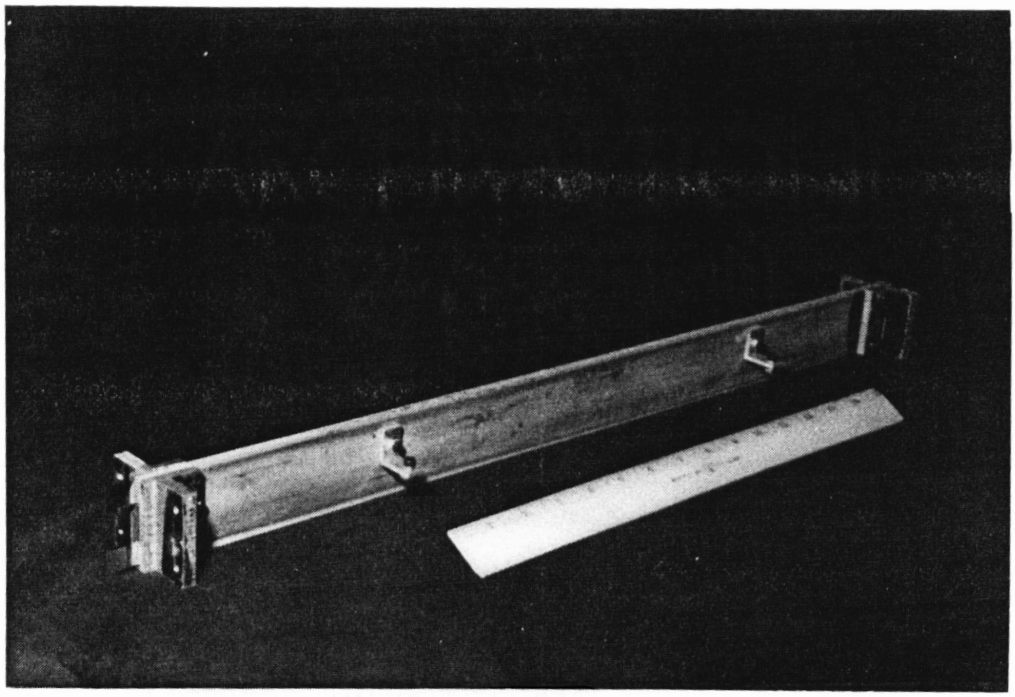

Figure 3-1: Photograph of One Substructure.
One of the identical beam components used to form coupled structures. The beam dynamics are dominated by bending; fundamental mode is at 55 Hertz.

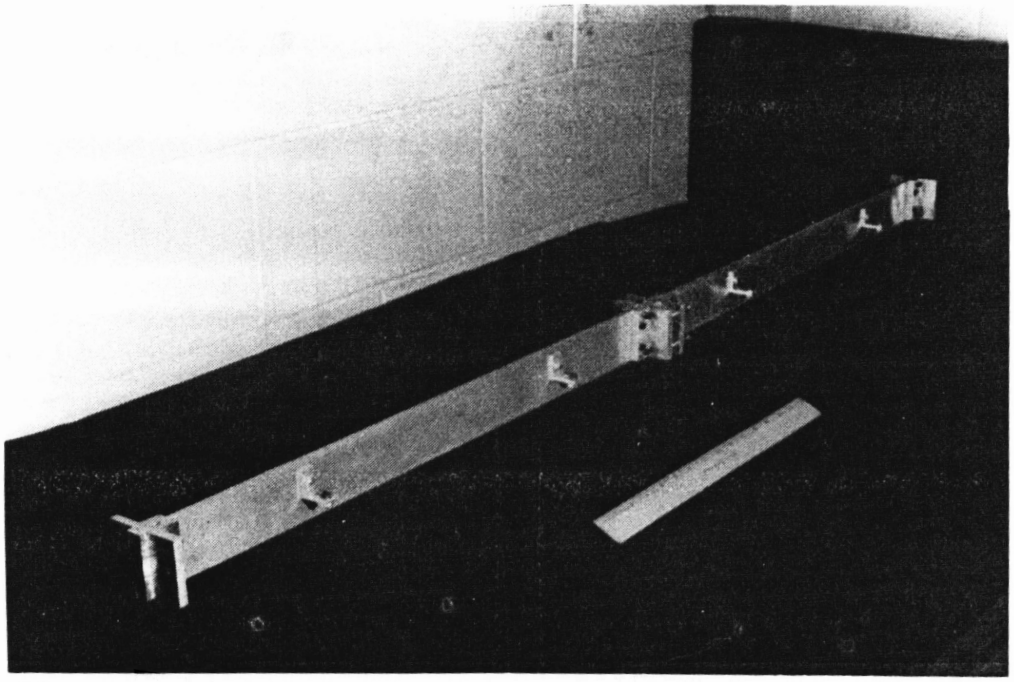

Figure 3-2: Photograph of Coupled Structure--Two Components.
Two identical components A and B are connected for form superstructure C. The components are rigidly clamped by the joint assembly.

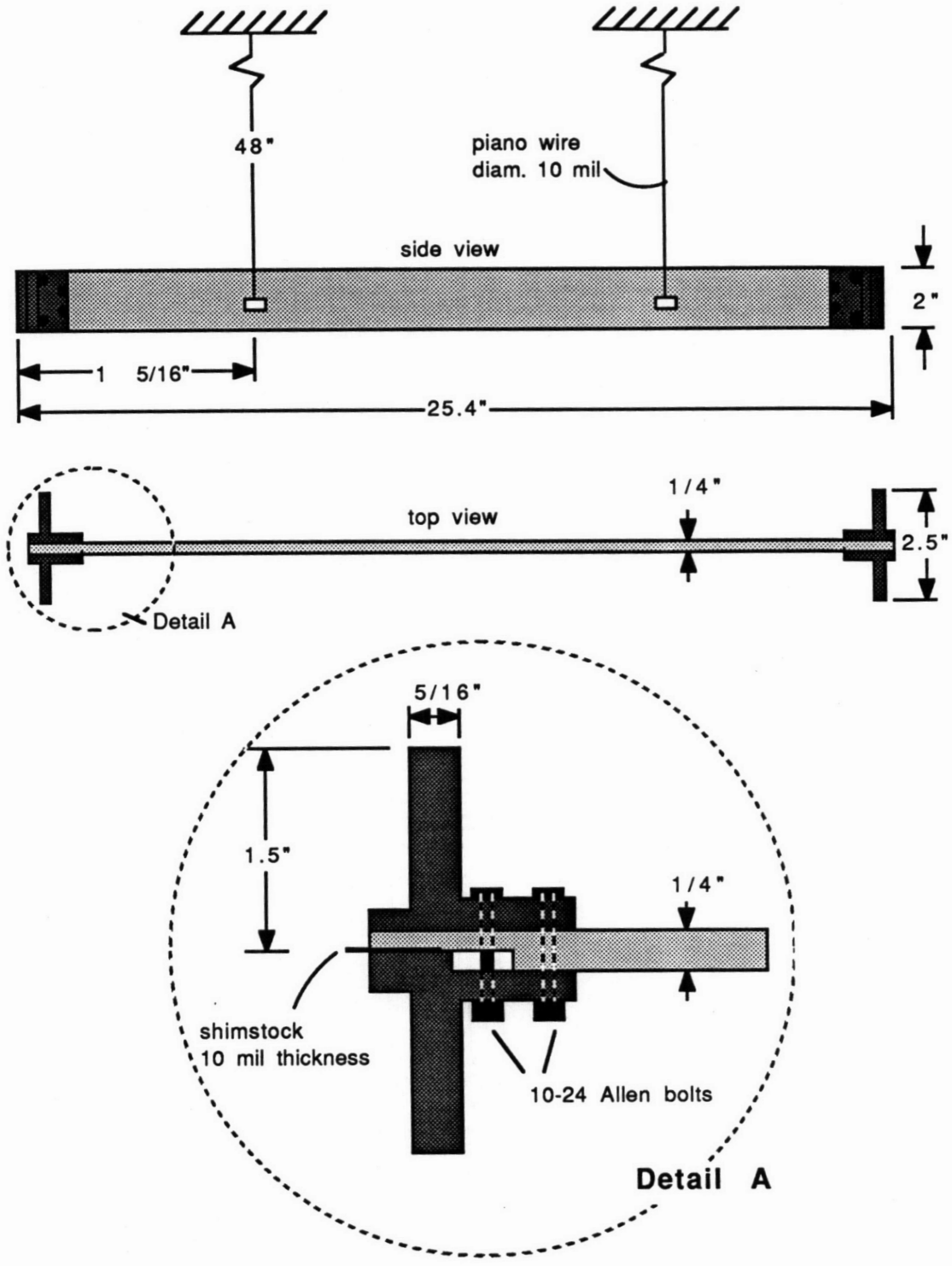

Figure 3-3: Geometry of Beam Component Used in Experimental Coupling.

The component is shown suspended in a free-free (or free interface) test configuration. Tip masses are used as joint connections to adjoining members. Dynamics are dominated by bending modes, five of which are below 1000 Hz. Fundamental mode is at 55 Hz.

An adjustable joint is used to connect the two components. Figures 3-4 and 3-5 display a photograph of the joint along with the important joint geometry. This joint has been designed and built to simulate certain dynamics and coupling of interest, rather than to represent any particular joint that would be used in space or for any other application. In particular, the joint is designed to provide either a clamped coupling between the components or to exhibit "slop" (deadband or freeplay) in another configuration. The joint is made rigid by tightening the bolts (which are tapped into only one component) against the lips of the adjoining component (refer to Figure 3-5). Thin shimstock maintains the alignment of the neutral axis and provides shear stiffness. Rotational freeplay, or deadband, can be produced by loosening the bolts and letting the joint rotate about the shimstock, which is moderately stiff in shear but weak in bending compared to the beam or joint. The joint can assume three states--component lips touching (or saturated) on either side of the joint, or a pseudo-rigid body rotation between the two saturation limits. It is important to realize that the joint does not display any deadband in shear deflection--this two degree of freedom joint exhibits deadband in only rotation. The superposition of multiple gap dynamics would only make the analysis more complicated.

The experimental design was chosen in order to satisfy several requirements for this study:

1) linear behavior of component.

2) coupled structure modes well above pendulum suspension modes.

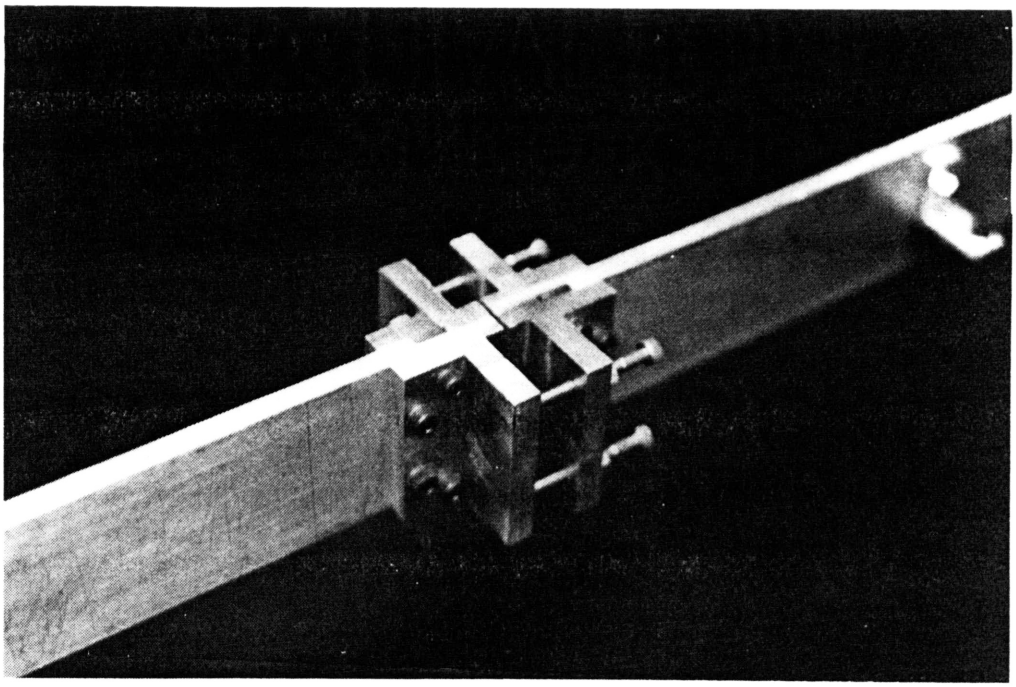

Figure 3-4: Photograph of Adjustable Joint Used to Connect Components.

The joint is moderately stiff in shear and can be made either stiff in bending or be made to exhibit rotational freeplay by loosening bolts on the lips of the joint.

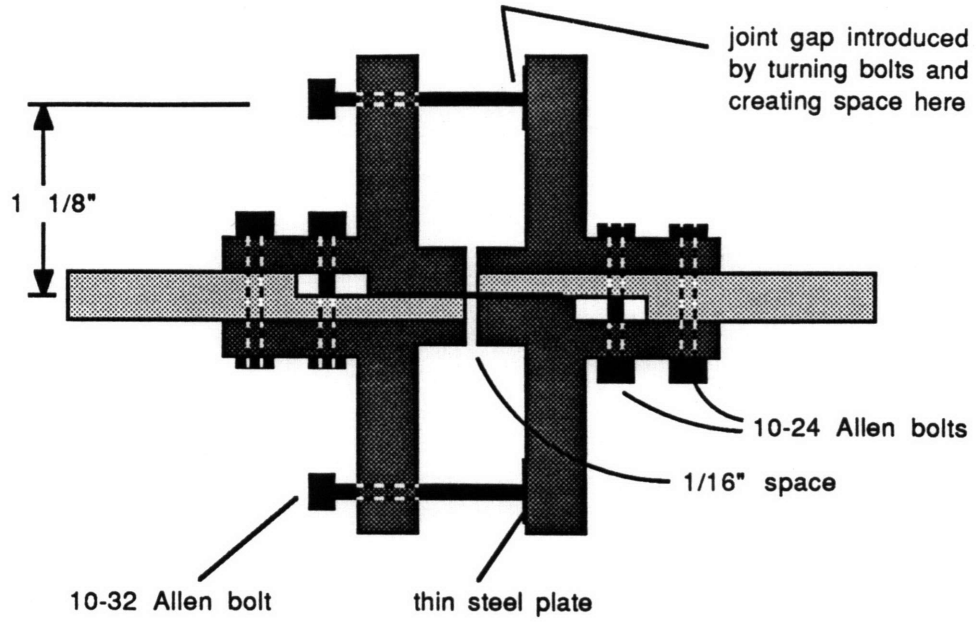

Figure 3-5: Joint Dimensions.
Shimstock maintains orientation of neutral axis and provides moderate shear stiffness.

3) beam dynamics dominated by bending modes, without interference from torsional modes.

4) straightforward coupling conditions at interface of linear structure in order to highlight the effects of joint freeplay of nonlinear structure.

5) joint exhibits freeplay in only one degree of freedom.

In order to satisfy the first requirement, each component was machined and assembled carefully, making certain there were no loose bolts or small gaps in the joint assembly. Special care was taken to machine the joint assemblies to close tolerances (+/- 1 mil) in order to ensure a tight fit. Lock washers were used to prevent nuts and bolts from loosening during dynamic tests, which would have adverse effects on the measured transfer functions. The beam and joint assemblies were

constructed from aluminum because it is much easier to machine than steel.

The overall size of the component was selected to be as large as possible subject to laboratory size constraints for the linearly coupled structure. A length of approximately two feet was felt to be sufficient. Beam dimensions, however, were determined by requirements (2) and (3): the placement of torsional modes at high frequencies dictated the ratio of beam height to beam length, while selection of bending mode frequencies was based on the ratio of beam thickness to length. A simple design analysis was based on the eigenfrequencies of a free-free uniform beam in order to arrive at approximate dynamic properties of the component, which in reality includes significant tip masses.

It was desired to have at least three bending modes below the first torsional mode to help simplify the modal analysis and coupling procedure for this experiment. In future experiments that more carefully simulate large space structural dynamics, high modal density and modal coupling will need to be included, but for this simple study these effects would only obfuscate the essential dynamics under investigation. Torsional modes were kept higher than the three lowest bending modes by maintaining a given beam length and reducing the rotational inertia of the beam along the longitudinal axis of the beam--in other words, a longer, more slender component. The first torsional mode was placed in between the third and fourth bending modes, and has apparently had little deleterious effect on measured beam dynamics.

The third requirement dictates that bending modes of the coupled structure (possibly three or four components) be above the pendulum modes of the suspension--one rotational and one translational mode. Given a suspension length of 48 inches, these modes were calculated to be on the order of 0.5 Hertz. One rule of thumb is to place suspension modes at least one decade below the lowest structural mode of interest in order to achieve a high degree of modal separation. Component with dimensions of 25.4 inches length and 1/4" thickness, including tip masses, have a fundamental mode at 57 Hertz; a 3-component structure has a fundamental mode at 6.7 Hertz. These dynamics were felt to be satisfactory.

The design of the joint presented special problems. The joint must be reasonable stiff when in the clamped configuration, yet be easily modified to exhibit rotational freeplay. The joint must carry bending moment and shear loads between components. Referring to Figure 3-5, the bending moment is transmitted through compression in the joint lips and tension in the shimstock, which is tightly secured in the joint assembly. Shear is carried through the shimstock. Four bolts, two in each lip assembly, are used to transmit compression load between the lips. A thin metal sheet is fastened to the surface of impact for the bolts in order to prevent wear of the softer aluminum. Lock nuts are used to secure the bolts in their lip assemblies.

When in the clamped configuration, the joint provides additional local bending stiffness to the beam, but adds to local shear flexibility. This added shear flexibility does not appear to affect the mode shapes of the

coupled structure, one of which is presented in Figure 3-6. To prevent any slop from occurring in the shear coupling, extreme care was taken to machine an excellent clamped-clamped boundary condition for the shimstock in the joint assemblies (see Figures 3-4 and 3-5).

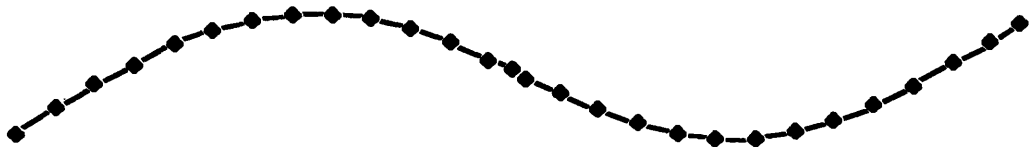

Figure 3-6: Mode Shape Displaying Joint Shear Stiffness.
Second mode of two-component structure, with antinode of shear at the joint.

3.2 Joint Behavior

A simple test rig was used to determine the static behavior of the joint. As shown in Figure 3-7, the beam was suspended vertically and clamped at the top. Lever arms were clamped to the structure below the joint and were used to apply a moment to the beam by means of hanging weights. Just below this point, magnetic positions sensors measure the slope of the beam (see Appendix A for equipment specifications). In this manner rotation was measured as a function of applied moment. A plot of the moment-rotation is shown in Figure 3-8 for the rigidly clamped joint; the curve represents both loading and unloading of the beam/joint assembly. Note the linearity and the lack of measurable hysteresis. The diagram in Figure 3-7 indicates that both joint and beam flexibility are included in this plot.

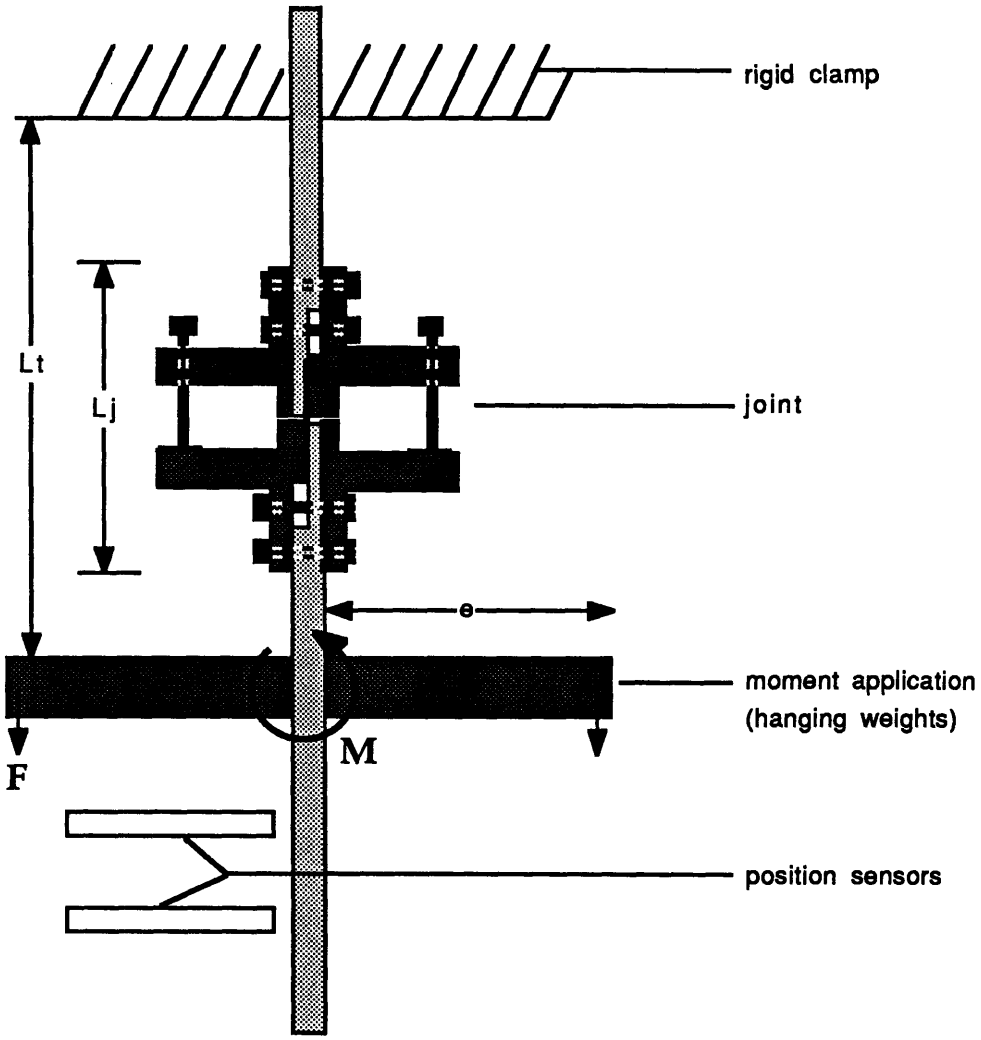

Figure 3-7: Test Rig for Static Test of Joint.
Joint and beam section are clamped and are subject to applied moment from hanging weights. Position sensors measure rotation of beam. While there could be many definitions of joint length, the chosen convention will be Lj for this chapter.

Figure 3-9 shows the moment deflection curve for the joint with deadband. Hysteresis is again small or unmeasurable; a small stiffening effect can be seen on the linear portion of the moment-rotation curve. The curve could be shifted horizontally by a redefinition of the zero angle, but it is noteworthy that a small moment is necessary to swing the joint from one saturation point to another. This is an indication of the small amount of shimstock bending stiffness or of possible joint asymmetries.

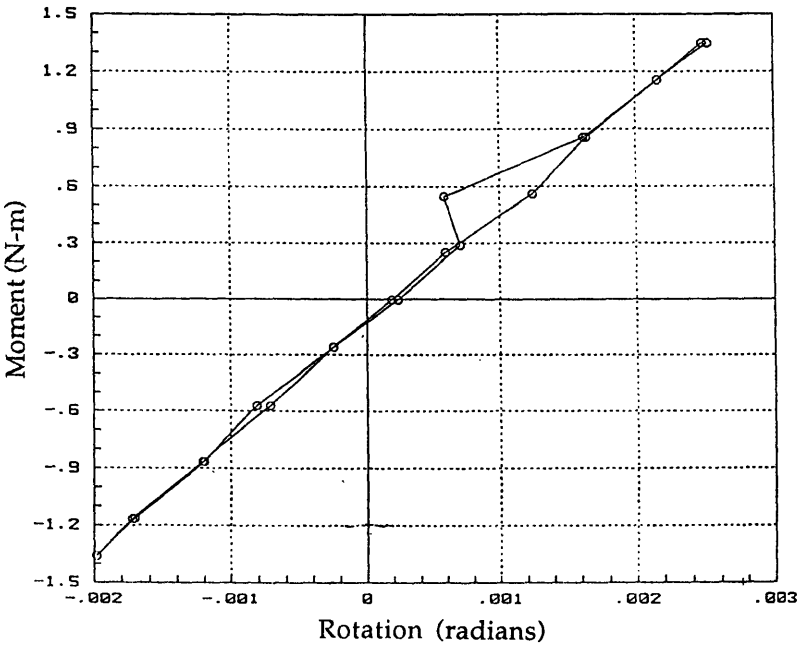

Figure 3-8: Moment-Rotation Curve for Linear Joint.
(lip bolts tightened)

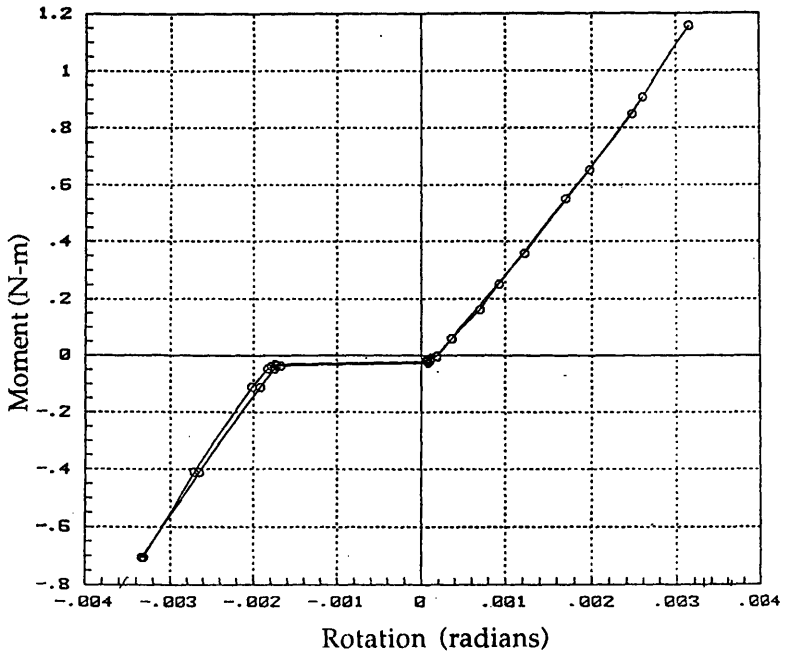

Figure 3-9: Moment Rotation Curve for Nonlinear Joint.
Deadband nonlinearity is introduced by loosening the lip bolts and letting the joint rotate about the shimstock. The joint retains shear stiffness.

The tendency of the joint to remain saturated against one lip, a small but measurable effect, may have been responsible for some of the observed behavior at low amplitude dynamic forcing presented in Chapter 5.

One unresolved problem in the joint measurements of Figures 3-8 and 3-9 is that the slopes of the linear regions of the nonlinear and linear curves are in disagreement by as much as 30%. The discrepancy may be due to the fact that the bolt tips were not "flattened" and were left pointed, giving less definitive impact or saturation conditions. A more likely explanation is that during the nonlinear test, both bolts on the lip may not have contacted the adjoining lip at the same load level, perhaps resulting in a different load relationship and the observed stiffening effect in the nonlinear plot. Both of these problems detract from the overall accuracy of this study.

The joint is measured to be stiffer than an equal section of beam. If the measured beam stiffness is written as $(EI)_b$, and the unknown joint stiffness as k_j then the total rotational deflection at the measurement location of Figure 3-7 can be written as a contribution of rotations of the beam section and the joint section

$$\Theta_{tot} = \Theta_{beam} + \Theta_{joint} \tag{3-1}$$

$$\Theta_{tot} = \left[\frac{L_t - L_j}{(EI)_b} + \frac{1}{k_j} \right] M \tag{3-2}$$

where M is the applied moment and L_t and L_j define beam and joint lengths over which rotation occurs. While the definition of "joint" length is arbitrary, here it is chosen as that length over which the beam is reinforced with the joint assembly, a distance of 2.56 inches. From Figure 3-9, the slope of the measured moment-rotation curve of the joint/beam section was calculated to be 407 Newton-meters/radian. The total deflection of this section due to a moment M is written as

$$\frac{\Theta_{tot}}{M} = S_1 = \frac{1}{407} \quad \text{rad/Nm} \tag{3-3}$$

The joint stiffness is calculated by

$$k_j = \left[S_1 - \frac{L_t - L_j}{(EI)_b} \right]^{-1} \tag{3-4}$$

For a value of L_t of 4.75 inches and measured beam stiffness of 33.8 Nm^2, the ratio of joint stiffness to beam stiffness was calculated to be

$$\frac{L_j k_j}{(EI)_b} = 2.3 \tag{3-5}$$

While the specific value of this joint stiffness is not important to the study, it does indicate the stiffening effect that might be expected in the dynamic tests of the coupled structures. Most importantly, the linear moment-deflection curve of the clamped joint gives confidence that the

joint will be well-behaved for the linear case, which will serve as a good basis for comparison when the joint is given deadband rotation.

3.3 Dynamic Tests of Components

A modal analysis was conducted for the components and coupled structures in order to determine a mathematical description of their dynamic behavior. There are generally two parts to a modal analysis--the first involves accurate measurement of the experimental frequency response functions, and the second consists of post-test determination of modal parameters (modal frequencies, damping, and modal residues). A further step is to determine spatial quantities of mass, stiffness and damping matrices based on these modal parameters in order to validate finite element models. Often modal parameters are sufficient as they are for this study. This chapter will be concerned with the experimental issues pertaining to the accurate measurement of the FRFs; Chapter 4 will address the analytical issues of parameter identification.

Modal analysis is typically performed for a variety of reasons--machine diagnostics, model verification, or model identification. Flight structures, such as the Galileo spacecraft[25], usually undergo a modal test in order to validate analytical finite element models that are used for load prediction analyses. When modelling uncertainty is high, as it may well be for future spacecraft, a modal test of the superstructure or components may itself be used to identify a mathematical model. In this spirit, the experimental components in this study are dynamically tested in the laboratory. This approach will hopefully help to identify test

considerations and constraints, even for these simple structures, that could affect the accuracy of the component mode synthesis procedure.

In most modal tests a great deal of care is taken to avoid corruption the true dynamics of the test article due to mass loading of sensors, and to avoid stiffness and damping interference from suspension and excitation mechanisms. Techniques already exist for removing or compensating for most of these corrupting influences--vacuum testing[26], freefall testing[26], zero spring rate devices[27], modal isolation of suspension[13], compensation for mass loading[13]--and will therefor not be addressed in detail in this study. Similar source of FRF corruption exist in the present experimental study, but for simplicity most of their effects will be defined "into" the component and thus will not need to be subtracted out of the final results. In particular, the mass of sensors will be included in the component and additional damping from air and suspension wires will be assumed to be part of the component damping. Stinger effects, however, will be removed by curve-fitting. The influence of these effects on the overall dynamics of the component is small, and probably has little or no influence on the results of this study.

3.3.1 Experimental Setup and Equipment

The experimental setup for modal testing is pictured in Figure 3-10; the diagram in Figure 3-11 also shows the spectrum analyzer and computers used. A complete list of equipment is provided in Appendix A. Components are tested in a "free-free" or "free-interface" configuration by suspending the structures from long piano wires. The 48" length of cables

places the suspension modes more than a decade below the fundamental modes of test specimens, so that these pendulum modes appear as rigid body modes (one rotational and one translational mode) in the dynamic range of the structures. Free interface testing is a commonly used technique because of its ease and good quality of measurements. Fixed-interface modal testing has also been used, but the condition that one or more degrees of freedom be grounded is difficult to enforce and often leads to poor results. A third option is to test "in situ", as is often done with machine diagnostics, and involves the use of compliant mounts.

A Signology® SP20 spectrum analyzer acts as the nucleus of the test equipment. The SP20 generates an analog signal--sine wave, random, or other--which is amplified by a Crown® amplifier and sent to a Bruel & Kjaer® electromechanical shaker. The shaker generates an axial force up to +/- 12 pounds on the structure. The shaker is coupled to the structure by a thin member called a stinger which is axially stiff but weak in flexure. The stinger helps to ensure that only an axial force is transmitted to the structure. A Kistler® load cell measures the actual force applied to the structure, which can have a frequency content different from that of the excitation signal sent to the shaker. PCB® Structcel accelerometers, which have a dynamic range between 1 and 1000 Hz and masses of .11 grams, measure the acceleration response at any points of interest on the structure. Charge amplifiers convert the charge signals from the load cell and accelerometers to voltages, which are then measured by the spectrum analyzer. The SP20 is supported by an IBM® XT. Data is later sent to a DEC® MicroVax II for analysis and plotting.

Accelerometers are calibrated prior to each test, and display sensitivity changes of +/- 5% on a daily basis. The load cell was calibrated only once because of the difficulty (the stiffness of the compression bolt changes the manufacturer's conversion factor) and may be a source of error in the measurements.

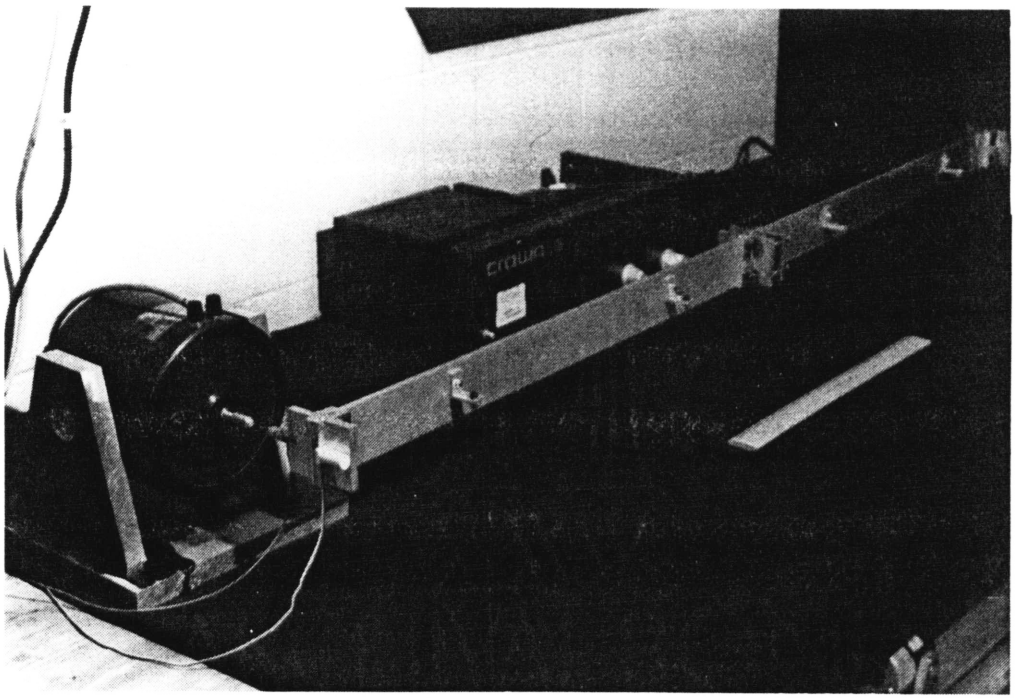

Figure 3-10: Photograph of Experimental Setup for Modal Tests.
Superstructure C is shown in the free interface test configuration, suspended by four feet of piano wire. The structure is excited by an electromechanical shaker through a flexible stinger coupling.

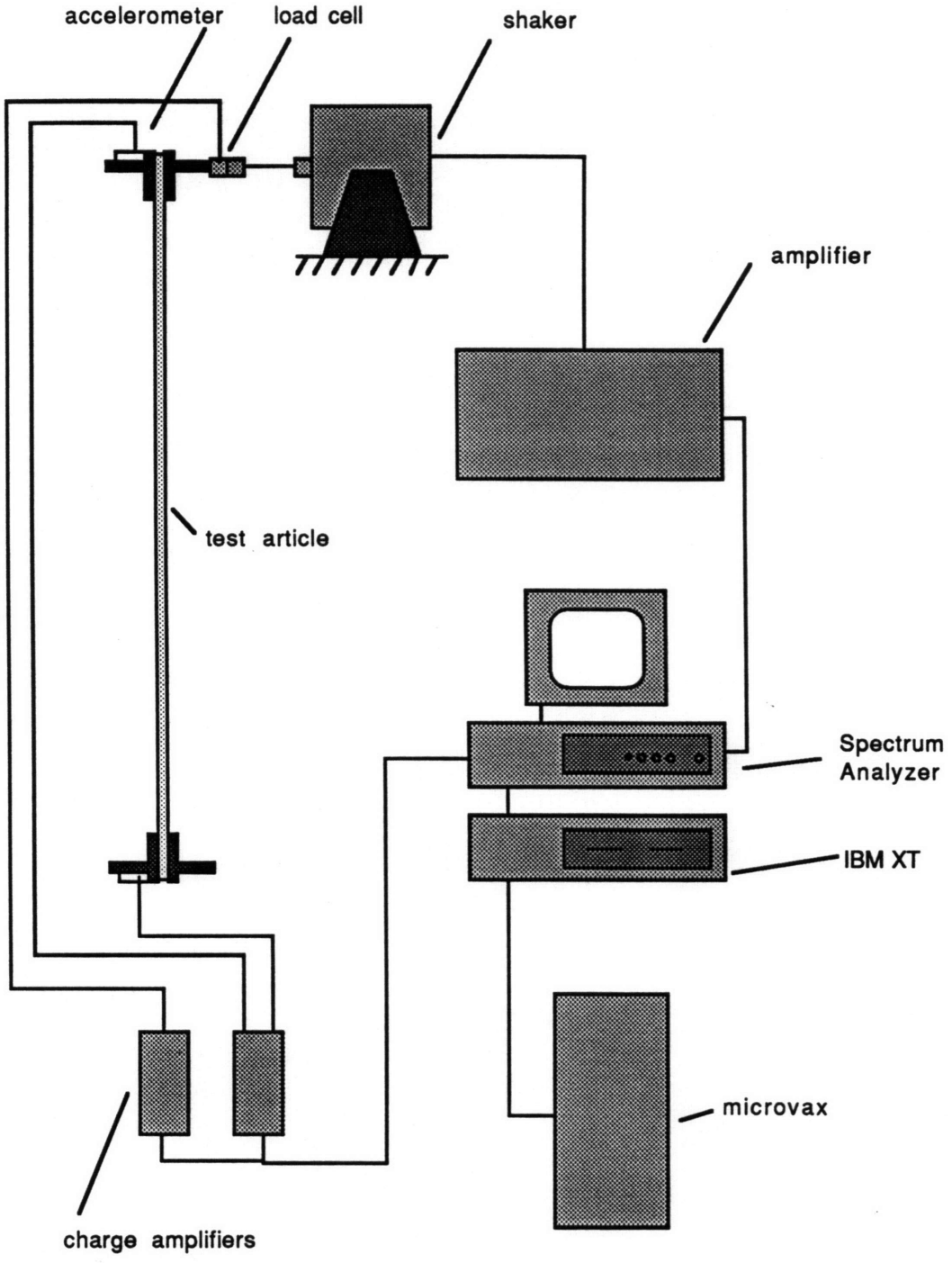

Figure 3-11: Diagram of Experimental Setup for Modal Tests.
Structure is suspended horizontally from 48" piano wires, and is shown from above in this diagram. MicroVax II is used for post processing.

3.3.2 Selection of Force Excitation

The selection of forcing function is an important step in the modal analysis procedure. Four general types of excitation are commonly used in modal analysis--steady state, random, periodic, and transient. Table 3-1 summarizes some of the strengths and weaknesses associated with each of these forms. In addition, there are four general means of applying these forms of excitation--shaker, impact hammer, step relaxation, or actual operating load. Each of these excitation methods and means of implementation have their advantages and areas of application, but no method is best for all situations.

Most recent modal testing is conducted using an electromechanical shaker which is attached to the structure through a flexible stinger. Usually, single shaker testing is used, but recent algorithms have been developed to permit the multiple-shaker tests which have the advantage of evenly distributing energy about the structure and help to provide better parameter estimation in the presence of closely spaced modes[28]. One drawback to shaker testing is that the applied force level drops to near zero at resonance for lightly damped structures, leading to measurement problems at the structural modes. Impact hammer testing is also commonly used but has the disadvantage of inconsistent results and noise sensitivity. A disadvantage of the step relaxation method is that it requires special test apparatus. A thorough modal test would compare measured FRFs using different methods to provide confidence in the test results.

Table 3-1: Possible Excitation Methods for Modal Testing.

Excitation Method	Strengths	Weaknesses
Random	Easy, fast, after initial setup for single input	Low force level only, low damping may not be measured correctly due to leakage
Burst Random	Same as random, no leakage	Low force level only more complicated input
Sine Sweep	Variable force level, variable freq. resoltion good for nonlinear systems	Long test time
Normal Mode Excitation	Forces a single normal mode	Requires precise tuning to isolate mode
Chirp	No leakage	Requires special hardware for input signal
Transient	Easy, quick to set up	Not good for complex structures or high damping

Burst random testing, sine sweep and normal mode excitation were all used in this experimental study because of their availability and their ease of implementation. Burst random was used to produce the transfer functions because of the short test time required, while the sine sweep was used to verify the accuracy of the random tests. Mode shapes were verified and measured using normal mode excitation. One aspect of random testing is that it can provide a "best" linear estimate of a mildly nonlinear structure, as discussed by Goyder[29], and has the effect of smoothing out

discontinuous jump phenomena. This feature was considered important for the tests of the nonlinear beam-joint assembly. One disadvantage to random testing is that moderate to high levels of nonlinearity lead to substantial noise in the measurement of the frequency response function.

A problem called leakage can occur when a discrete Fourier transform is calculated from the measured force time history. The problem arises because of the need to measure a finite time record of a process which is assumed to be periodic with infinite time length, distorting the true frequency content of the measured frequency over a range of frequency lines in the DFT. A solution to this problem is to use a window such as the Hanning window to force the time history to zero at either end of the time record. Another solution is to use a burst random or chirp signal with no window, which is also zero at the beginning and end of the time record. Burst random excitation was required by the spectrum analyzer to determine transfer functions suitable for a recursive parameter identification algorithm, and was therefor selected as the most suitable form of excitation.

The force time history for the burst random signal is shown in Figure 3-12. The time record length of 1600 milliseconds is determined by the number of points in the time record (4096 were selected for maximum resolution) and the sampling rate. Note that the signal begins about 3% into the time record, and ends at 1300 milliseconds. These limits were determined by trial and error along with operator judgement to produce the most "clean" transfer functions. Coherence measurements were not available due to analyzer software error, but should be measured in future

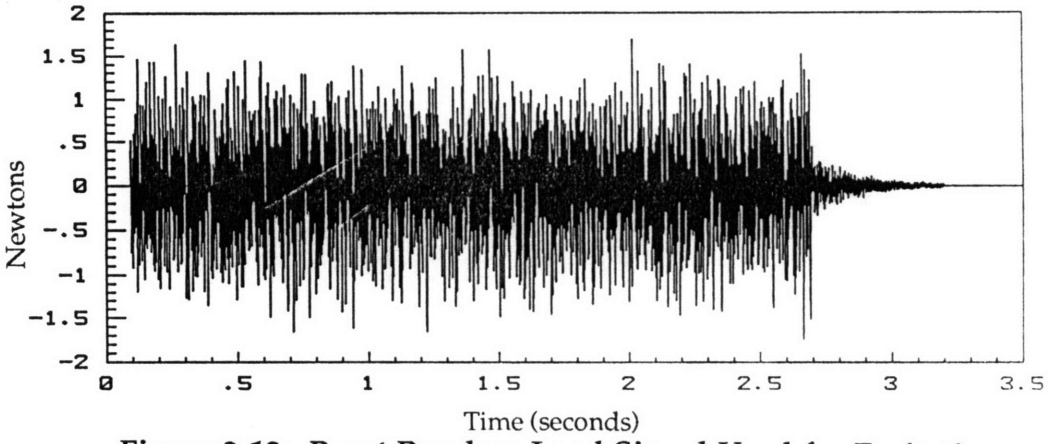

Figure 3-12: Burst Random Load Signal Used for Excitation.
The structure is forced using broadband random excitation applied by the shaker, connected to the joint lip by a thin flexible stinger. A load cell measures the actual force applied and is plotted above.

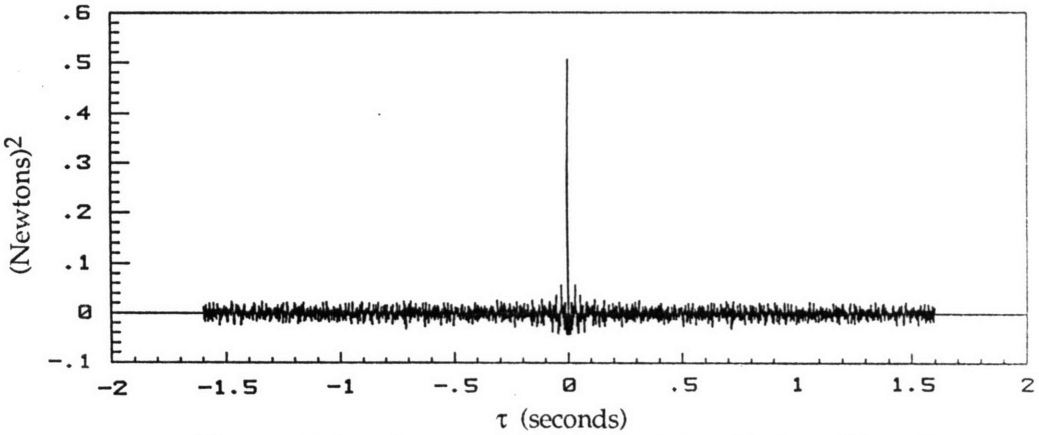

Figure 3-13: Autocorrelation of Load Time Signal.

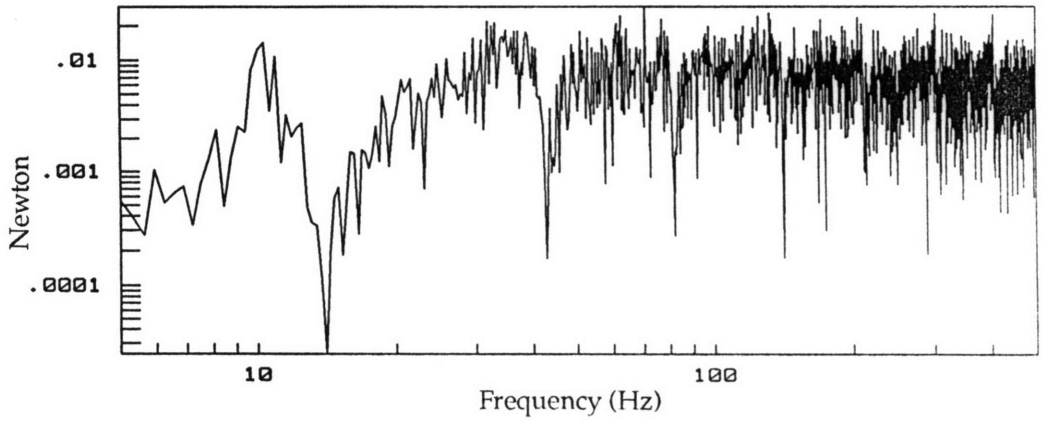

Figure 3-14: Discrete Fourier Transform of Load Time Signal.
The load excitation is "pink" and not white; deep zeros appear at the structural resonances (two-component structure in this case).

experiments. Fifteen averages were used to compute transfer functions. The burst random signal is on for 1300 milliseconds and off for 10000 milliseconds; the off-time allows the structural vibrations to damp out and let the structure achieve zero initial conditions before the next random burst.

Force amplitude was selected to be small, as to not excite any extraneous vibrations of the suspension. A white noise signal was output from the spectrum analyzer in order to drive the electromechanical shaker. The autocorrelation of the measured load signal is shown in Figure 3-13 to be almost a white noise signal; the rms value of the force level is approximately 0.7 Newtons. Figure 3-14 shows the discrete Fourier transform force time signal in Figure 3-14, which is corrupted by dynamics of the test specimen. Zeros appear at the structural modes and are deep because of the low damping. A clever technique, not used in this study, to compensate for this problem is to create a time signal with more energy at the zero frequencies and less energy at the poles, based on a previously measured transfer function. This produces more accurate measurements of the structural response near the resonances and anti-resonances.

3.3.3 Forcing Stinger

The most difficult, and frustrating, part of the modal testing was the accurate use of the stinger. Three problems persisted:

1) interference of stinger-structure resonances with structural modes.

2) wear and tear of the stinger from repeated repositioning of the shaker for different modal tests.

3) orientation of shaker and stinger such that only an axial force was applied--a requirement for the modal tests.

The first two problems were surmounted by the design of Figure 3-15, which shows the latest stinger. A photograph of an earlier, similar stinger is shown in Figure 3-16. A 3/4" section of 25 mil wire was used to provide the flexural stiffness. The wire was press fit into short sections of 3/8" aluminum rod, one of which was used to place the load cell into compression by a bolt which passes through the annular load cell and is bolted into the lip. This stinger section would wear after repeated use (as the stinger and shaker were unbolted and moved) and would have to be remachined. The other end of the stinger is shown in Figure 3-15 to interface to a reverse-threaded rod, which is then connected to the shaker. Attachment of the shaker then requires no torque on the thin wire section, which prolongs its longevity and preserves its dynamic behavior. A superior design would have been to construct the stinger assembly from steel. The shaker sits on a table top that is not connected to the suspension system for the test article.

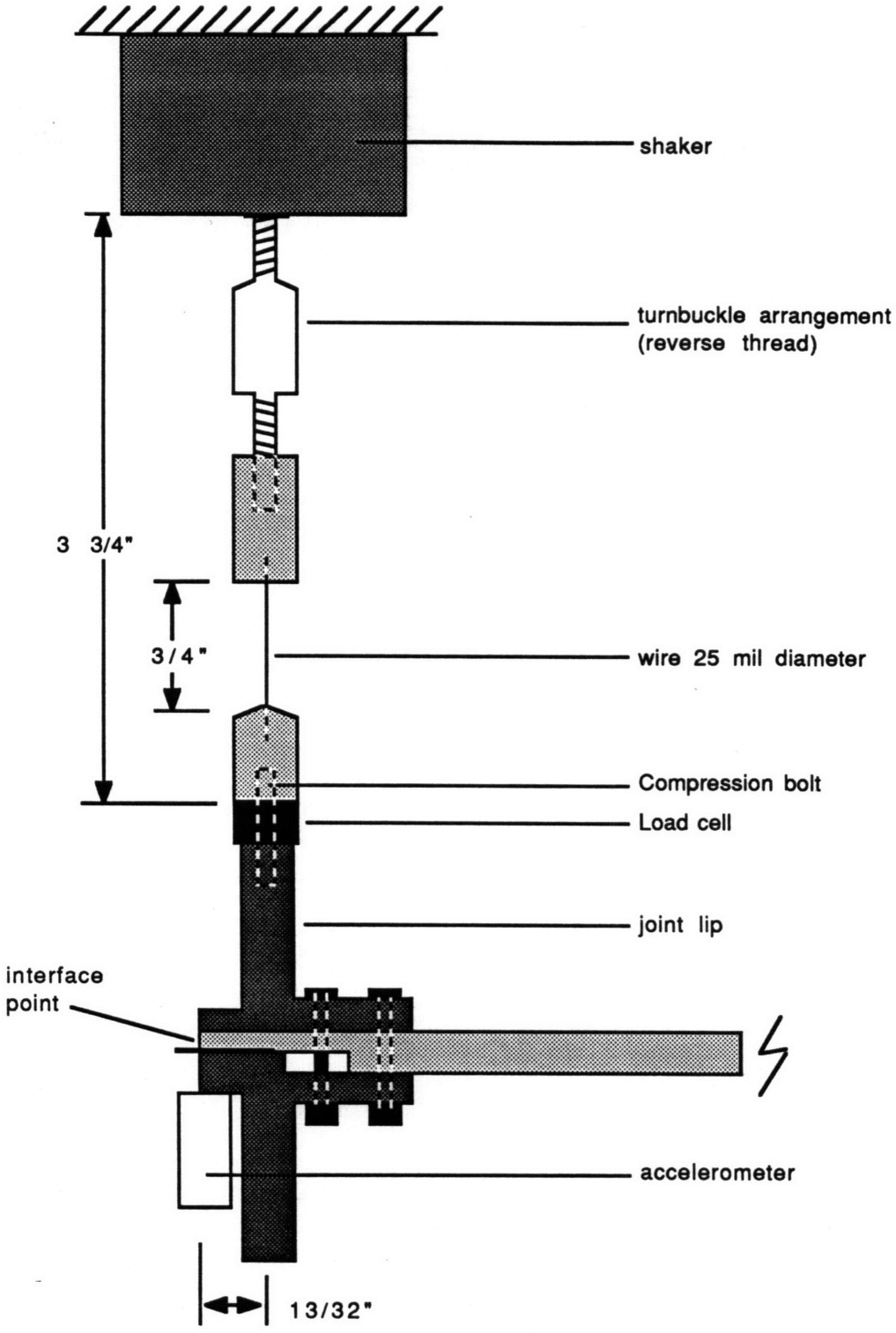

Figure 3-15: Diagram of Forcing Stinger.

Coupled shaker-beam resonances are below the structural modes. A compression bolt places the load cell into compression so that it can measure both compression and tension. Lock nuts, not shown, secure the turnbuckle assembly against stinger and shaker.

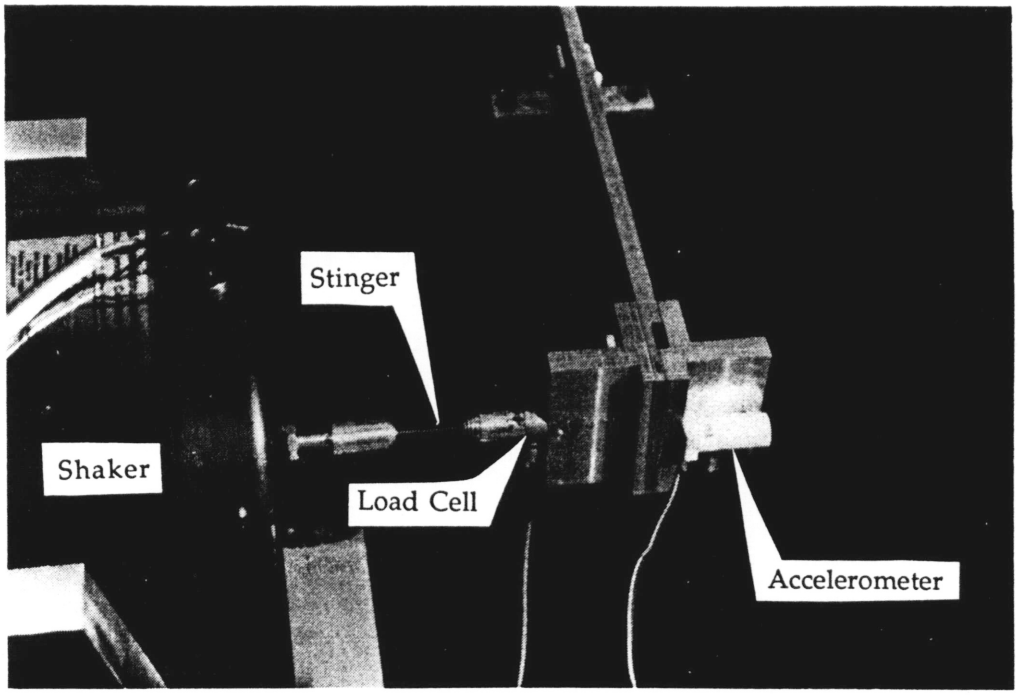

Figure 3-16: Photograph of Forcing Stinger.
The shaker is connected to the structure via a thin flexible stinger. Load cell and accelerometer are used to measure force applied and linear response at the interface.

A stinger-beam resonance occurs when the beam mass oscillates axially with the flexural stiffness of the stinger wire to produce motion perpendicular the axial forcing direction. The motion causes cross-coupling measurements in the load cell and accelerometers and leads to a corrupted transfer function. These effects are exacerbated when this stinger mode occurs near a structural mode. This problem is overcome by machining a longer stinger, which locates the stinger-beam resonance in a frequency range below the test range.

3.3.4 Force Application and Response Measurement

Figure 3-17 shows the two configurations used to apply forces to the test structures, for reasons which will be presented in Section 3.4.1. A force and moment must be applied at the interface of the components, which in this case is at the very ends of the members. The force was achieved by exciting parallel the joint lip as in Figure 3-17; moment was applied by forcing perpendicular to the joint lip and using the lip as a lever arm. Lever arm dynamics were assumed to be neglible in the frequency range below 1000 Hertz. An important requirement for most modal tests is that only one force or moment be applied to the structure at any one time, otherwise superposition effects would corrupt the measurement of the modal parameters. This condition required the use of a stinger to remove non-axial force components or reaction moments from the excitation. Multi-shaker testing can be conducted only if the excitation signals are uncorrelated. The results of transfer function measurements in the present study were found to be satisfactory.

One important note is that these forcing locations were not at the exact interface, but were in error by 13/32" or 1.6% of the beam length. In retrospect the test article should have been designed differently; this measurement problem, however, is generic in modal analysis of actual structures. Calculations indicate that this position error induces a 4.5% error in the estimate for the first component eigenvector at 55 Hertz; this error increases to 30% at the third mode above 325 Hertz. Modal frequencies are still measured correctly. Accelerometers, on the other hand, were placed at or very close to the actual point of interface. The error in forcing location is not serious and can be compensated for. Rather than detract from the results, this event has elucidated a problem worthy of future attention.

Accelerometers were attached to the structure with wax. Manufacturer's specifications for the accelerometers and wax indicate a nearly linear response of these two items in the frequency range of 1 to 1000 Hertz, the range in which most tests were conducted. Accelerometers measured linear acceleration at the beam tips (interface points) as is shown in Figure 3-17. Tip rotation of the beam was also measured by placing two accelerometers on the joint lips and assuming the lip to be "rigid" enough to deduce the beam rotation at the tip. This configuration is shown in the third figure of Figure 3-17.

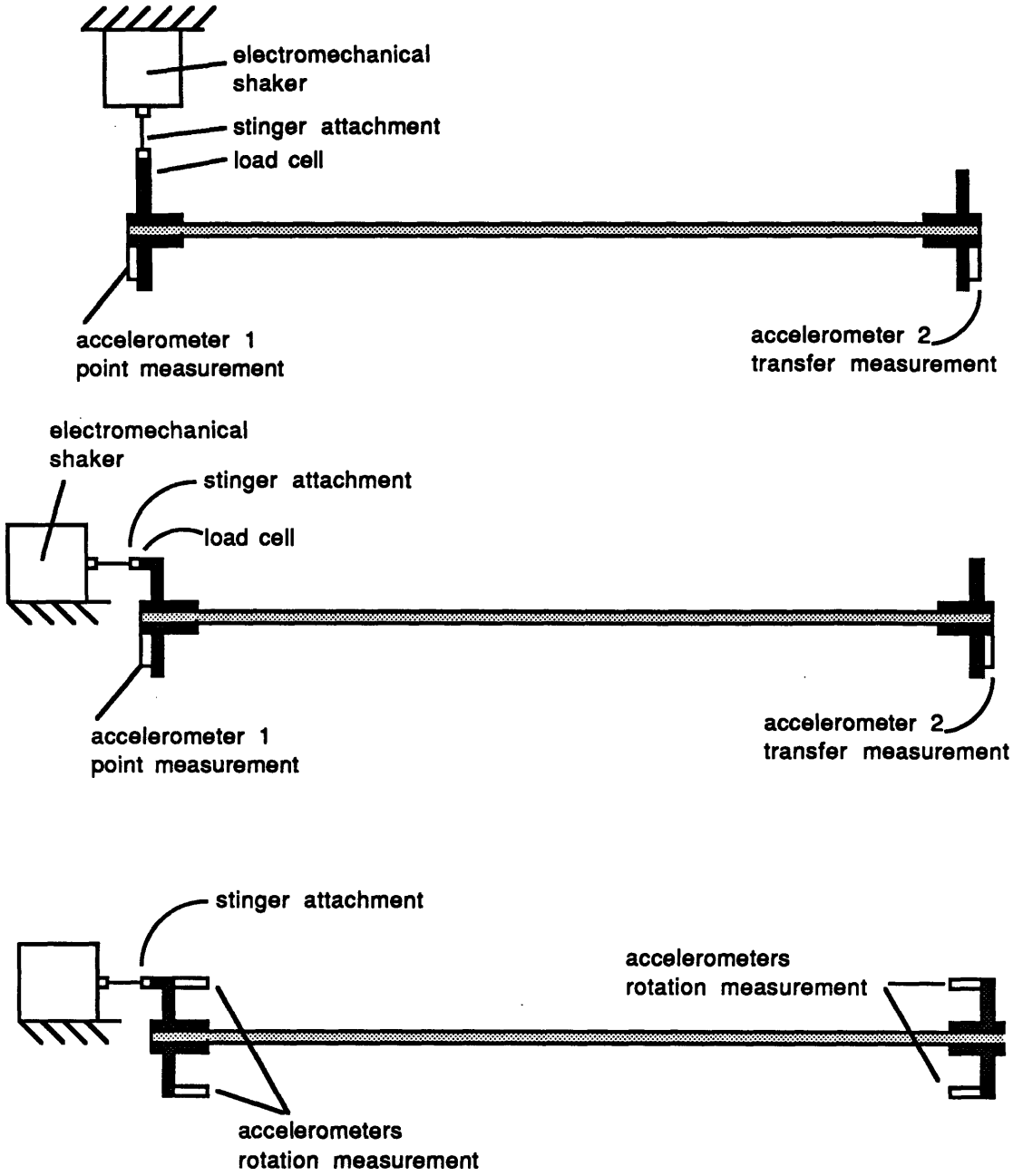

Figure 3-17: Geometry of Force Application on Structure.
Structure is shown from above; it is tested in a free-free configuration. 3-17(a) shows force/deflection test; 3-17(b) shows moment/deflection test; 3-17(c) shows moment/rotation test.

3.3.5 Determination of Frequency Response Function

Time histories of force and response are used to estimate the transfer function relating the two. 4096 points are measured in each time record which are transformed to the frequency domain by the fast Fourier transform (FFT). Complex conjugate symmetry reduces the length of the frequency domain block to 2049 points (including the Nyquist frequency point). Low pass anti-aliasing filters are used to filter out high frequencies from the time histories, and since they are not perfectly efficient still have some distortion of high frequency components in the measured data. Accordingly, only 78% of the frequency vectors, or 1601 points, are retained and are free from aliased high-frequency data down to a level of -75 dB. The spectrum analyzer calculates the complex-to-complex FFT as:

$$X(k) = \sum_{i=0}^{N-1} x(i) \exp^{-\left(\frac{2\pi ki}{N}\right)} \qquad k = 0,1,2,...,N-1 \qquad (3\text{-}6)$$

where x(i) is a time history and X(k) is a complex frequency vector of the same size. The power spectral densities (PSD) are calculated from the FFT by the relation

$$S_{xx}(k) = \left(\frac{T^2}{P}\right) x^*(k)\, X(k) \qquad k = 0,1,2,...,(N/2)-1 \qquad (3\text{-}7)$$

where P is the time record length (1600 milliseconds) and T is the time increment (P=NT). The T^2 term is included since it was left out in the FFT computation. The transfer function is determined from the averaged

auto-spectrum of the force $S_{ff}(k)$ and the averaged cross-spectrum of force and acceleration $S_{xf}(k)$ by

$$H_{xf}(k) = \frac{S_{xf}(k)}{S_{ff}(k)} \qquad k = 0,1,2,...,N/2-1 \qquad (3\text{-}8)$$

3.4 Experimentally Measured Frequency Response Functions

3.4.1 The Complete Frequency Response Matrix

A definition of the sign conventions used for the measurement of component transfer functions is presented in Figure 3-18. Two responses (translational and rotational deflections) and two forces (force and moment) are defined at each of two points.

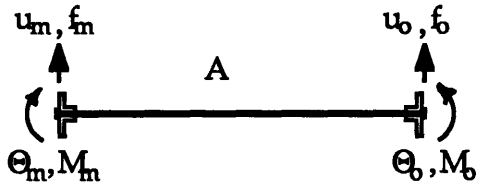

Figure 3-18: Sign Conventions for Single Component Deflections and Forces

The frequency response matrix that relates the forces to deflections is given by

$$\begin{bmatrix} u_m \\ \Theta_m \\ \hline u_o \\ \Theta_o \end{bmatrix}^a = \left[\begin{array}{cc:cc} h_{11} & h_{12} & h_{13} & h_{14} \\ h_{21} & h_{22} & h_{23} & h_{24} \\ \hdashline h_{31} & h_{32} & h_{33} & h_{34} \\ h_{41} & h_{42} & h_{43} & h_{44} \end{array}\right]^a \begin{bmatrix} f_m \\ M_m \\ \hline f_o \\ M_o \end{bmatrix}^a \qquad (3\text{-}9)$$

Eq. (3-9) is a *receptance* matrix since it relates force to displacement. The measured component FRFs that will be presented are termed *inertances,* which relate force to acceleration. Chapter 4 will address the simple conversion of inertances to receptances; the following discussion can be left in terms of receptances with no loss of generality since the results apply to inertances as well.

The objective of dynamic testing is to determine each entry of the FRF matrix of Eq. (3-9). Typically, any one row or column of the matrix is measured--usually by exciting at one degree of freedom and measuring responses at all degrees of freedom--which is sufficient to determine all the remaining entries of the FRF matrix. For the test structure of this study, two assumptions provide possible ways to reduce the number of FRF measurements:

1) reciprocity
2) structural symmetry

Reciprocity is typically assumed in modal analysis, given by

$$\frac{x_i}{f_j} = \frac{x_j}{f_i} \tag{3-10}$$

The second assumption is that due to structural symmetry, the point and transfer FRFs should be the same no matter which side of the structure is subject to excitation--a reasonable assumption given the construction of the components. This assumption dictates that the diagonal blocks of Eq. (3-9) are identical, given the chosen sign conventions. Thus, only two 2x2 blocks need to be determined. If the structure were truly symmetric, then the eigenvectors calculated from the measurements should be perfectly symmetric and anti-symmetric. The analysis of Chapter 4 and Appendix B shows this to be the case to within a few percent.

Thus, only two blocks corresponding to the two left columns of Eq. (3-9) need to be measured. However, this number can again be reduced[10] by looking at the upper block

$$\begin{bmatrix} u \\ \theta \end{bmatrix} = \begin{bmatrix} h_{11} & h_{12} \\ h_{21} & h_{22} \end{bmatrix} \begin{bmatrix} f \\ M \end{bmatrix} \tag{3-11}$$

or

$$x = h(j\omega)\, f \tag{3-12}$$

Given a modal model, each of the receptances in Eq. (3-11) can be rewritten as

$$\frac{x_i}{f_j} = \sum_{r=1}^{N} \frac{\Phi_{ri}\Phi_{rj}}{\left(\Omega_r^2 + 2j\zeta_r\Omega_r\omega - \omega^2\right)} \tag{3-13}$$

where N is the number of modes, Ω_r is the natural frequency of the r^{th} mode and Φ_r is the mass-normalized eigenvector of the r^{th} mode. The product of eigenvector entries in the numerator is known as the *modal constant*, and usually is determined from the curve-fitting of transfer functions. Given this modal model, we can rewrite $\mathbf{h}(j\omega)$ of Eqs. (3-11) and (3-12) as

$$\begin{bmatrix} \frac{x}{f} & \frac{x}{M} \\ \frac{\theta}{f} & \frac{\theta}{M} \end{bmatrix} = \sum_{r=1}^{N} \frac{1}{\left(\Omega_r^2 + 2j\zeta_r\Omega_r\omega - \omega^2 \right)} \begin{bmatrix} A_r & C_r \\ B_r & D_r \end{bmatrix} \tag{3-14}$$

where

$$\begin{aligned} A_r &= \Phi_{r1}^2 \\ B_r &= \Phi_{r2}\Phi_{r1} \\ C_r &= \Phi_{r1}\Phi_{r2} \\ D_r &= \Phi_{r2}^2 \end{aligned} \tag{3-15}$$

It can be seen that $B_r = C_r$ and that $D_r = C_r^2/A_r$, thus all four parameters can be deduced from A_r and C_r. Physically, this means that no rotational deflections need to be measured--simply deflection at the interface must be measured for both force and moment excitation at the interface. This analysis holds also for the transfer FRFs for u_o and θ_o; thus only h_{11}, h_{12}, h_{31}, and h_{32} need to be measured to determine the complete FRF matrix of Eq. (3-7). Eq. (3-9) is rewritten below and shaded to reflect the entries that are necessary to measure in order to define the entire matrix, subject to the stated assumptions. "Boxed" entries were also measured and are discussed in the following section.

$$\begin{bmatrix} u_o \\ \Theta_o \\ \hline u_p \\ \Theta_p \end{bmatrix}^b = \left[\begin{array}{cc:cc} h_{11} & h_{12} & h_{13} & h_{14} \\ h_{21} & h_{22} & h_{23} & h_{24} \\ \hdashline h_{31} & h_{32} & h_{33} & h_{34} \\ h_{41} & h_{42} & h_{43} & h_{44} \end{array}\right]^b \begin{bmatrix} f_o \\ M_o \\ \hline f_p \\ M_p \end{bmatrix}^b \qquad (3\text{-}16)$$

3.4.2 Single Component Frequency Response Function Measurements

Figures 3-19 presents the measured FRFs for one of the components in the range 10 to 1000 Hertz. This range was chosen on the basis that five modes were felt to be sufficient for the component mode synthesis procedure; it was hoped that the first three modes could be identified accurately and that the last two would provide information on residual terms resulting from higher modes. The "accurately modelled" range would then be some fraction, perhaps as little as one-half, of the measured range. Although Section 3.1 discussed the simplification that only four FRFs needed to be measured to define the entire FRF matrix, two additional ones--θ_m/M_m and θ_o/M_m--were measured anyway and used in the CMS coupling with raw data.

Several typical characteristics of point and transfer inertances can be seen in these plots (otherwise known as collocated and noncollocated inertances). The point inertance has zeros in between each of the measured modes, which results from the fact that each of the modal residues has the same sign (refer to Eq. (3-13)). In the region between the modes, the relative signs of the entire modal terms are opposite and will

add to zero at some frequency. For the transfer inertances there are no zeros present--modal residues are of alternating sign, causing the modal terms to have the same sign in the frequency region between modes and thus constructively add. Had these plots been receptances rather than inertances, the pole-zero structure would have been the same but the overall FRF would have dropped off at -40 dB/decade. This is a result of the ω^2 term that scales inertances to receptances.

The quality of these measurements were felt to be good. The shaker was repositioned slightly until the no further improvements in modal response or cleanliness of the FRF were possible. Usually the measure of coherence is used to assess the quality of the measurements. Higher quality transfer functions were determined when the maximum number of points was used in the FRF calculation (4096); use of a fewer number led to poorer resolution of poles and zeros. Zoom measurements were taken to confirm the location and damping of the poles; the extra time and effort required for the zoom measurements was not justified by the moderate increase in resolution, since the broadband measurements were felt to be sufficient for the purposes of this study. Note the interference of stinger-beam resonance at about 10 to 18 Hertz, depending on the forcing configuration. The effects of the errors in the location of force and moment excitation are somewhat evident in the measurements, and are manifested in the attenuation of modal peak responses at the fourth and fifth modes. Modes above the seventh, while they do exist for the structure, are difficult to measure because they are not being properly excited--at these high frequencies, a node line exists at or near the forcing and measurement locations.

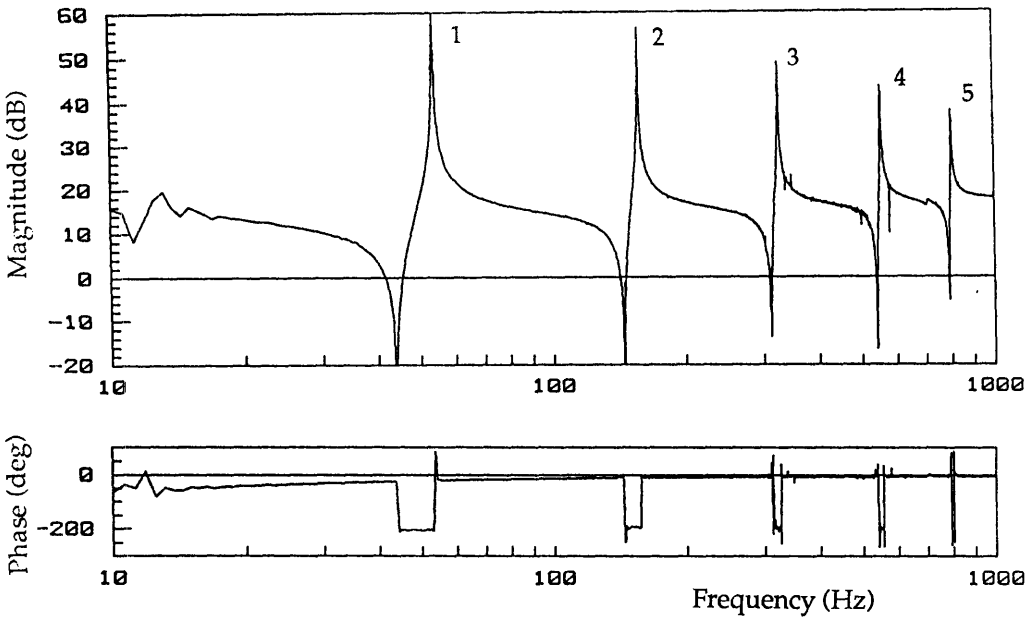

(a) u_m/f_m

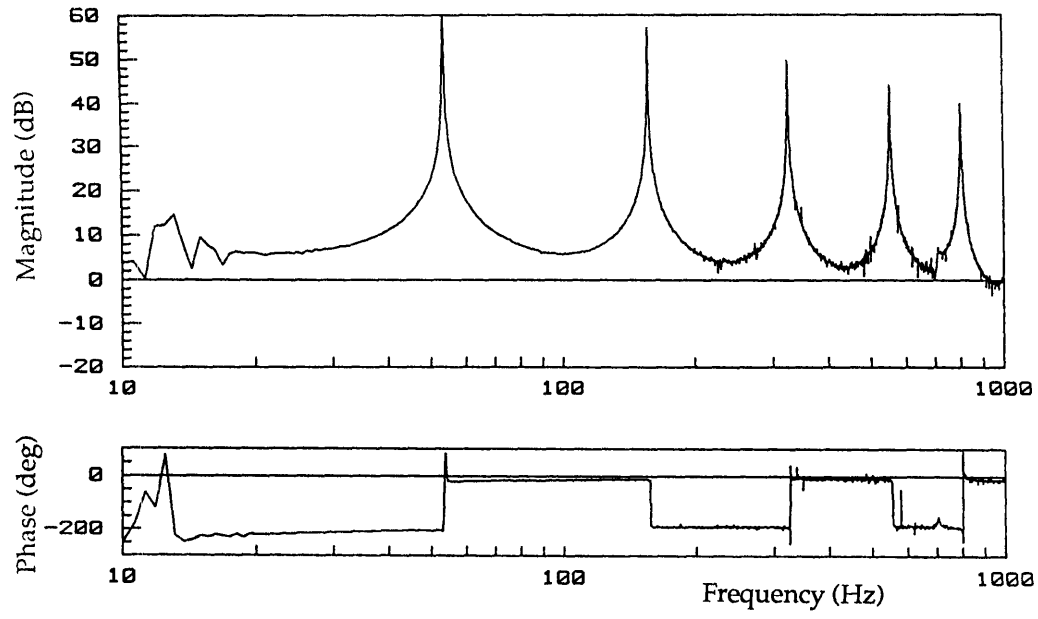

(b) u_o/f_m

Figure 3-19: Six Experimental Inertances for Single Component.

These are used to define the full FRF matrix for the component.

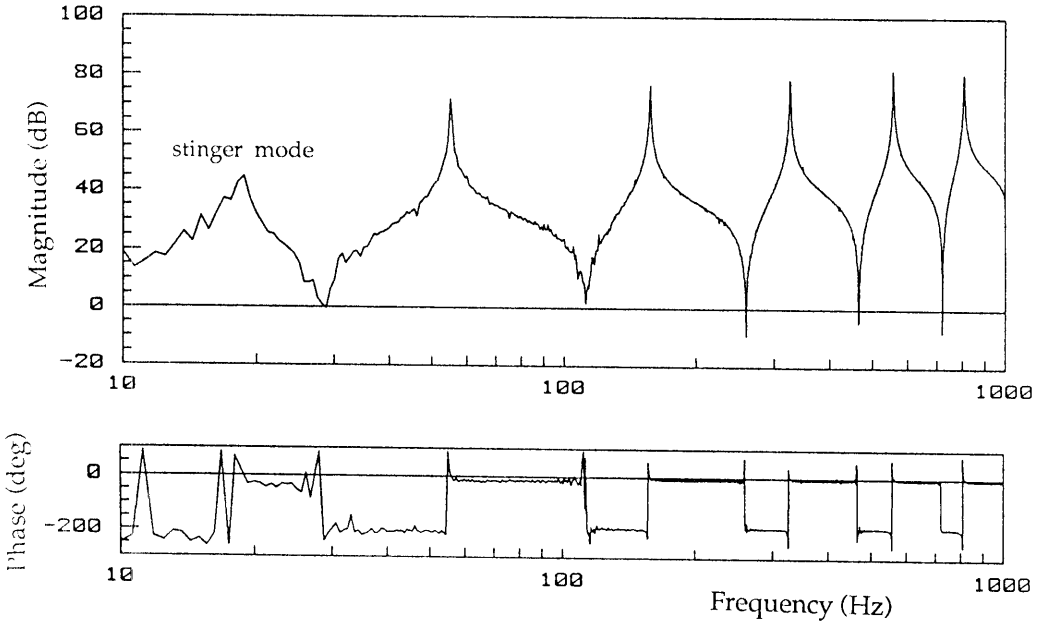
100
80
60
40
20
0
-20
Magnitude (dB)
stinger mode
10
100
1000
0
-200
Phase (deg)
10
100
1000
Frequency (Hz)

(c) u_m/M_m

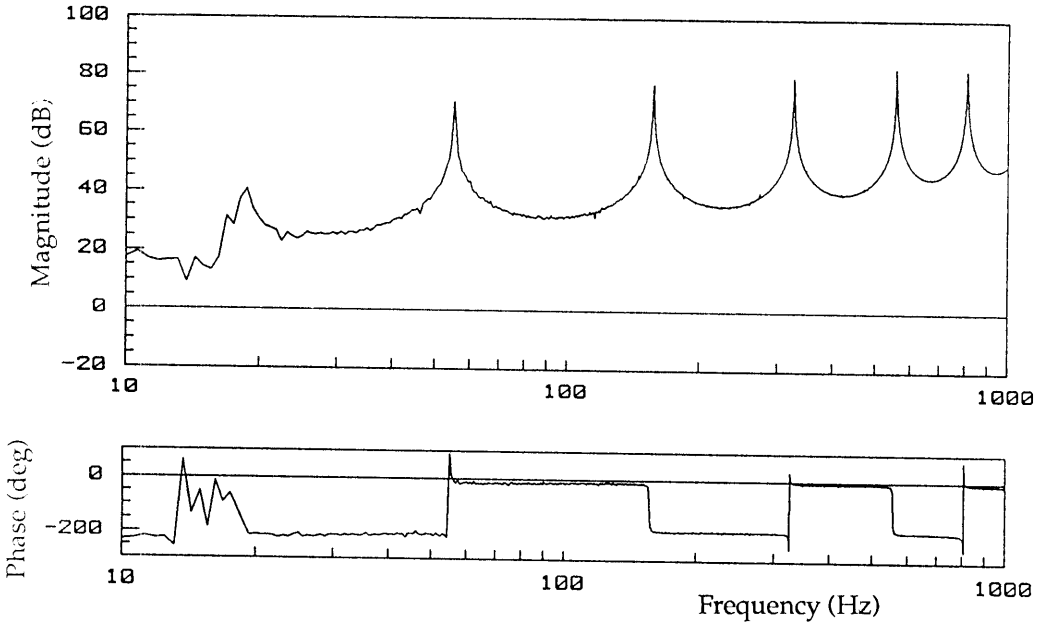
100
80
60
40
20
0
-20
Magnitude (dB)
10
100
1000
0
-200
Phase (deg)
10
100
1000
Frequency (Hz)

(d) u_o/M_m

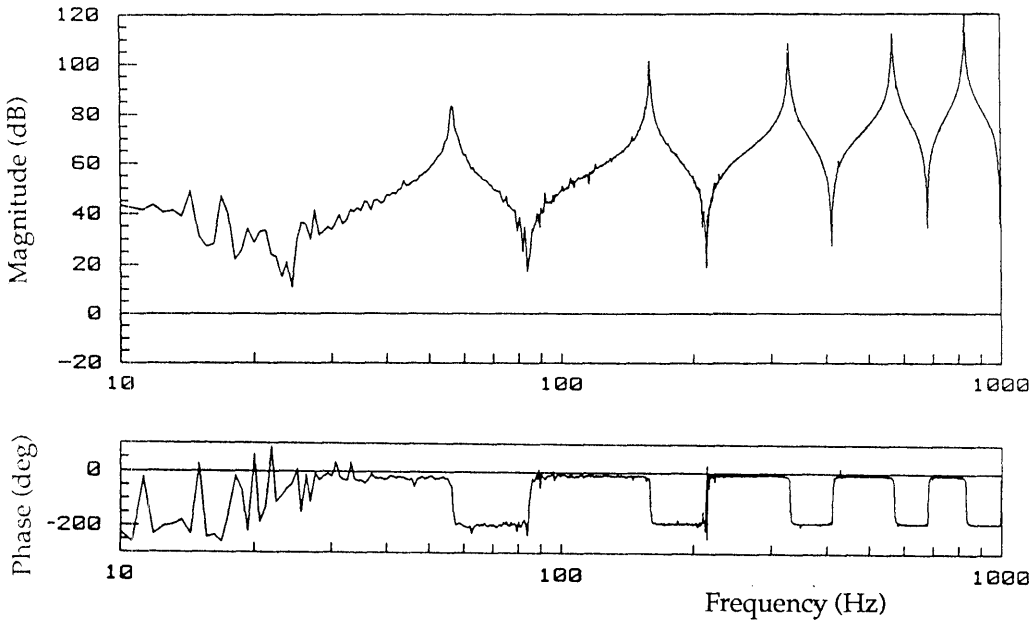

(e) θ_m/M_m

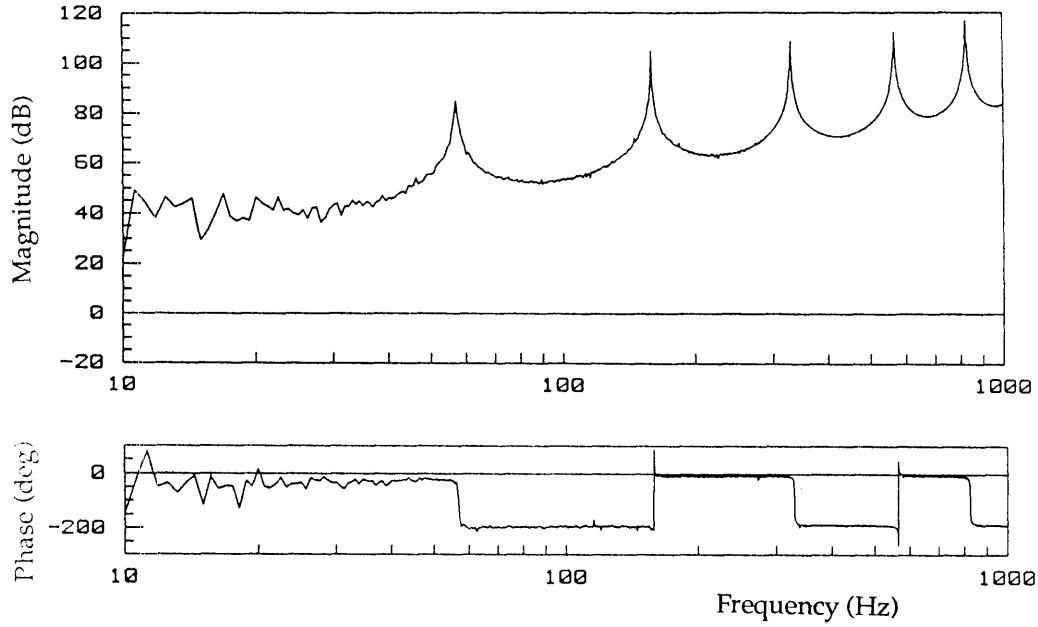

(f) θ_o/M_m

3.4.3 Two-Component Configuration

Two components were rigidly clamped together by the variable joint of Figure 3-4 and were subject to a modal test similar to the one for the single component. At first the forcing stinger interfered with the first mode but this problem was later alleviated by a new stinger design. Figure 3-20 lists the conventions for deflections and forces for the two-component FRFs presented in Figure 3-21. For simplicity only the point and transfer inertances for force/translation measurements are presented; stinger interference can be seen at the first mode in Figures 3-21(a) and (b).

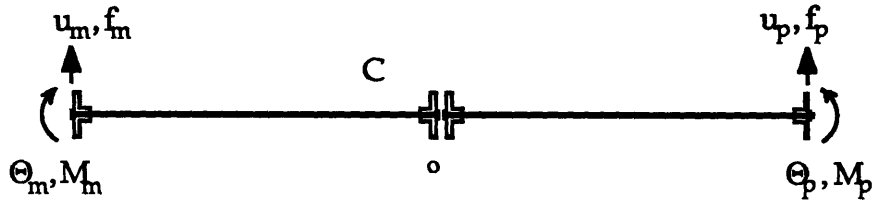

Figure 3-20: Sign Conventions for Two-Component Structure.

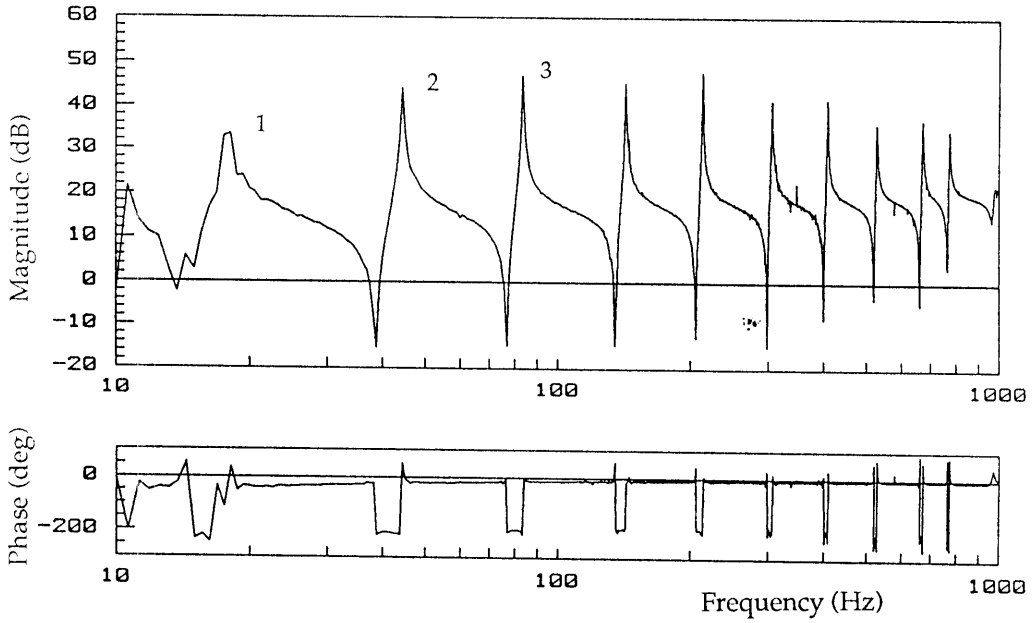

(a) u_m/f_m

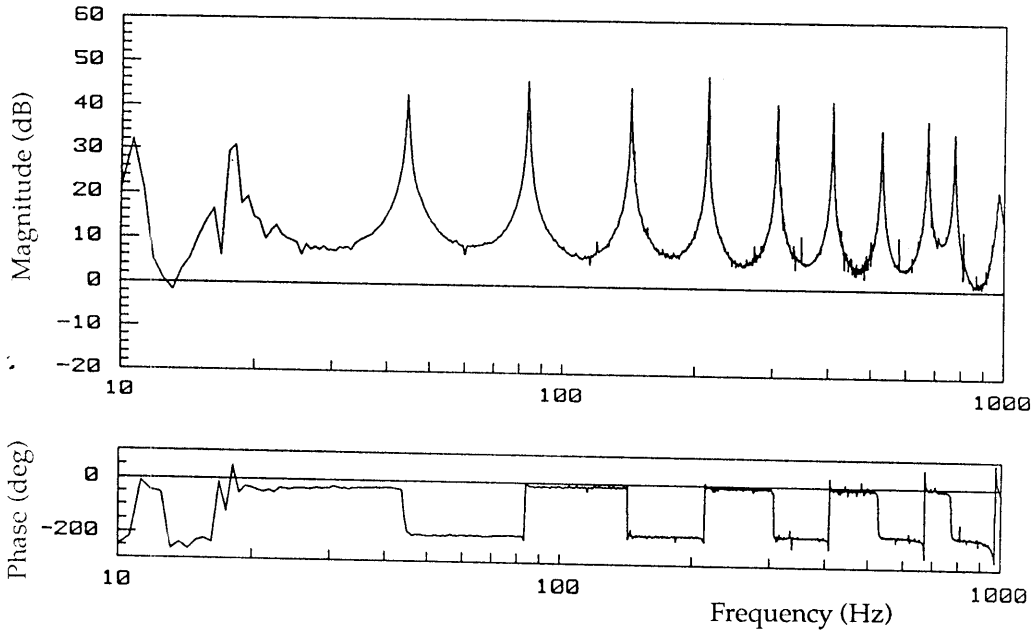

(b) u_p/f_m

Figure 3-21: Experimental Inertances for Two-Component Structure.

3.4.4 Three-Component Configuration

Sign conventions for a three-component structure are given in Figure 3-22. Measured frequency response functions (force/translation only) are given in Figure 3-23, and are presented on the same scales as the FRFs for the one- and two-component structures. Unfortunately the first mode at 6 Hertz is below the plotting scale; the first mode can be seen in Figure 3-23(c) and (d) which are plotted from 2 to 200 Hertz. Once again, stinger interference can be seen near the first mode. Another observation worth pointing out is that the modes above 900 Hertz are seriously attenuated due to the fact that node lines of the higher modes move directly to the forcing location, which is positioned slightly in from the end of the beam.

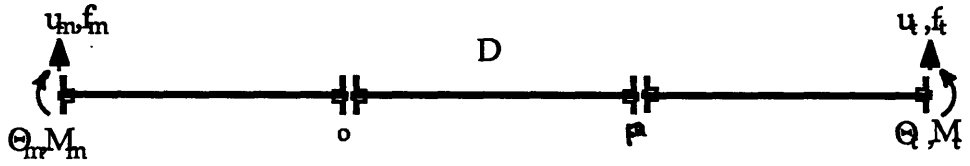

Figure 3-22: Sign Conventions for Three-Component Structure.

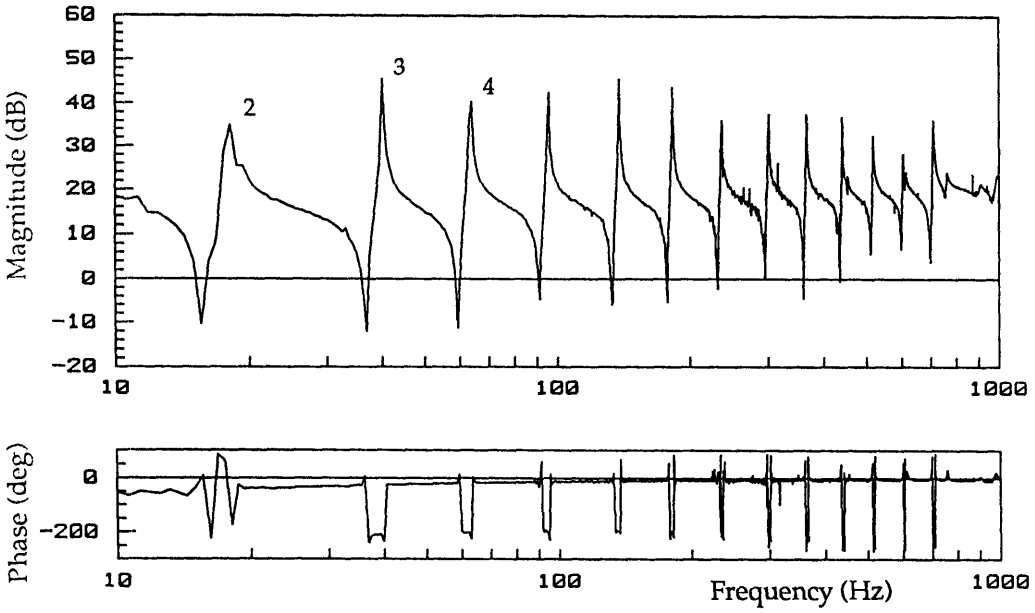

(a) u_m/f_m

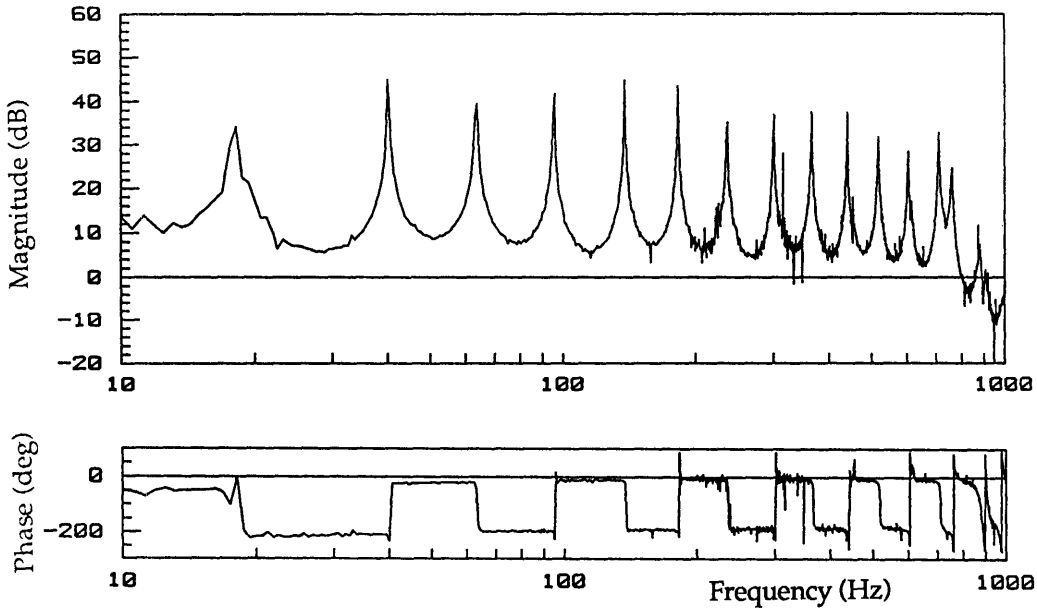

(b) u_t/f_m

Figure 3-23: Experimental Inertances for Three-Component Structure.

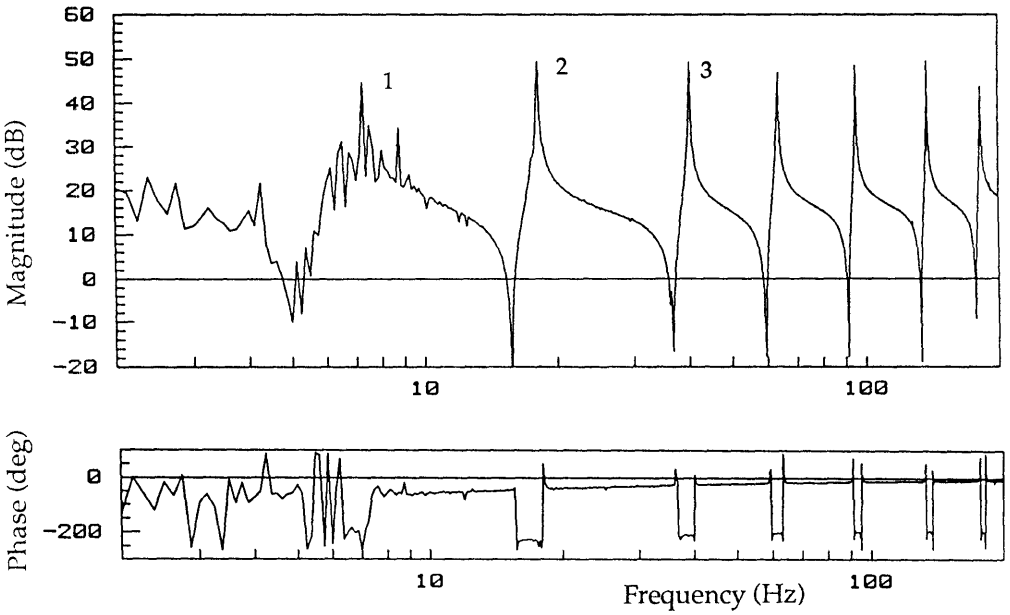

(c) u_m/f_m 2-200 Hertz

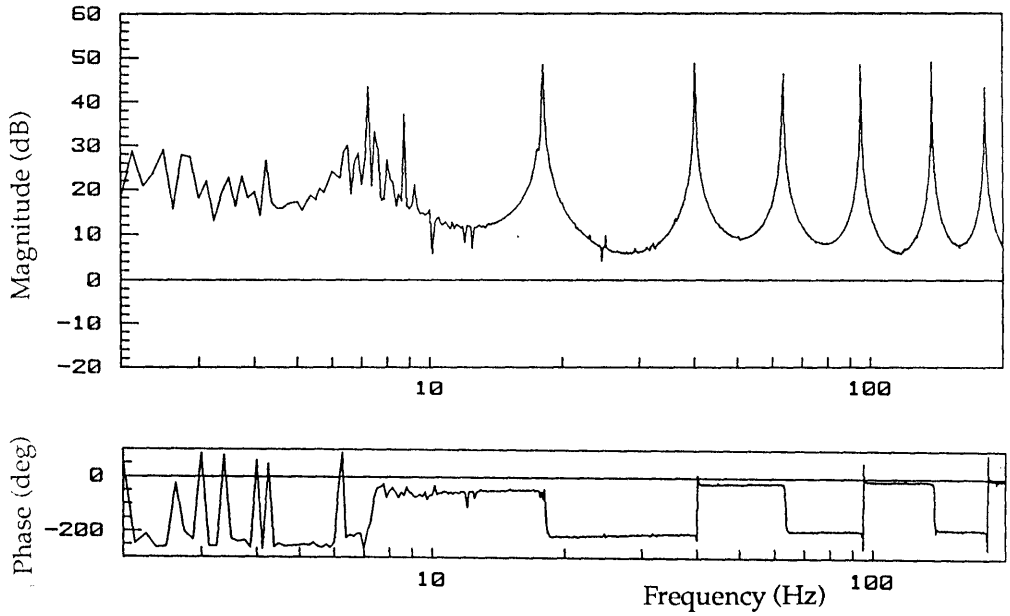

(d) u_t/f_m 2-200 Hertz

3.4.5 Measured Mode Shapes

The single- and double-component structures were forced with a sine wave exactly at their natural frequencies--a "normal mode" excitation--and the corresponding modes shapes were then measured. The structures were forced in a configuration identical to the first setup of Figure 3-17. Accelerations were measured by moving an accelerometer along the length of the beam, defining the mode shapes. Mode shapes for the first three modes of the single component are presented in Figure 3-24, and those for the two-component structure are given in Figure 3-25. The plots resemble typical free-free modes shapes for a beam.

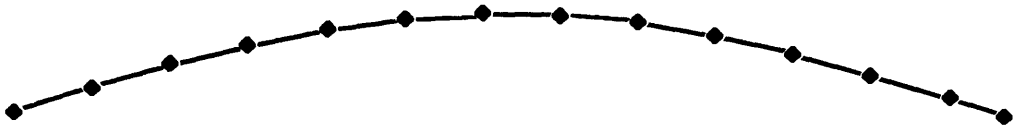

Mode 1 at 55 Hertz

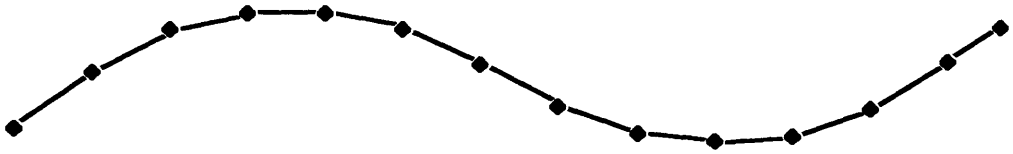

Mode 2 at 156 Hertz

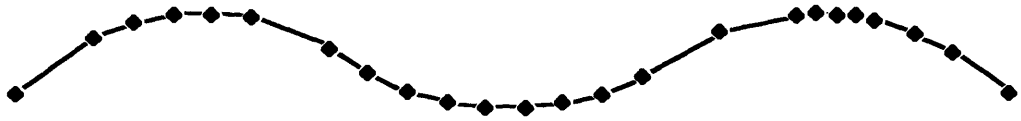

Mode 3 at 325 Hertz

Figure 3-24: Measured Mode Shapes for Single Component.
(first three bending modes)

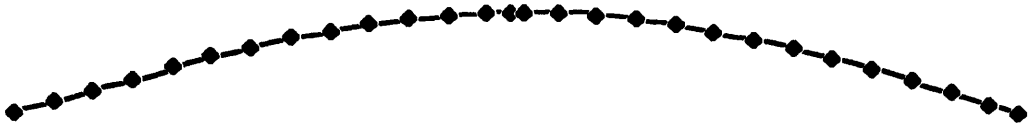

Mode 1 at 18 Hertz

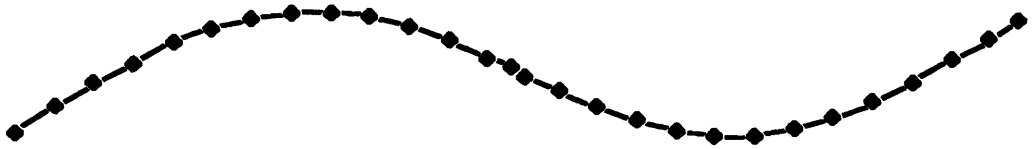

Mode 2 at 44 Hertz

Mode 3 at 83 Hertz

Figure 3-25: Measured Mode Shapes for Two-Component Structure
(first three bending modes)

Chapter 4
Linear Component Mode Synthesis

4.1 Application of Component Mode Synthesis to Experimental Structure

In this section the theoretical frequency domain component mode synthesis procedure outlined in Chapter 2 will be applied to the experimental structure, with one minor difference. Whereas the theoretical derivation of Chapter 2 dealt with *receptances* $h_{ij}(j\omega)$, representing displacements due to force, the experimental CMS procedure utilizes inertances $\alpha_{ij}(j\omega)$, or accelerations due to force, because of readily available sensor measurements. The receptances can be recovered by

$$h_{ij}(j\omega) = -\frac{1}{\omega^2}\alpha_{ij}(j\omega) \tag{4-1}$$

The CMS procedure can otherwise be implemented as previously described. For simplicity of notation, $H_{ij}(j\omega)$ and $h_{ij}(j\omega)$ will hereafter refer to inertances rather than receptances.

Figure 4-1 defines the sign conventions used in the coupling procedure for this case study. Two identical components A and B are rigidly connected at point (o). Points (m) and (p) are arbitrary points that define interior degrees of freedom, though in this case these points are chosen to be points of interface at the opposite end of each component. This convention facilitates multiple-component coupling; a second

advantage is that one frequency response matrix can be used to define both components since the components are assumed to be identical to within machining tolerances. While it would be better to measure the FRF matrix for each component, in practice this may not always be possible, as for the repeatable (and nearly identical) bays of a truss structure.

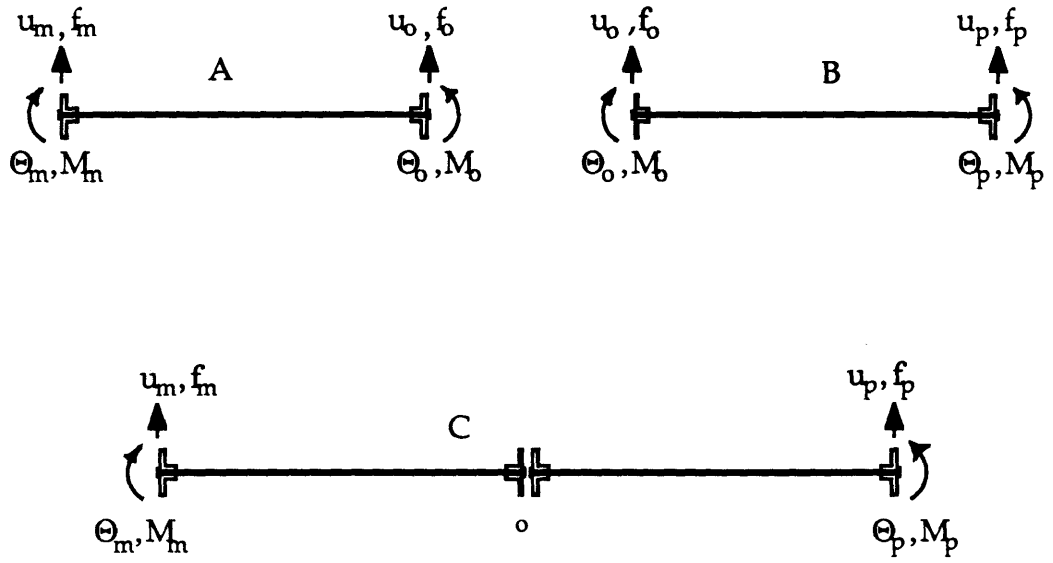

Figure 4-1: Sign Conventions Used in Coupling.
Components A and B are rigidly coupled at point (o) to form superstructure C. Points (m) and (p) are arbitrary interior degrees of freedom.

At each point there are two degrees of freedom--one translation and one rotation. Both a force and moment also act at these points. The inertance matrix $\mathbf{H}_{ij}(j\omega)$ that relates the displacement and force vectors for component A is given in Eq. (4-2). The vectors for force and deflection, as well as the inertance matrix, are partitioned according to the interior and interface degrees of freedom. The inertance matrix for component B is assumed to be identical to that of component A, and is given by Eq. (4-3).

$$\begin{bmatrix} u_m \\ \Theta_m \\ \hline u_o \\ \Theta_o \end{bmatrix}^a = \left[\begin{array}{cc:cc} h_{11} & h_{12} & h_{13} & h_{14} \\ h_{21} & h_{22} & h_{23} & h_{24} \\ \hdashline h_{31} & h_{32} & h_{33} & h_{34} \\ h_{41} & h_{42} & h_{43} & h_{44} \end{array}\right]^a \begin{bmatrix} f_m \\ M_m \\ \hline f_o \\ M_o \end{bmatrix}^a \qquad (4\text{-}2)$$

$$\begin{bmatrix} u_o \\ \Theta_o \\ \hline u_p \\ \Theta_p \end{bmatrix}^b = \left[\begin{array}{cc:cc} h_{11} & h_{12} & h_{13} & h_{14} \\ h_{21} & h_{22} & h_{23} & h_{24} \\ \hdashline h_{31} & h_{32} & h_{33} & h_{34} \\ h_{41} & h_{42} & h_{43} & h_{44} \end{array}\right]^b \begin{bmatrix} f_o \\ M_o \\ \hline f_p \\ M_p \end{bmatrix}^b \qquad (4\text{-}3)$$

The coupling at interface point (o) must include compatibility of both translation and rotation because the joint is assumed to be rigidly clamped. Naturally, a pinned joint would require only compatibility of deflection. The clamped compatibility condition is written to be consistent with the defined sign conventions to be

$$\begin{bmatrix} u_o \\ \theta_o \end{bmatrix}^c = \begin{bmatrix} u_o \\ \theta_o \end{bmatrix}^a = \begin{bmatrix} u_o \\ -\theta_o \end{bmatrix}^b \qquad (4\text{-}4)$$

Similarly, the force equilibrium is written as

$$\begin{bmatrix} f_o \\ M_o \end{bmatrix}^c = \begin{bmatrix} f_o \\ M_o \end{bmatrix}^a + \begin{bmatrix} f_o \\ -M_o \end{bmatrix}^b \qquad (4\text{-}5)$$

Z^a and Z^b are computed as the inverses of the component inertance matrices H^a and H^b of Eq. (4-2) and Eq. (4-3). Matrix assembly, as shown in Figure 4-2, is used to assemble the inverse inertance matrix Z^c for the coupled structure C.

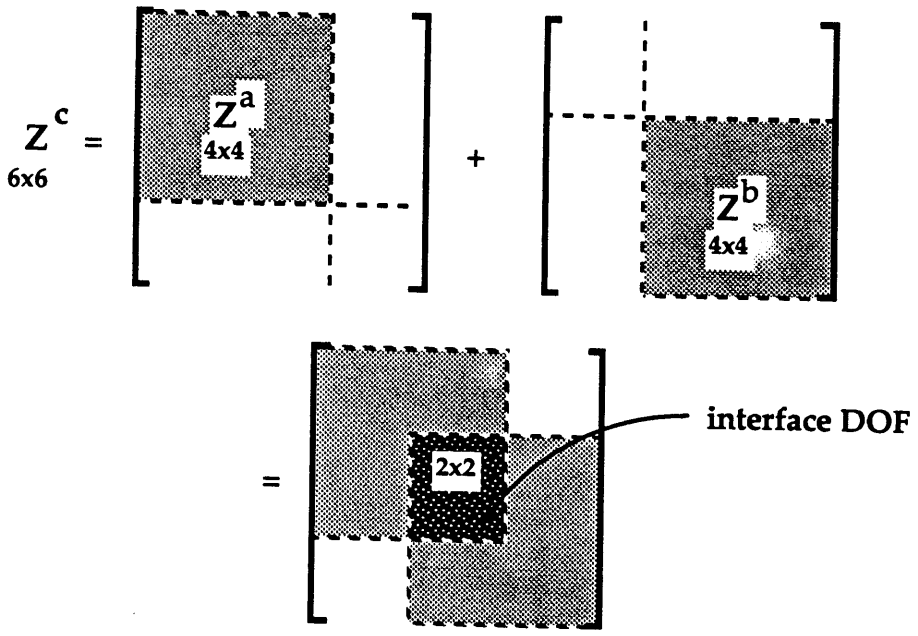

Figure 4-2: Matrix Assembly of Inverse Inertance Matrix of Coupled Structure.
Shaded areas show nonzero matrix entries; the overlap at the interface DOF is shown in dark shade. This overlap region corresponds to degrees of freedom u_o and θ_o for a clamped joint.

The desired inertance matrix for the coupled structure C is obtained by the inverse of Z^c. This set of procedures--component matrix inversion, assembly, and superstructure matrix inversion--is carried out at each frequency point of interest, or at each frequency point available in the measured FRFs if experimental data is used.

4.2 CMS Results Using Raw Frequency Response Functions

The component mode synthesis can be performed using experimentally determined frequency response functions at each frequency point in the measurements. A difficult step in this process is the construction of the complete inertance matrix $H_{ij}(j\omega)$ as outlined in section 3.4.1. While all the measurements are available, some effort and judgement are required to make the data consistent with the sign conventions. In particular, the FRFs measured by the spectrum analyzer sometimes required a sign change in order to achieve the correct relative phase between point and transfer inertances. In this simple experiment these errors were relatively easy to identify since the relative phase of the measurements were known in advance, but in practice these errors may not be so easy to spot.

Figure 4-3(a) compares a CMS prediction of the transfer inertance u_o/f_m to the actual inertance measurement of the coupled two-component structure. 1600 frequency points were used in the range 0 to 1000 Hertz, giving a frequency resolution of 0.625 Hertz. The prediction matches the true FRF well in terms of the damping, frequency, and modal amplitudes near the superstructure modes (except the first). However, several "ghost" modes and zeros are present in the prediction, and occur near the frequencies of the component modes. These errors are due to inconsistencies in the measured data. Figure 4-3(b) shows a component transfer function for purposes of comparison. Were the superstructure measurements not available for comparison, it may be difficult to label some of the predicted modes as "true" and others as "incorrect". These re-

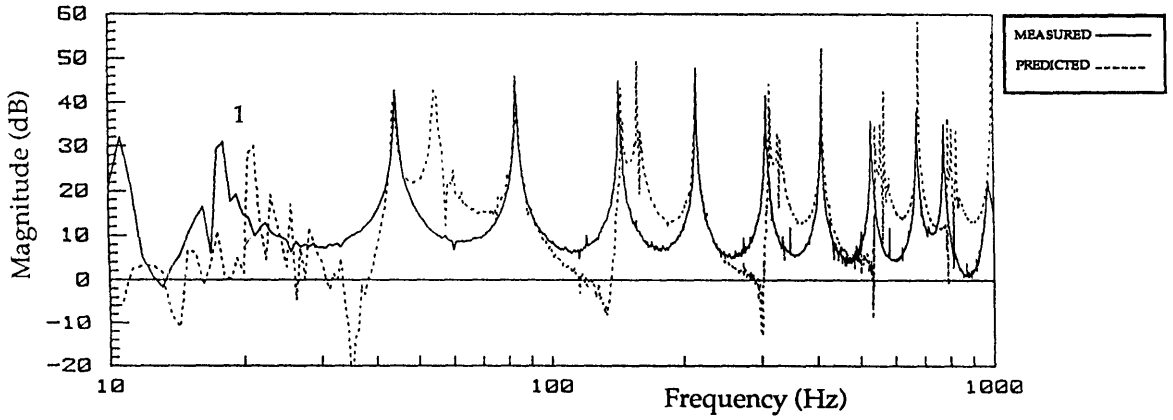

(a) CMS Prediction u_o/f_m

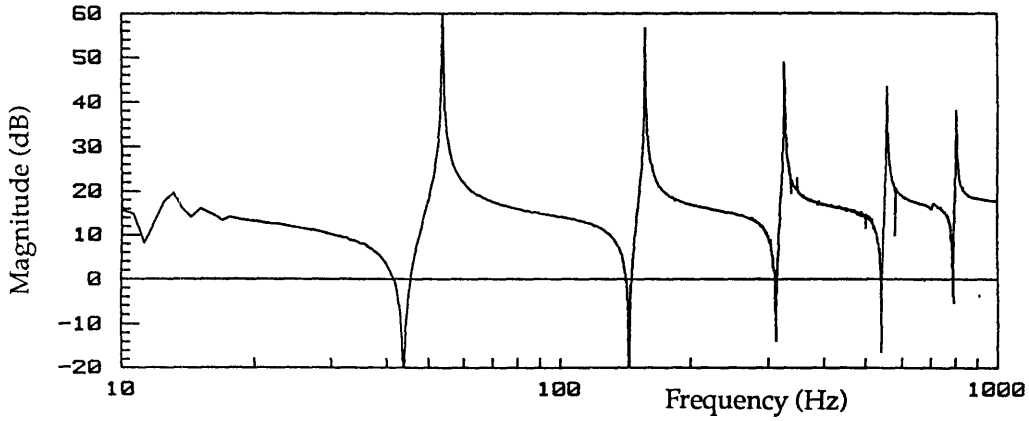

(b) component FRF u_m/f_m for comparison

Figure 4-3: Results of CMS Using Raw Measurements.
This procedure predicts superstructure modes but also creates several "ghost" resonances near the component modes, one of which is shown for comparison in 4-3 (b).

sults are consistent with the experimental results of Ewins[6]. The following section describes a means to overcome these prediction problems.

4.3 CMS Using Unified Frequency Response Functions

4.3.1 Modal Model

Ewins has shown that a better CMS estimate is possible by careful curve-fitting and adjustment of the measured frequency response functions by means of a consistent modal model. Two sources of error are removed by this procedure. Firstly, the low frequency contributions of suspension and forcing stinger dynamics can be eliminated. Secondly, the inconsistencies between different experimental FRFs are removed by using a consistent set of modal frequencies, damping values, and mode shapes.

The generic modal model for an inertance frequency response function is given by

$$\frac{\ddot{x}_i}{f_j} = \sum_{r=1}^{M}\left\{\Phi_{ri}\Phi_{rj}\right\} - \sum_{r=M+1}^{M+N}\left\{\frac{\omega^2\Phi_{ri}\Phi_{rj}}{\Omega_r^2 + 2j\zeta_r\Omega_r\omega - \omega^2}\right\} - \sum_{r=M+N+1}^{\infty}\left\{\frac{\omega^2\Phi_{ri}\Phi_{rj}}{\Omega_r^2}\right\} \quad (4\text{-}6)$$

where M is the number of rigid bod modes, N is the number of kept dynamic modes, and Ω_r and ζ_r are the natural frequency and damping of

the r^{th} mode. Φ_{ri} is the mass-normalized eigenvector for the r^{th} mode, and the product of the eigenvector entries in the numerator is known as the modal constant, A_r. The summation in Eq. (4-6) is represented graphically in Figure 4-4. The first term in Eq. (4-6) is a residual inertance with units of inverse mass, and results from rigid body modes, or any mode below the measured frequency range. The third term arises from the contribution of higher modes to the frequency range of interest, and corresponds to a residual flexibility. The second term is the familiar dynamic response. Note that each mode in this term has a low frequency and high frequency behavior: at frequencies well below the natural frequency ($\omega << \Omega_r$) a mode contributes virtually nothing to the response of the structure. At frequencies well above the natural frequency ($\omega >> \Omega_r$) each mode contributes a constant term to the response; this asymptote is termed the residual inertance of that mode.

4.3.2 Determination of Modal Parameters

The individually acquired FRFs must be curve fit in order to extract the necessary modal parameters--natural frequencies, damping ratios and modal residues, from which the eigenvectors may be determined. A total of four FRFs need to be fit, as these are all that are necessary to define the FRF matrix for one of the components (see section 3.4.1). There are modal analysis software packages available that can perform multi-degree-of-freedom analyses to fit a modal model to several measured transfer functions simultaneously. Techniques such as SDRC's polyreference algorithm[28] are effectively used to identify closely spaced modes and to

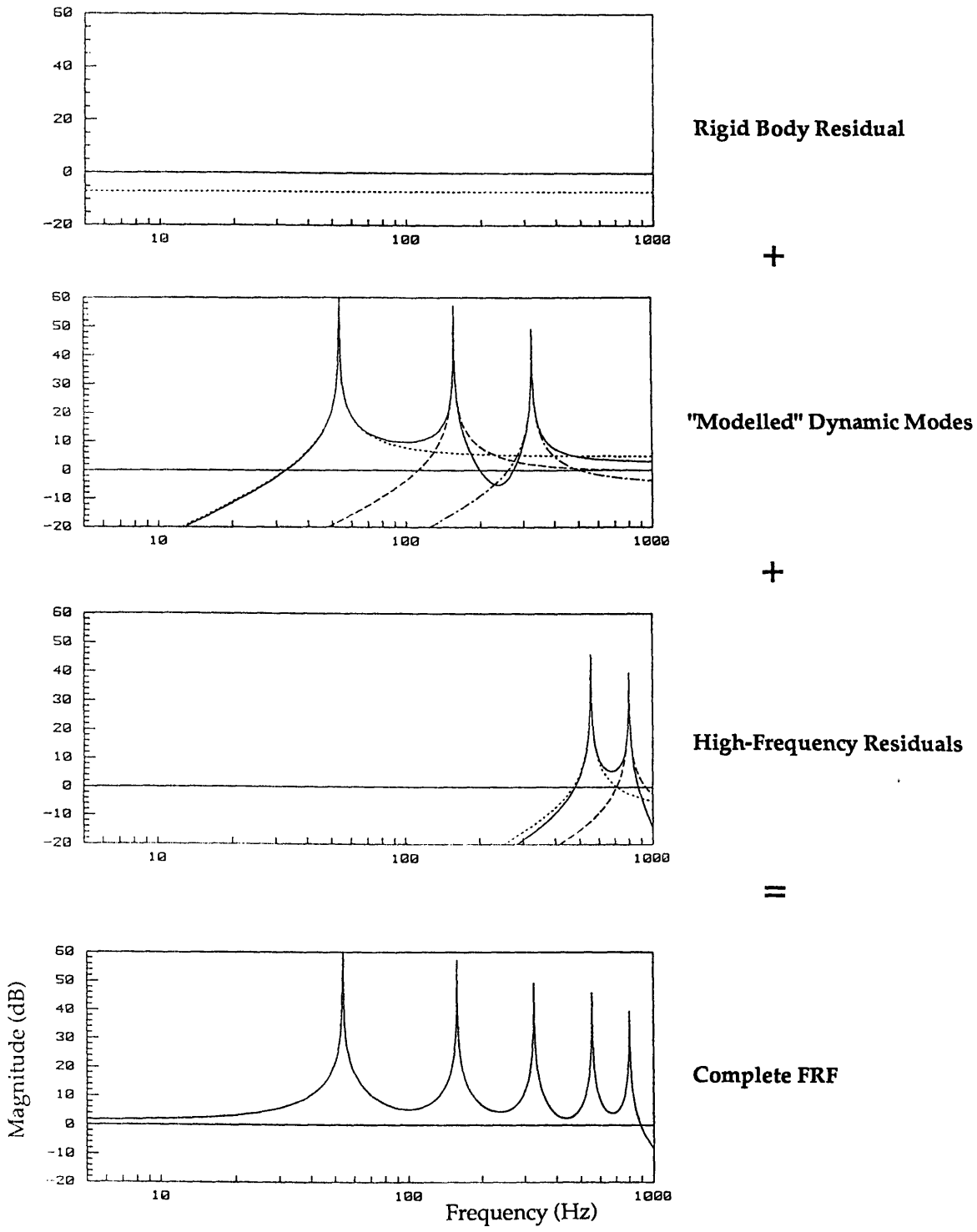

Figure 4-4: Contribution of Dynamic and Residual Terms to Modal Model.

Dynamic Modes are augmented by low-frequency residual terms resulting from rigid body modes, and also by the residual contributions from high-frequency modes, which in practice may or may not be measured.

develop modal models for complex systems. For the purposes of this study, for which experimental modes are well separated and the number of measured transfer functions are low, a simple identification procedure based on Eq. (4-6) is sufficient.

The identification procedure that was used in this study involves fitting a second order model to each mode in the transfer function separately and including a constant term based on analytical rigid body modes. Each transfer function was curve fit in the region from 0 to 1000 Hertz, in which five dynamic modes and constant inertances from rigid body modes were present. The curve fit algorithm uses a frequency domain approach based on Chebychev polynomials. The analytical derivation of the rigid body modes--rotation and translation--was based on mass and geometry measurements of the component, and is presented in full in Appendix B. These rigid body terms can also be determined by the low-frequency residual terms of the measured FRFs of Figure 3-19, which agreed well with the analytical predictions. Contributions from higher out-of-range modes, corresponding to the third term of Eq. (4-6), were neglected, which will necessarily reduce the accuracy of the model above approximately 800 Hertz. The modal model for the particular FRF is simply the sum of these dynamic and rigid body contributions. A typical curve fit is compared to the measured FRF in Figure 4-5--note the stinger dynamics that are removed in the neighborhood of 10 to 18 Hertz.

The curve-fit algorithm produces a pair of complex conjugate poles and a residue for each mode that is fit, and from these quantities the modal parameters are extracted. The poles given by the algorithm are

$$A \pm jB \tag{4-7}$$

The poles of a second order system are given by

$$-\zeta_r\Omega_r \pm j\Omega_r\sqrt{1 - \zeta_r^2} \tag{4-8}$$

An excellent approximation for the damping and natural frequency, given that the damping is on the order of fractions of one percent of critical, is given by

$$\zeta_r = \frac{A}{B} \tag{4-9}$$

$$\Omega_r = B \tag{4-10}$$

The eigenvectors can be determined from the modal constants, which are shown in Eq. (4-6) to be the product of two eigenvector entries for a given mode--one entry corresponding to forcing location, and the other to response location. Thus, given forcing at one location and response at several locations (as was the case for this study) the eigenvectors may be determined if any one of the measurements involves a collocated force and response. The corresponding eigenvector value is then simply the square root of the modal constant. Note that in order to determine the eigenvector at any point, one is required to measure either a force or response at that location, a requirement that cannot always be met.

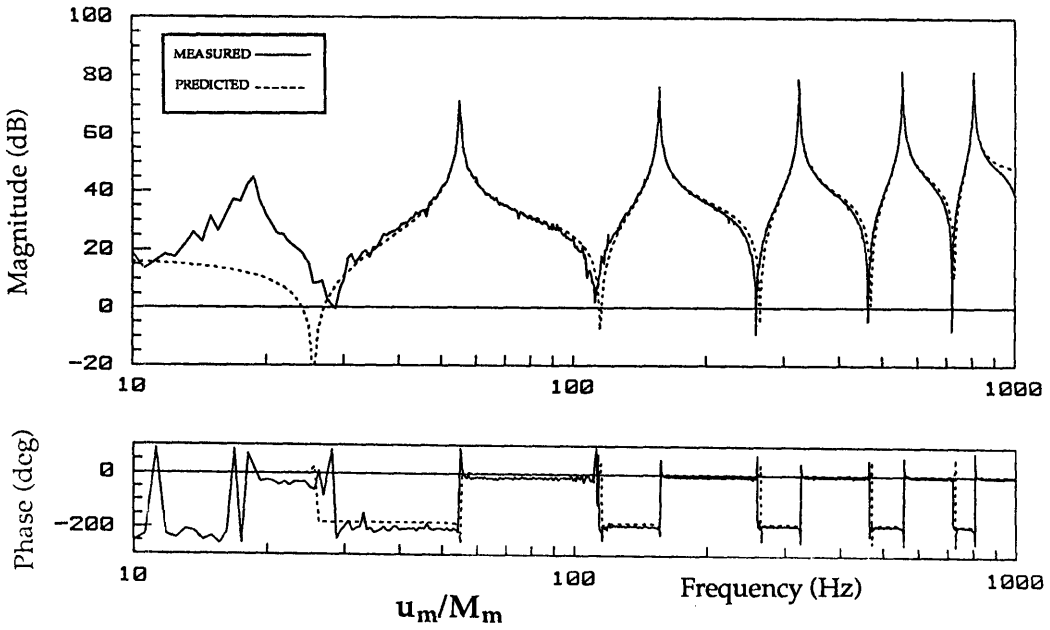

Figure 4-5: Typical Curve-Fit of Component FRF.
Note that stinger resonances at approx 19 Hertz are removed.

4.3.3 Unified Modal Model of Component

The identification of modal properties for the four frequency response functions has naturally led to inconsistencies in estimates for these parameters, which now need to be adjusted for consistency. In each case the corrections were only a few percent, and were derived by taking the arithmetic averages of the available estimates. Although structural symmetry was assumed in order to set equal the diagonal blocks of the component FRF matrix in Eq. (3-9) the calculated eigenvectors were not forced to be symmetric and antisymmetric, although Table 4-2 and Figure 3-23 show that this is almost the case. During the determination of eigenvectors from modal constants, the assumption of reciprocity ($x_i/f_j = x_j/f_i$) allowed two estimates for two of the eigenvector entries. The unification procedure is presented more fully in Appendix C, and the modal model for the standard component is summarized below.

Table 4-1: Measured Natural Frequencies and Damping Ratio for Modal Model of Component

Mode	Ω_r (Hertz)	ζ_r (%)
1	54.4	.184
2	156.8	.095
3	325.8	.104
4	556.4	.123
5	804.6	.148

The eigenvector matrix is composed of two rigid body modes (translation and rotation) and five dynamic modes.

$$\underset{4x7}{\Phi} = \left[\Phi_{01} \quad \Phi_{02} \quad \Phi_1 \quad \Phi_2 \quad \Phi_3 \quad \Phi_4 \quad \Phi_5 \right] \tag{4-11}$$

Note that the row length of four corresponds to the displacement vector for each component. The experimentally determined eigenvectors are listed in Table 4-2; these were calculated from the modal residues that were fit to the measured transfer functions (see Appendix C). Given the consistent modal model, the entire 4 by 4 frequency response function $H_{ij}(j\omega)$ can be recalculated by Eq. (4-6) by letting i,j go from 1 to 4.

Table 4-2: Experimentally Determined Eigenvectors for Two Rigid Body and Five Bending Modes.

Units	Rigid Body Modes		Dynamic Modes				
	Φ_{01}	Φ_{02}	Φ_1	Φ_2	Φ_3	Φ_4	Φ_5
$\ddot{u}_m$ $(kg)^{-1/2}$	0.914	1.553	1.350	0.963	0.793	0.672	0.508
$\ddot{\theta}_m$ $m(kg)^{-1/2}$	0.0	4.813	16.507	26.194	34.999	53.023	78.469
$\ddot{u}_o$ $(kg)^{-1/2}$	0.914	-1.553	1.247	-1.041	0.826	-0.682	0.579
$\ddot{\theta}_o$ $m(kg)^{-1/2}$	0.0	4.813	-16.559	26.274	-35.028	53.028	-79.142

4.3.4 CMS Using Unified Modal Model--Clamped Joint

Component mode synthesis is carried out at 1600 frequency points using the frequency response functions developed from the consistent modal model. The CMS prediction is compared in Figure 4-6 to the actual

measured transfer function of the two-component structure for the point inertance u_m/f_m and the transfer inertance u_o/f_m.

Figure 4-6 demonstrates the dramatic improvement in component mode synthesis when the unified modal model of the component is used. Several discrepancies still exist, however. The first predicted mode (dashed line) is strongly influenced by the rigid body asymptotic adjustments made to the component FRFs, and remains in disagreement with the measured first mode. Since the rigid body modes were based on an analytical model and the dynamic modes were based on experimental measurements, any error in sensor calibration would lead to this type of low-frequency error. The problem of identifying or including the correct out-of-range residual terms, such as the rigid body modes, is a typical and recurring problem in modal analysis. An example of the sensitivity of the CMS prediction to changes in the magnitudes of the rigid body modes is presented at the end of this chapter. Note also the poor superstructure prediction above 800 Hertz; this is a result of not including high frequency residual terms in the component modal model.

Modes 7 to 10 show errors in frequency estimates that are likely due to errors in positioning the force transducer and the accelerometers precisely at the point of interface, as documented in Figures 3-15 and 3-16. This difficulty is generic in modal analysis and experimental component mode synthesis. If significant deflections occur between the measurement location and the actual interface, the measured component FRFs will be in error. Eigenvector estimates derived from these measurement will also be in error. This measurement error will increase with frequency, since the

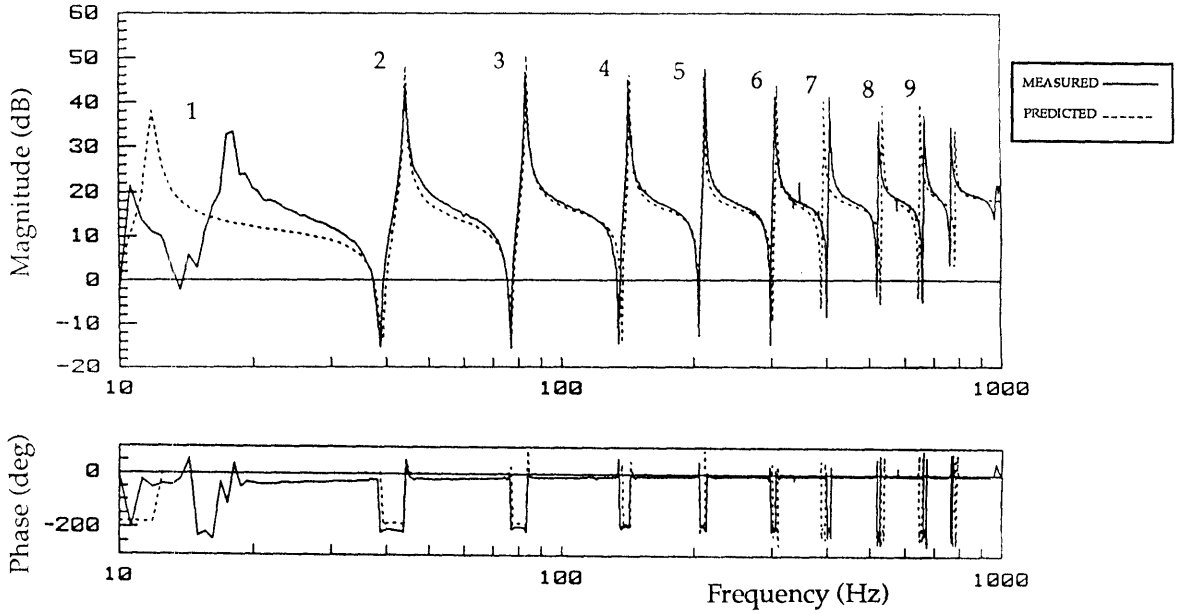

(a) u_m/f_m

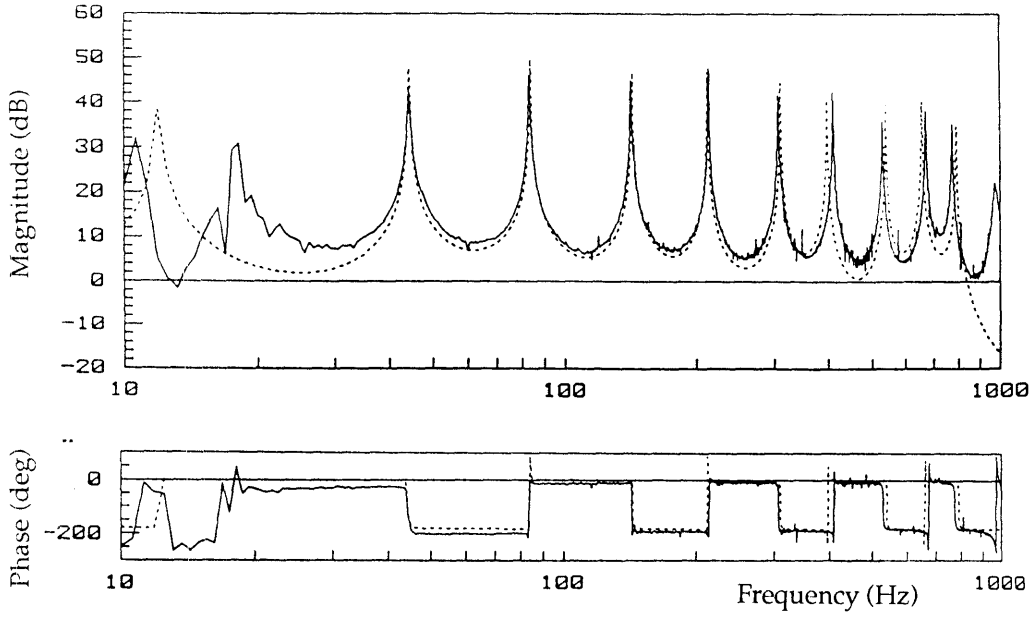

(b) u_o/f_m

Figure 4-6: Results of Unified CMS--Two Components.
Prediction is compared with actual measurement of coupled structure.

higher mode shapes have more closely spaced nodes and antinodes. It is worth noting that in Section 3.4.4 it was discussed that at 50 Hertz the eigenvector entries were likely to be in error by only 4.5%, but that this error had grown to 30% at 325 Hertz. The seventh superstructure mode, at around 400 Hertz, shows the first signs of significant frequency prediction error, and may be due to this problem in eigenvector identification.

4.3.5 CMS Using Unified Modal Model--Pinned Joint

The component modal models can be used to predict the dynamics of a superstructure for any interface compatibility. In particular, these models are used to predict the behavior of two identical components coupled by only deflection at the interface--a pinned joint. Procedures for CMS are carried out as before, except that the compatibility and equilibrium equations are modified to reflect the new coupling conditions:

$$u_o^c = u_o^a = u_o^b \tag{4-12}$$

$$f_o^c = f_o^a + f_o^b \tag{4-13}$$

Matrix assembly represented by Figure 4-2 is altered to accommodate the coupling of only one degree of freedom. The results of the pinned coupling are presented in Figure 4-7; note that the former even modes (shear coupling) of Figure 4-6 are still present, but that the former odd modes (bending coupling) have changed. Instead, modes are present that

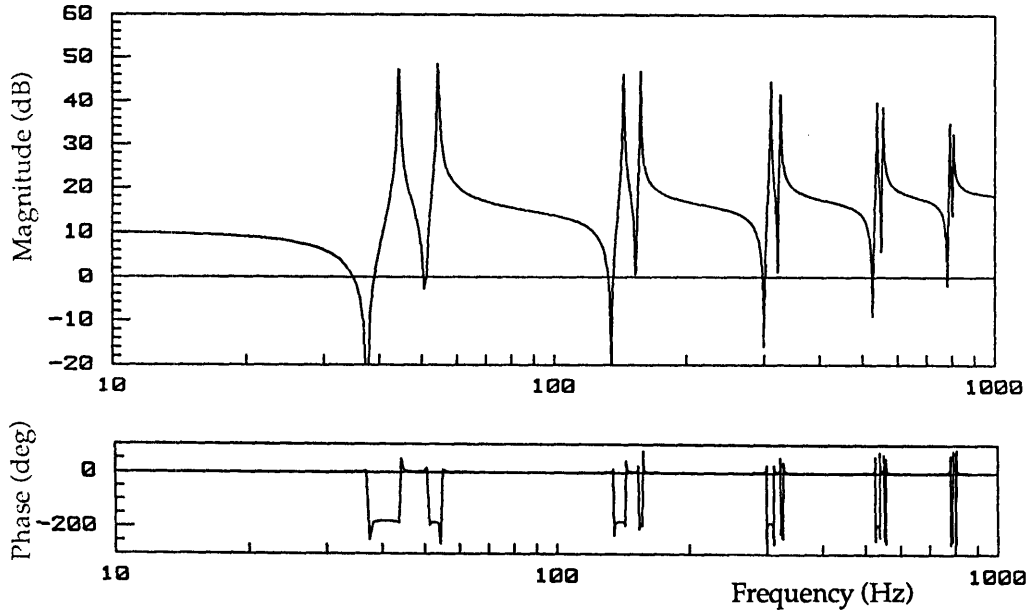

(a) u_m/f_m

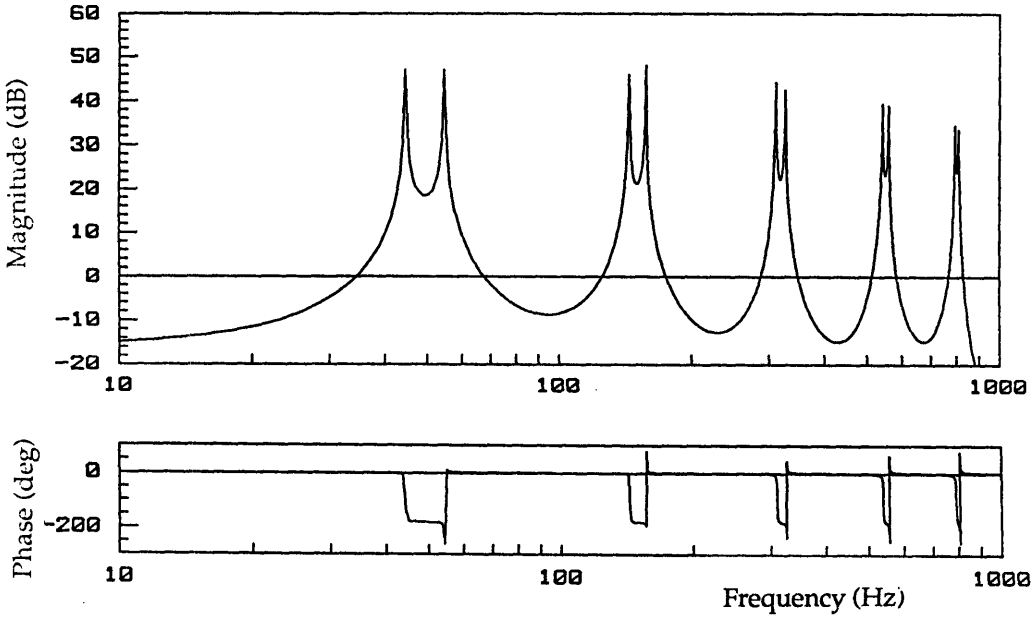

(b) u_o/f_m

Figure 4-7: Results of Unified CMS--Two Components, Pinned Joint.

Shear modes remain in addition to individual component resonances.

occur at the natural frequencies of the individual components and are thus internal resonances. Since the model assumes two "identical" components, these modes are actually two modes superposed; in an actual structure the modes would be closely-spaced and not identical.

4.3.6 CMS of Three-Component Structure--Clamped Joint

The component mode synthesis procedure is easy to implement for coupled structures consisting of more than one component, although the matrix inversions will eventually become unwieldy as the number of components becomes very large. The coupling of a three-component structure is compared to the measurement of the physical structure in Figure 4-8 for two different frequency scales.

Agreement between prediction is good but shows low and high frequency estimation errors similar to those of the two-component case. In this case the two lowest modes are predicted poorly; obviously the CMS procedure has limitations to accurately predicting low superstructure modes. Further investigations will need to be conducted to determine the cause of the low frequency estimation error in this study.

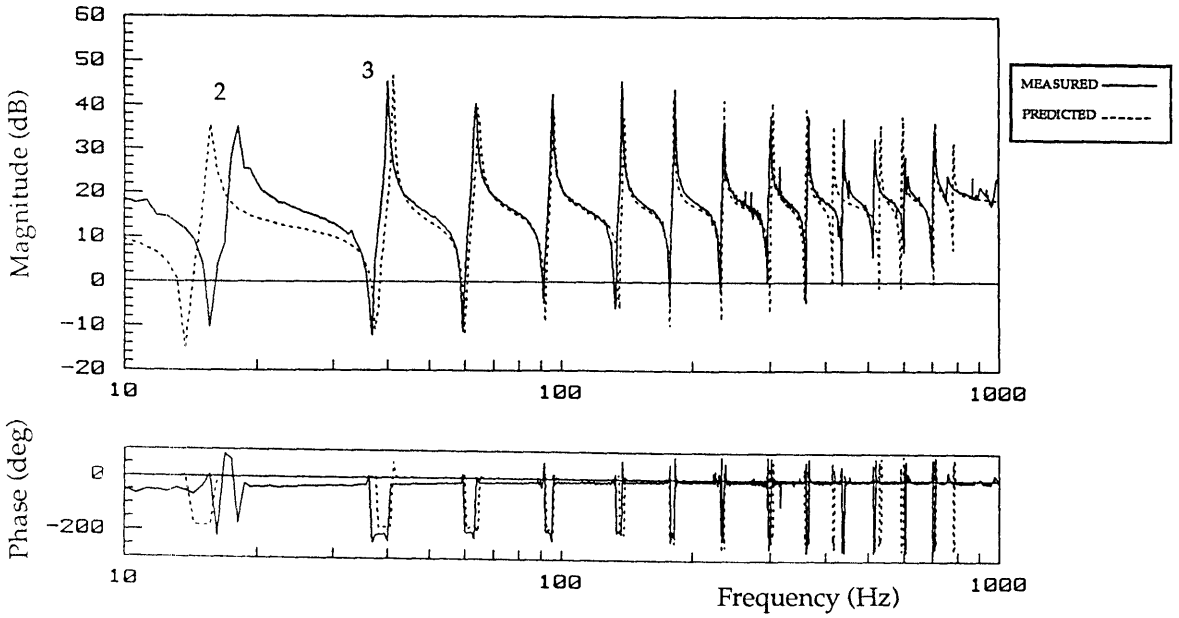

(a) u_m/f_m

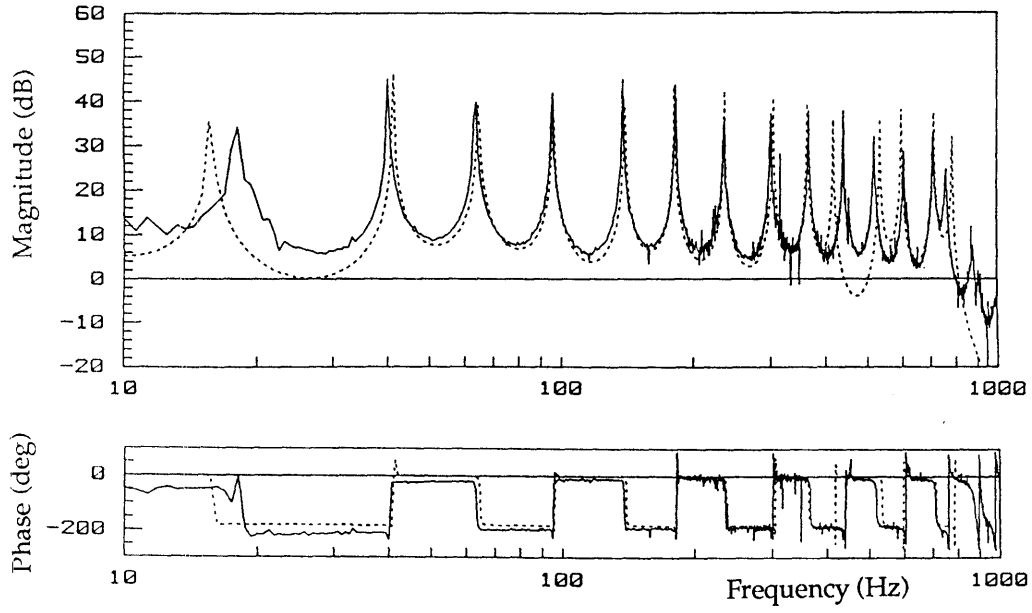

(b) u_t/f_m

Figure 4-8: Results of Unified CMS--Three Components.
Note that the prediction is reasonably accurate for the range in which component modal data is available. Figures 4-8 (c) and (d) display the same comparison, but for the range 2-200 Hertz.

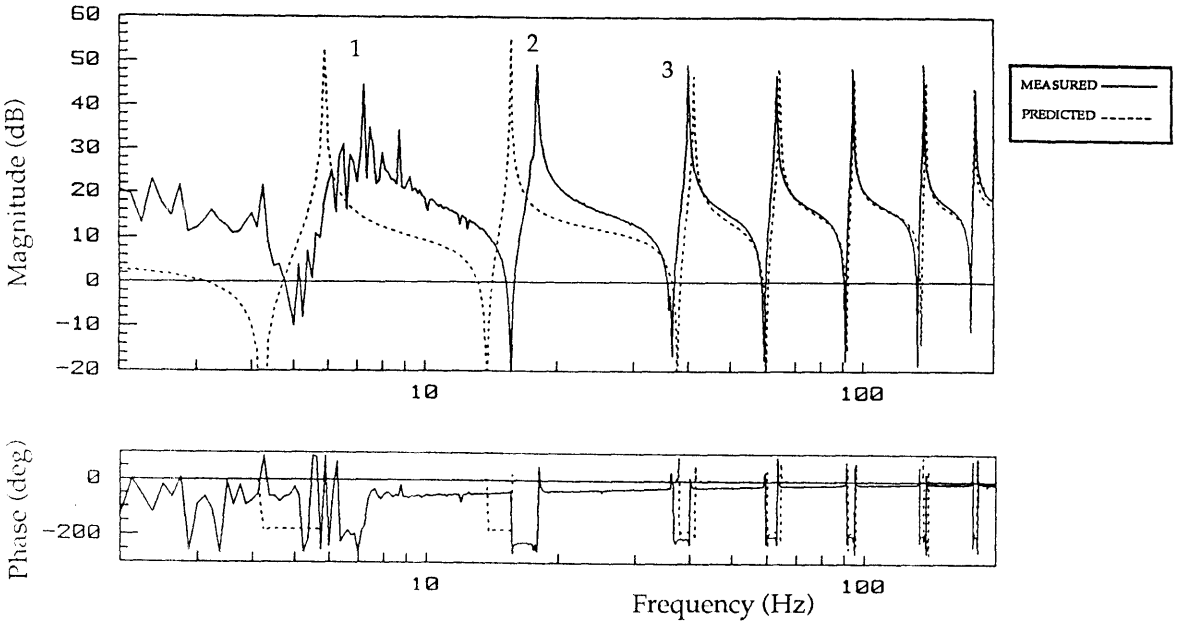
60
50
40
30
20
10
0
-10
-20
Magnitude (dB)
1
2
3
MEASURED
PREDICTED
10
100
Phase (deg)
0
-200
10
100
Frequency (Hz)

(c) u_m/f_m

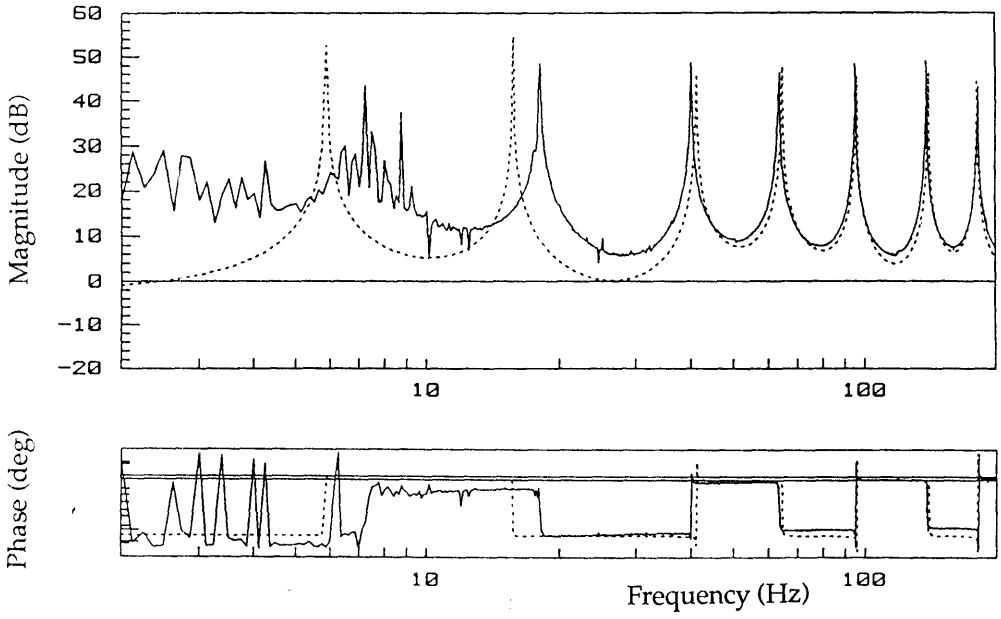
60
50
40
30
20
10
0
-10
-20
Magnitude (dB)
10
100
Phase (deg)
10
100
Frequency (Hz)

(d) u_t/f_m

4.4 Compensation for Effects of Transducer Positioning Error

In retrospect the eigenvector estimation error could have been prevented by designing the experiment such that the component was excited at the "exact" interface. As was pointed out earlier, the problem of measuring the exact interface inertances is generic to experimental substructuring and modal analysis. Given the current configuration, the eigenvectors could have been better identified by using a more physically correct modal model from which to estimate the vectors. A reasonable approximation of the desired quantities was achieved by the method of Appendix C, which assumes that a point inertance was measured at point (m). In reality, the forcing location was slightly offset from the beam tip (where the accelerometer was located) and therefor the point inertances are actually slightly noncollocated. By placing an accelerometer at exactly the forcing location, all the necessary information (for this model) can be obtained to estimate the true eigenvector entries at the interface, at least for the deflection degrees of freedom. This procedure was checked to assess the accuracy of the eigenvectors as determined by Appendix C; these corrections were not incorporated into the present analysis. Significant improvements in the prediction of higher coupled structure frequencies would be expected. Unfortunately neither rotation nor moment were measured or applied at the exact interface and no estimates of the corresponding eigenvectors can be "backed out" of the available data. One can make the assumption, however, that negligible rotation occurs between the joint lips and the exact interface and that the "approximate" eigenvectors already determined are nearly correct. This assumption may

be well justified by examining the experimental mode shapes of Figures 3-24 and 3-25.

4.5 Problems in Repeatability

The results of the component mode synthesis prediction of Figure 4-6 were extremely encouraging. A second set of FRF measurements was obtained of the coupled structure using a new stinger which did not interfere with the first mode. Unfortunately, the coupled structure had been separated and reassembled since the time of the initial measurements of Figures 3-19. Figure 4-9 displays a comparison of the new FRF with the CMS prediction in the range 5-500 Hertz. The new two-component FRF, while displaying a "healthy" first mode clear of stinger corruption, is now in some disagreement with the CMS prediction.

Two explanations are offered. A likely cause of the error is that the joint clamp holding the shimstock had loosened, resulting in a joint that was less stiff. In addition, the components were reconnected in a fashion that left more space between the joint assemblies. This produced a longer coupled beam and lower natural frequencies. These events place a limit on the accuracy of this study. Accordingly, the use of FRFs from the "reassembled" beam was limited to the determination of joint rotation in Chapter 5, and were used only as a basis of comparison in the nonlinear measurements of Chapter 6.

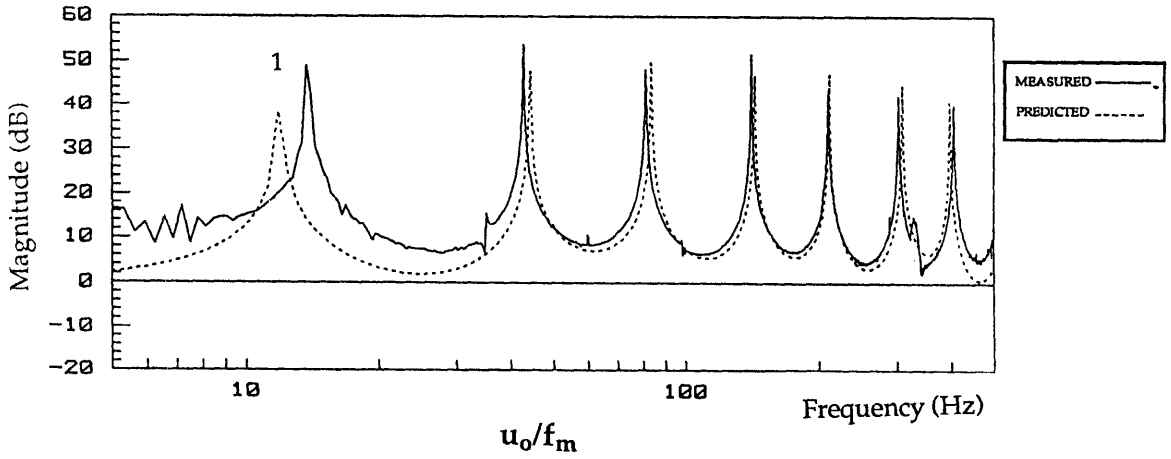

u_o/f_m

Figure 4-9: Comparison of CMS Prediction to Two-Component Structure After Reassembly.

The coupled structure was separated and reassembled; the natural frequencies of the resulting structure are lower and in error with the CMS prediction.

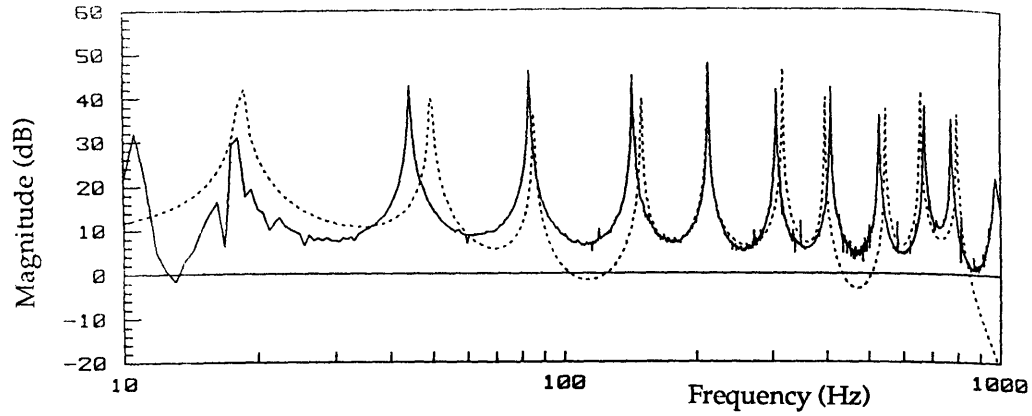

u_o/f_m

Figure 4-10: Sensitivity of CMS Results to Errors in the Rigid Body Modes (Two-Component Structure).

The rigid body modal residues were all multiplied by 2.5 in order to simulate a structure with less inertia, corresponding to a 58% error in each rigid body eigenvector. The true measurement is shown for comparison.

The task of accurately predicting low frequency modes of the coupled structure has been difficult, and it was desired to assess what impact the magnitudes of the rigid body modes had in this region. Figure 4-10 shows the attempt to modify the rigid body modes in order to place the first predicted superstructure mode at the measured modal frequency. It turns out that a 58% change in rigid body modal vector magnitude was required, but that in the process all higher modes were inaccurately predicted. It is unlikely that a simple scaling error on the load cell is responsible for the observed discrepancies, and further investigation is needed.

Chapter 5
Introduction of Joint Freeplay Into Coupled Structure

This chapter presents the effects on the measured transfer function of the coupled structure when a gap nonlinearity is introduced into the coupling joint. These results will remain case-specific unless a generalization can be made about the size of the gap relative to the relevant deflections and geometry of the structure. Before the transfer function results are presented, therefor, it is worthwhile to review relevant experimental work in the literature and to develop a nondimensional parameter that references the gap size to the local linear rotational deformation near the joint.

5.1 Relevant Experimental Work in the Literature

Structural nonlinearity is usually something to avoid when conducting modal tests. Amplitude scaling, superposition, single valued solutions--all these "linear" assumptions are violated by a nonlinear system. Since modal analysis is based on these linear assumptions, even small amounts of nonlinearity can corrupt transfer function measurements. The questions become: is nonlinearity present in the test specimen, and is it "small" enough to ignore given the linear assumptions?

Unfortunately almost all structures and systems exhibit some nonlinear behavior outside of some "linear" range, usually defined by assumptions of small displacements about some operating or reference point. Some work has been done in the modal analysis of nonlinear systems, but it has chiefly involved identifying the presence of nonlinearity from the test data and then taking steps to avoid it. Busby et. al.[32] presents a good review of current work regarding modal analysis of nonlinear systems. Of course, many experimental studies of nonlinear systems tend to be case-specific by their very nature; however some analytical studies of simple mass-spring systems with deadband or clearance nonlinearity have been conducted[33,34] that demonstrate the attenuation, multiple solution, and frequency shift phenomena observed in this thesis. Averaging and describing function techniques are also available for the linearization of simple nonlinear models, and have been implemented in experimental and analytical case studies[3,24,30] using state space or spatial model analysis. Relevant papers of analytical and experimental studies of nonlinear systems are presented in the bibliography.

5.2 Development of Non-Dimensional Deadband

The chosen non-dimensionalization of the joint is a ratio of the joint rotation (due to deadband) to the local rotational deformation near the linear joint. If this parameter is small, the structure could be assumed to be quasi-linear; that is, the structural deflections are due almost entirely to linear flexibility. If the nonlinear deflection size were known to be of

the same magnitude as the local deflection of the linear structure, then it might be assumed that the structure would not behave linearly at all. Linear, rather than nonlinear, joint rotation was chosen as a reference because this quantity was relatively easy to measure, and only needed to be measured once. The local rotation near the nonlinear joint may be significantly different and difficult to measure.

In Figure 3-9 the measured load deflection curve of the nonlinear beam joint assembly was presented. No hysteresis was observed, and the slopes of the saturated portions of the load deflection curve appeared reasonably linear. The general model of the joint with deadband is presented in Figures 5-1(a) and (b). Note that as the points (q) and (s) are brought closer to the actual interface point (o), the flexibility of the beam is removed and the slope m of the moment-rotation curve approaches the limit set by the steel compression bolts and the steel shimstock. In practice the joint deadband was measured by saturating the joint against each lip and measuring the deflection change with a micrometer.

The local rotational deflection near the linear joint is measured as shown in Figure 5-2. Forcing is applied to the structure in the same manner as for the nonlinear tests--broadband random excitation at point (m). Transfer functions between $u_{1\text{-}4}$ and f_m were measured; a third-order polynomial was fit to these measurements to determine the transfer function relating joint curvature θ' to force excitation f_m.

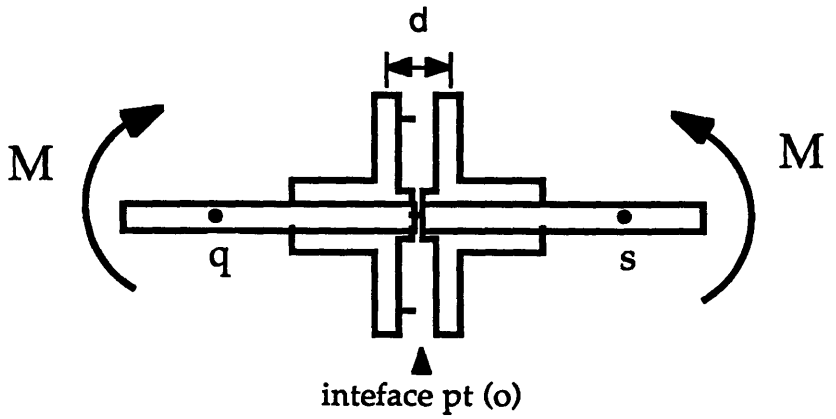

(a): Hypothetical points used to define the moment-rotation curve of Figure 5-1(b)

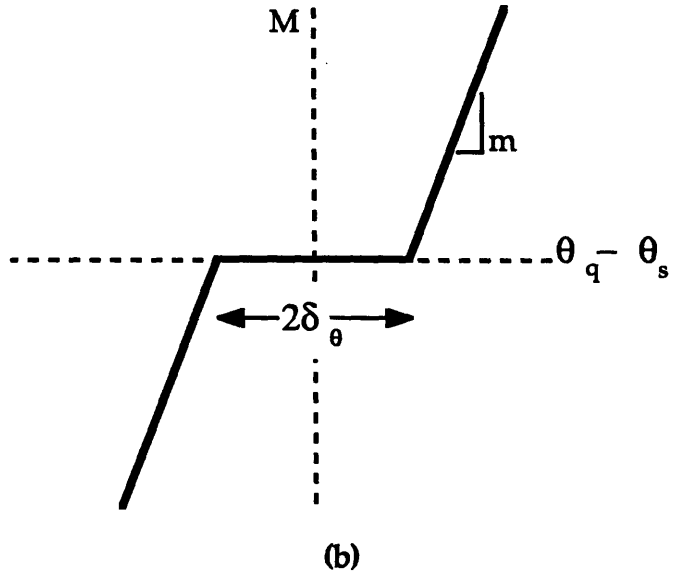

(b)

Figure 5-1: Convention Used to Define Joint Deadband.
As points (q) and (s) move towards interface point (o), the slope m changes. Thus the stiffness of the joint depends somewhat arbitrarily on the distance "d" chosen as the joint length.

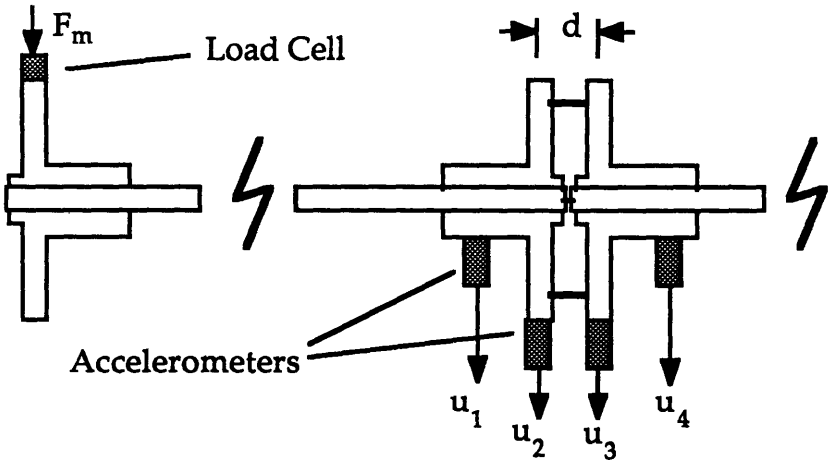

Figure 5-2: Sensor Placement for Measurement of Joint Rotation.
Structure is excited by burst random force at point (m).

In order to calculate the desired magnitude of joint curvature, and hence rotation, the θ'/f_m transfer function needs to be scaled by the appropriate force level used in each test. Accordingly, the averaged force time histories were recorded in each test of the linear and nonlinear structures and were used to calculate the discrete Fourier transform (DFT) of the force given by

$$X(k) = \frac{1}{N}\sum_{i=0}^{N-1} x(i)\exp^{-\left(\frac{2\pi i k}{N}\right)} \qquad k = 0,1,2,\ldots,N-1 \qquad (5\text{-}1)$$

where N is the number of time points, x(i) is value at time index i, and X(k) is the spectral value at frequency index k. The frequency resolution is given by $\Delta\omega = 2\pi/T$, where T is the length of the time record. For the case study N=4096, T=1.6 sec, and $\Delta\omega$= 0.625 Hertz or 3.93 sec^{-1}. The value X(k) can be interpreted as the random complex amplitude of the measured force time signal with frequency $k*\Delta\omega$. Joint curvature is scaled by the

magnitude of the force DFT at each frequency point; approximate joint rotation is determined by the product of the curvature θ' and the chosen distance d.

Linear joint rotation is assumed to be a linear function of forcing amplitude. A reference forcing level is chosen to be that presented previously in Figure 3-12, for which the rms value of the force is approximately 0.7 Newtons. This reference level will hereafter be referred to as F_o. Figure 5-3 shows the magnitude of joint rotation calculated using the reference force level. This spectral representation of joint rotation, in effect a DFT, needs to be scaled to reflect the actual forcing level F of any individual test. Table 5-1 lists the reference values of linear joint rotation calculated from Figure 5-3. Note in Figure 5-3 that at the frequencies pertaining to the even modes--44, 143, and 306 Hertz--the rotation is nearly zero. This of course is consistent with the measured even mode shapes, for which a point of inflection exists at the joint interface.

Table 5-1: Linear Rotational Deformation Near Joint Calculated with Reference Force Level F_o.

Mode	Joint Rotation (radians)
1	.005
3	.0026
5	.0006

The joint nondimensionalization is proposed to be

$$\delta_\theta^* = \frac{\delta_\theta}{\theta' d} \tag{5-2}$$

and is a function of gap size, forcing amplitude and mode number. The denominator represents the rotational deformation across the joint of the linear structure, and is interpreted as a peak sine amplitude. The value is taken from Table 5-1 and is scaled according to the force level F/F_o. For a given gap size and forcing amplitude, a different δ_θ^* is calculated for each mode.

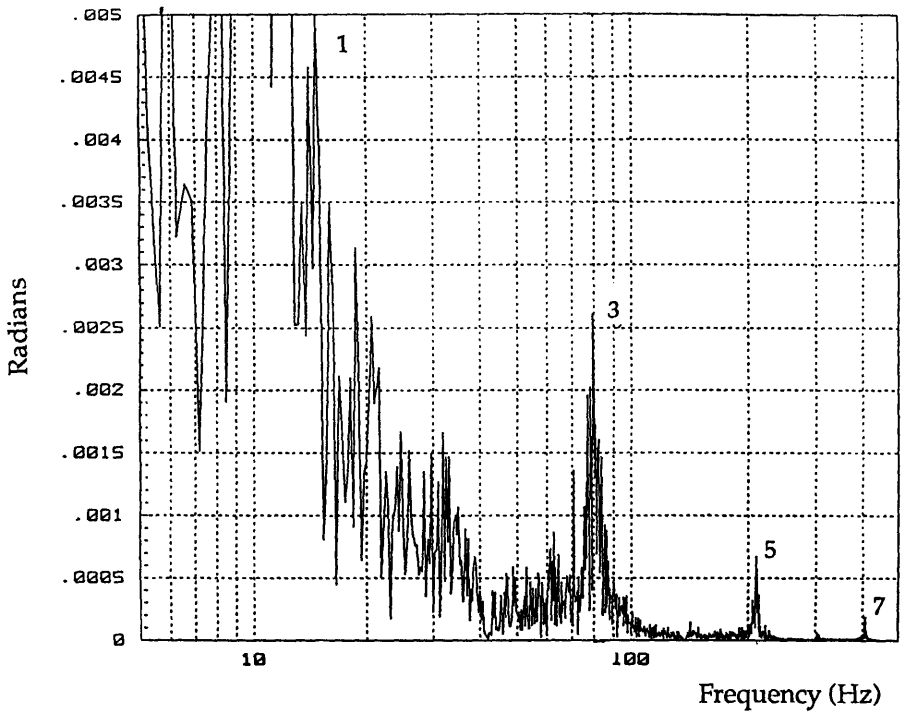

Figure 5-3: Measured Local Rotation Across Linear Joint.
Note that only the "odd" modes have joint rotation; the even modes have a point of inflection at the joint for the two-component structure.

5.3 Effect of Gap Size on Measurement of Frequency Response Function

Various amounts of joint rotational freeplay δ_θ are introduced by loosening the bolts between the lips of the joint, and are measured by saturating the deadband and measuring the deflection change of the joint lips with a micrometer. Special care was taken to back each of the bolts off by the same distance, although this was difficult to enforce rigorously. The frequency response of the superstructure with loose joints is then measured, subject to burst random force excitation at point (m) with a normalized force level F/F_o of 1.7 The forcing amplitude is kept constant for all the tests shown in Figures 5-4 and 5-5.

The requirement that the structure be linear for modal test methods to be applicable is waived for the purpose of identifying the effect of deadband on FRF measurement. One result of using burst random excitation is that the measured FRFs will appear noisy, due to the effect that the deadband has on the measured power spectral densities and calculation of the transfer function, as shown in Eq. (3-8). However, Goyder[29] has shown that one advantage of testing by random excitation is that the resulting FRFs may be interpreted as the approximate linear response of the nonlinear structure, free of discontinuous jump phenomena. Another advantage to this mode of testing is the short time duration of tests.

The accuracy of the random test was confirmed by testing the structure using sine sweep excitation. This measured transfer function agreed well with the former--for those modes that were not affected by the

gap nonlinearity, there was a close match in the shape and magnitudes of the FRF. However, those modes that appeared excessively noisy in the random test exhibited typical jump behavior during the sine sweep, though the general response amplitude and mode location were approximately the same as in the random tests.

Several interesting effects can be seen in Figure 5-4. Firstly, the destruction of the FRF due to the gap occurs first at high modes, while the lower modes appear unaffected and still "linear". The destruction advances down in frequency as the gap size increases. The high frequency effect is understandable, since the rotational deflection of the high modes across the joint is less, and thus the joint nonlinearity will be saturated less of the time. Hunter[15] demonstrated a similar destructive effect on inertance measurements for a four DOF mass spring model. Secondly, the modes appear to be more highly damped, not a surprising result given that significant rattling was heard during the testing, and that the spectrum analyzer has a difficult time constructing a transfer function from noisy and nonlinear data. Thirdly, the mode peaks shift lower in frequency--an effect observed previously in other analytical and experimental studies[35,36]. However, only the odd modes gain damping and shift in frequency, since the odd mode shapes have an antinode of rotation at the joint and thus excite the deadband. These are the same modes that demonstrate the typical jump phenomena in the sine sweep test. The even mode shapes have a rotational node point at the joint; here the components are coupled only by shear force. These mode shapes do not excite the deadband and therefor the modes are not affected significantly, except when the noise from the other modes becomes

excessive and interferes at the even mode frequencies. This dependance on mode shape is consistent with the experimental results of Bohlen and Gaul[24]. Lastly, when the deadband is very large, the FRF resembles noise--a result of a severe breakdown in the assumption of linearity and the superposition principle. Modal analysis is not defined in this regime of structural response.

Figure 5-4b shows a comparison between the linear FRF, a highly nonlinear FRF, and the predicted linear FRF for two components coupled by pinned coupling. The modes of the nonlinear structure, coupled with a less stiff joint due to deadband, appear to shifting to those of the pinned joint FRF.

Figures 5-6 and 5-7 display the same information as Figures 5-4a and 5-5, but represent the information in a three-dimensional perspective. Shown are the modes 2, 3, and 4; mode 3 is the only one of the three to have an antinode of rotation at the joint. Accordingly, it is this mode that clearly demonstrates a shift to lower frequency and a decrease in amplitude, as well as in modal resolution, as the size of the deadband increases. The phase plot shows a measured increase in damping for mode three as a function of gap size.

5.4 Effect of Excitation Amplitude on FRF Measurement

The "dual" of the last series of measurements, in which gap size is varied at a constant excitation level, is to maintain the gap size and force

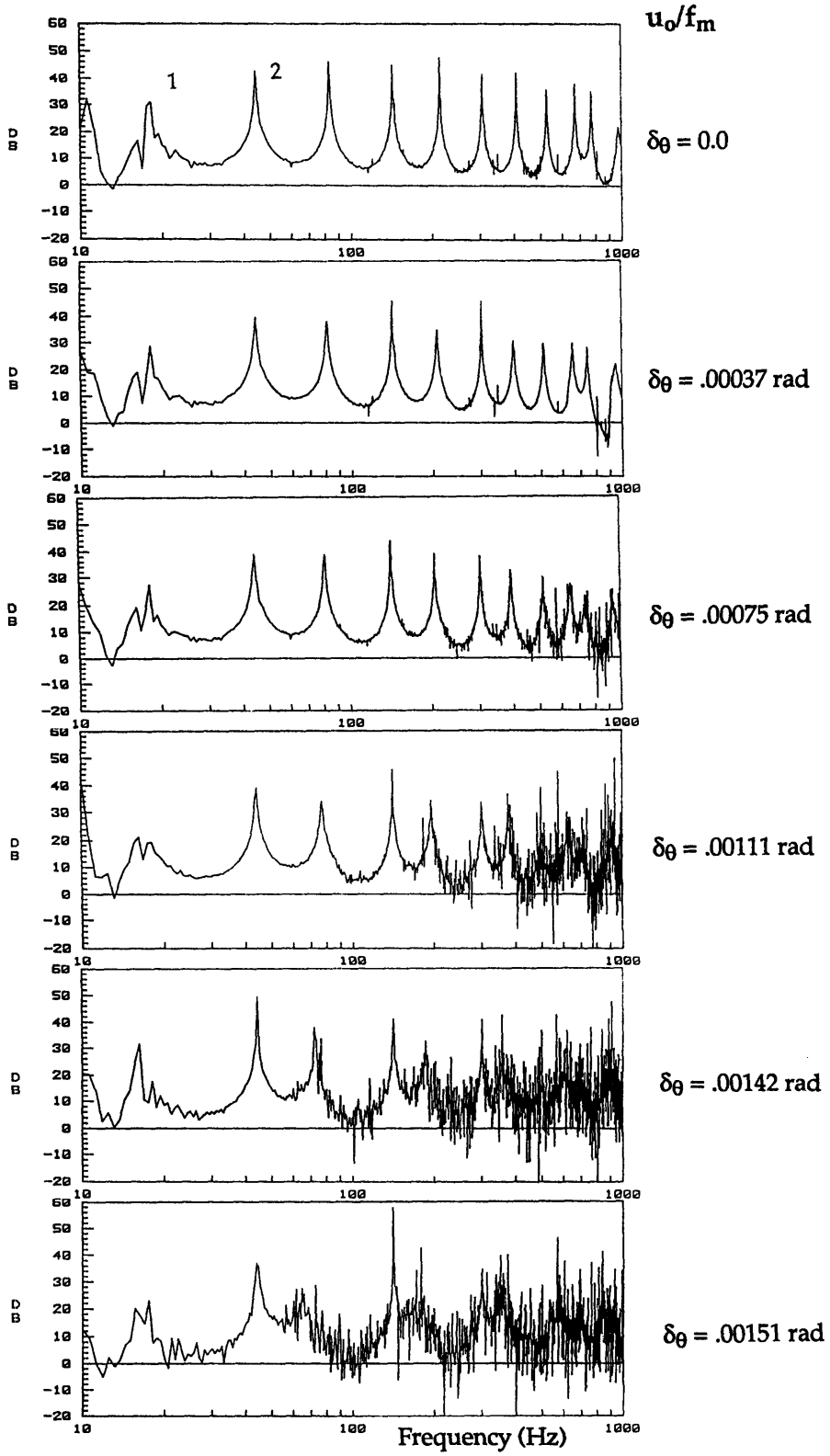

Figure 5-4: Effect of Gap Size on FRF Magnitude Measurement--Two Component Strucuture.

The superstructure inertances are shown for increasing sizes of deadband in the joint; a constant force level of $F/F_0 = 1.7$ was used for each of these measurements.

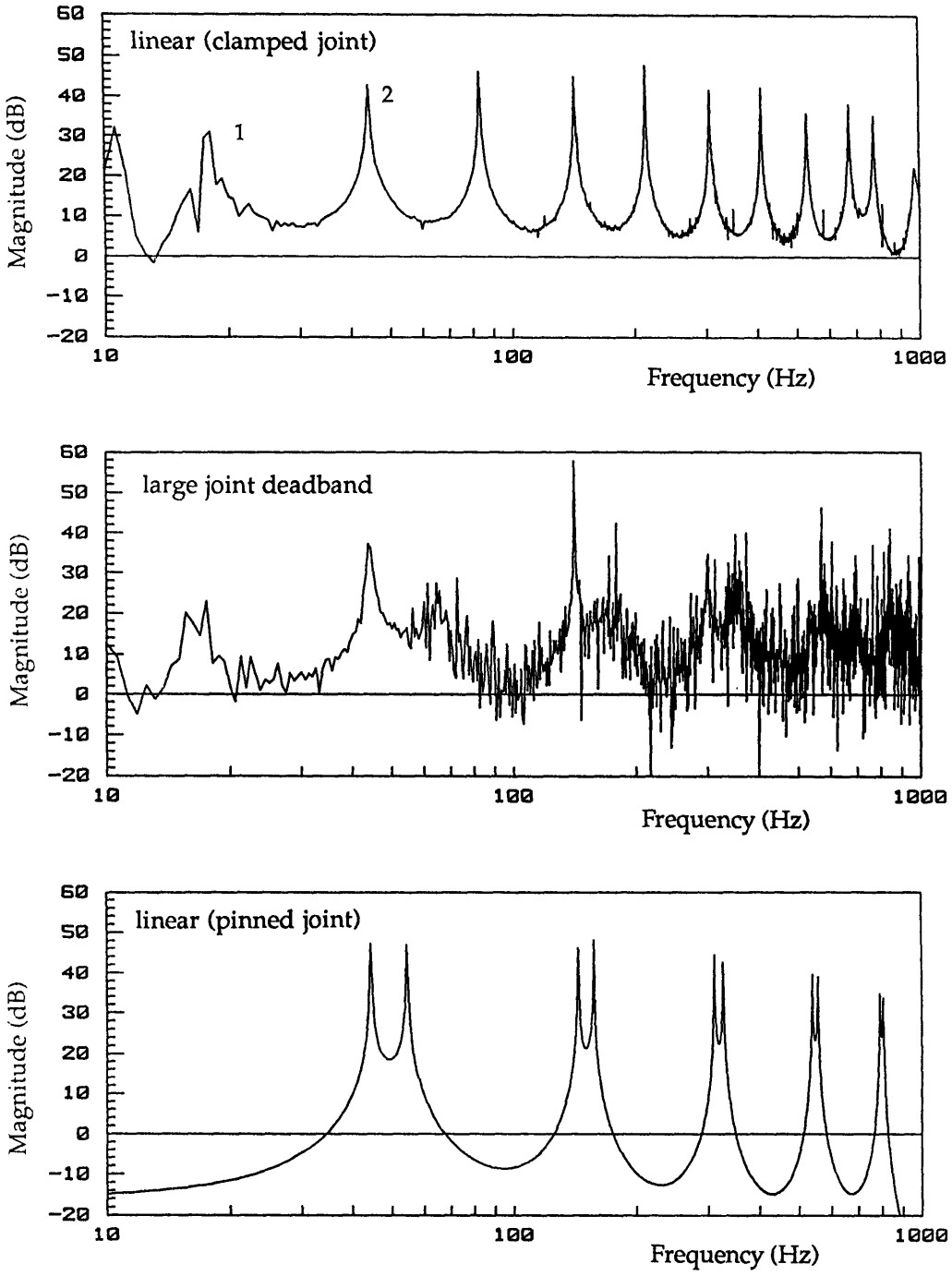

Figure 5-4 (b)

The structure with large joint deadband is compared to the linear structure (clamped joint) to the CMS prediction of the structure connected by pinned joint.

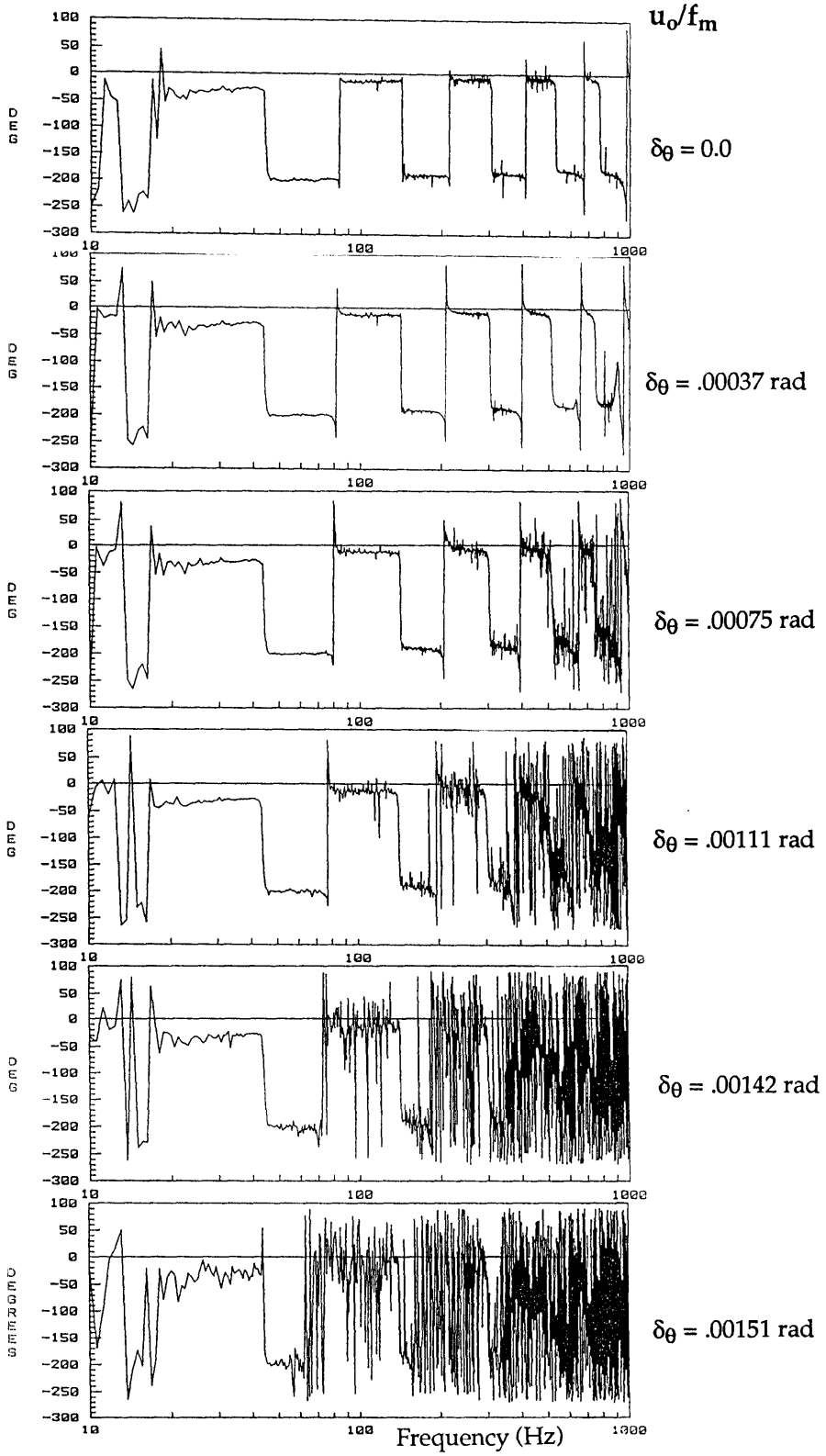

Figure 5-5: Effect of Gap Size on FRF Phase Measurement--Two Component Structure.

The superstructure inertances (corresponding to Figure 5-4) for increasing sizes of deadband in the joint; a constant force level of F/F_o = 1.7 was used for each measurement.

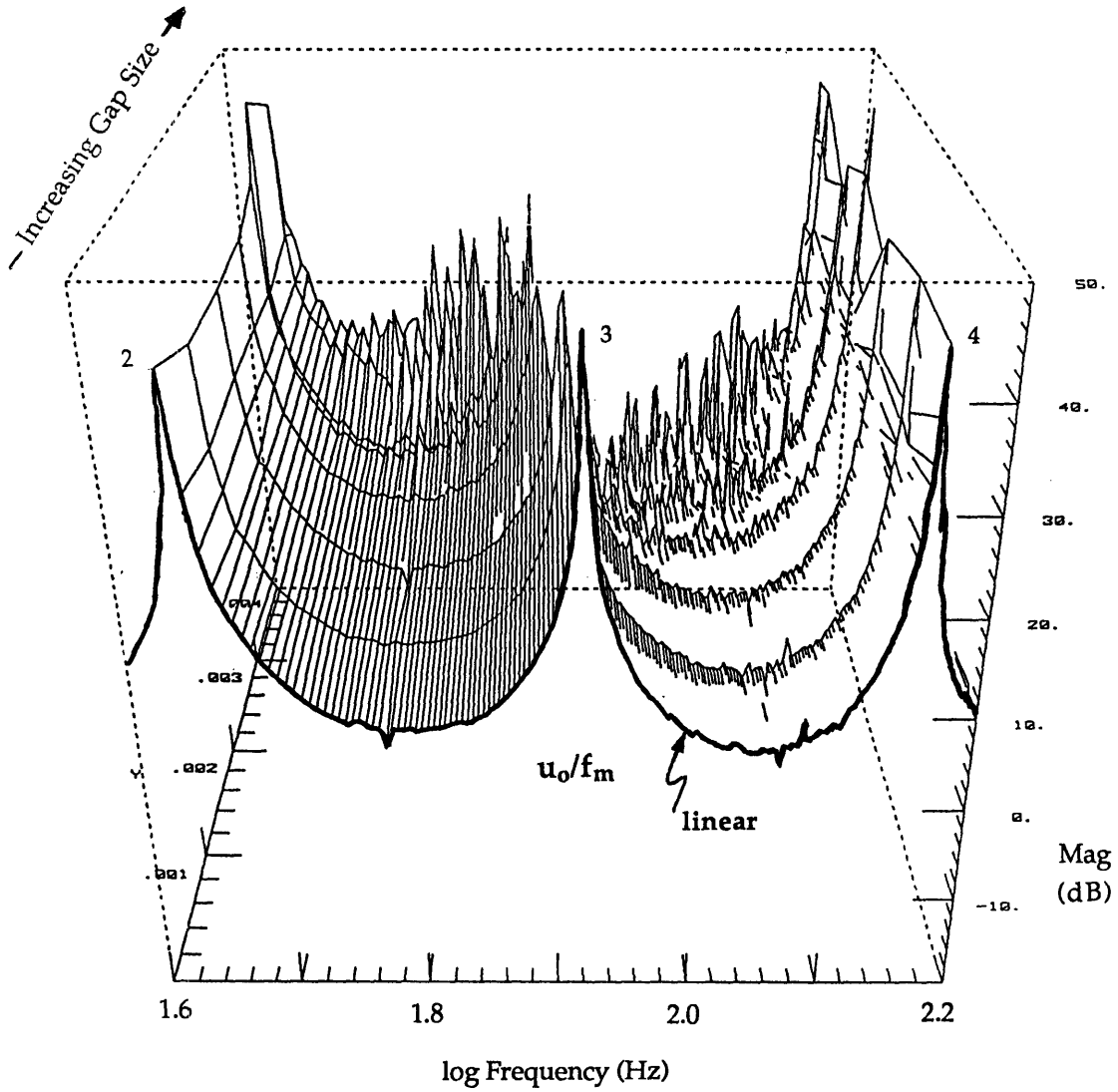

Figure 5-6: Perspective View of Effect of Gap Size on FRF Magnitude Measurement--Two Components.

Modes 2, 3, and 4 are shown for increasing values of gap size in the joint (into the page). Only mode 3 has bending coupling at the joint, and only mode 3 displays attenuation and frequency shift.

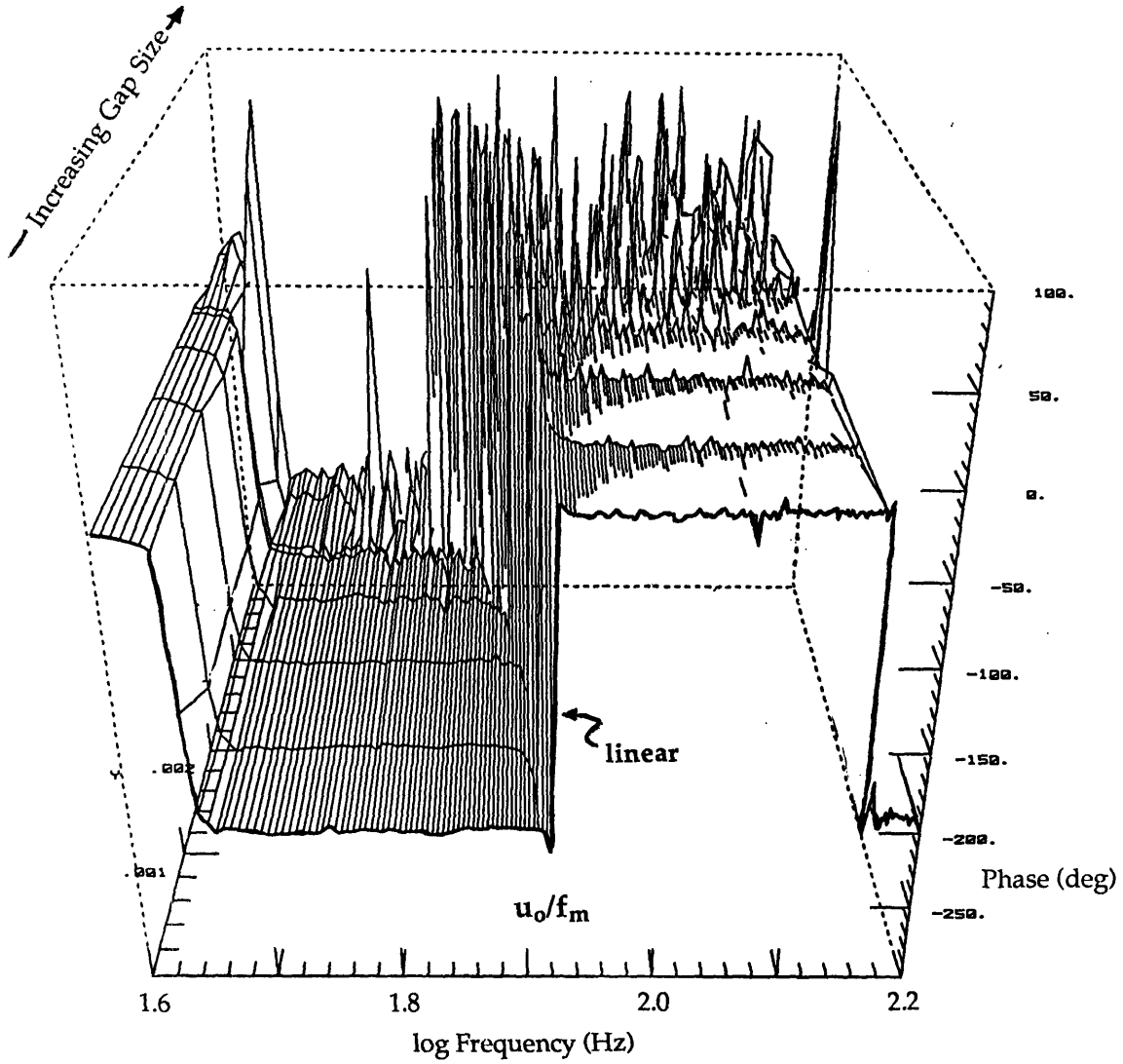

Figure 5-7: Perspective View of Effect of Gap Size on FRF Phase Measurement--Two Components.
Modes 2, 3, and 4 are shown for increasing values of gap size (into the page). Mode 3 displays corruption and increase in damping.

the structure at different force levels. Similar effects should be observed, and if the nondimensional parameter has been chosen correctly, the shifts in natural frequency should correlate for similar values of δ_θ^*. All force levels are referenced to F_o given by Figure 3-12.

Figure 5-8 shows the effect that various levels of forcing have on the measured transfer function, for a gap size (.00095 radians) that is "moderate" by comparison to those of Figure 5-4. One immediate observation is that despite rather high levels of forcing, the smooth linear transfer function is not recovered at all--symptoms that the gap still corrupts the calculation of the transfer function. Otherwise, for decreasing levels of excitation the odd modes do shift lower in frequency, become more highly damped and generally less defined. This effect is again more pronounced at high frequency. In all of these measurements, the joint gap saturates for at least one mode, as confirmed by the extreme rattling noise heard during testing.

A striking and unexpected result occurs at extremely low levels of forcing--so low that the joint does not saturate at all--and is shown in the last plot of Figure 5-8. A relatively "clean" transfer function is observed, with even modes at the expected locations, but with odd modes at frequencies somewhere between the clamped and pinned mode locations. It is surmised that the structure has achieved a new linear mode of vibration, one in which the joint, whether due to friction or a small bias in construction, remains saturated in a new configuration. In particular, the joint was observed to carry the bending moment through the lips on one side (which remain saturated) and the shimstock in the "center" of

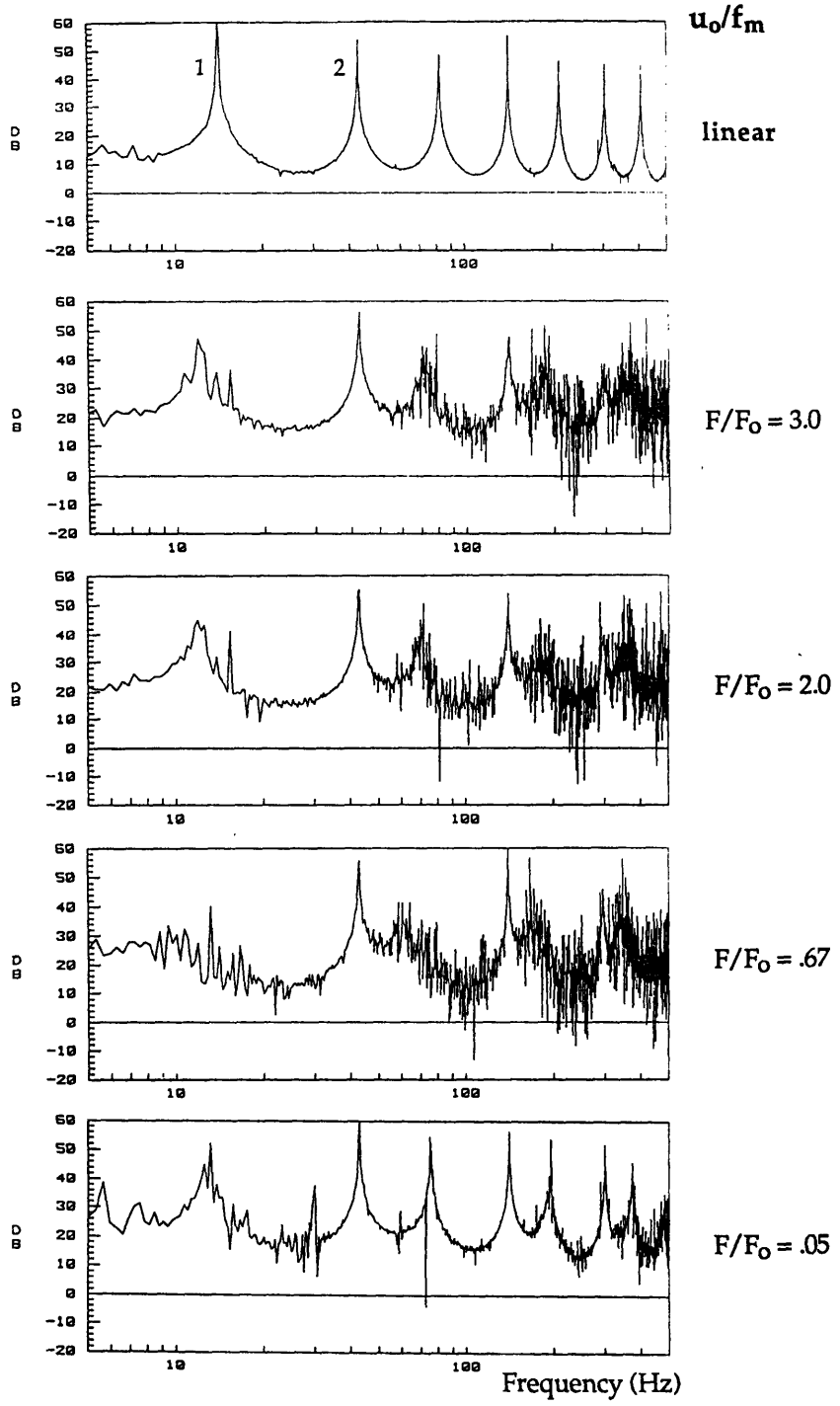

Figure 5-8: Effect of Gap Size on FRF Magnitude Measurement at Different Forcing Amplitudes.
A constant gap size of .0095 radians was used at different forcing levels, each referenced to F_o of Figure 3-12.

the joint. If the neutral axis of the beam were slightly biased towards this half of the joint, the observed behavior would become possible. Certainly this observation is strictly case-specific, but should serve as a warning that unusual effects may occur when testing "sloppy" joints at low amplitude.

5.5 Effect of Gap Size on Accuracy of Component Mode Synthesis

The effect of this deadband on the accuracy of the component mode synthesis prediction is now investigated, since the coupling procedure assumed a linear, fully compatible joint. The compatibility of Eq. (4-4) is known to be in error in the presence of joint deadband, in which case $\theta_o{}^a$ does not equal $-\theta_o{}^b$. Force equilibrium, given by Eq. (4-5), still holds. Figure 5-9 compares the CMS prediction of Chapter 4 (dashed line) to the measured transfer function of the coupled structure for two different sizes of joint deadband. In general, good predictions are made of those modes with rotation antinodes at the joint, and poor predictions are made of the others. One suspects that an improvement in CMS could be achieved if the joint dynamics could be accounted for in the coupling procedure, by an averaging or describing function technique, keeping in mind the effects of gap size, joint rotation, and the participation of modal vectors.

Assuming that the CMS prediction of Figure 4-6 is used to define linear prediction errors E_o for the modal parameters (damping, residues, natural frequencies), the change in error ΔE_o can be calculated by measuring the shift of these parameters for the nonlinear FRF measurements. The percent error in CMS modal frequency prediction due

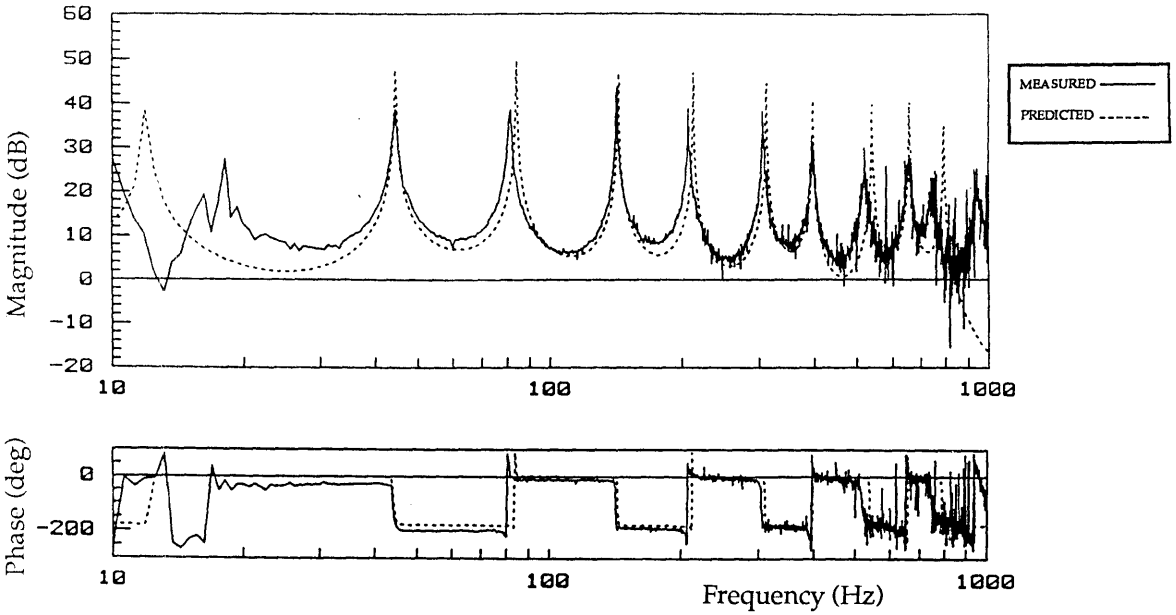

(a) u_o/f_m $\delta\theta$ = .00075 rad

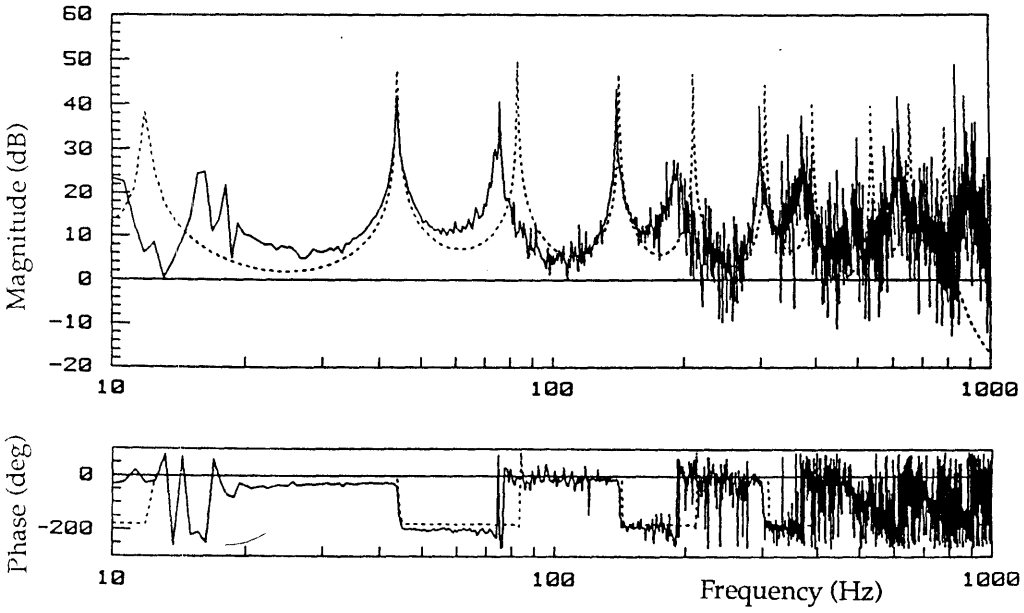

(b) u_o/f_m $\delta\theta$ = .00138 rad

Figure 5-9: Qualitative Effects of Deadband Effect on CMS Accuracy.

The CMS prediction is compared to a coupled structure with gap in the joint.

to varying the gap size at constant amplitude is plotted versus nondimensional gap size in Figure 5-10. Errors for the even modes were very near zero and are not plotted; only modes 1 and 3 are shown. The shift in frequency for both modes 1 and 3 are approximately the same for similar values of $\delta\theta^*$. The shift in natural frequencies of the nonlinear structure, represented by the error in CMS prediction, would not increase indefinitely--eventually the gap size would become so large that the structure would exhibit resonances typical of a pinned joint coupling, as shown in Figure 5-4b. These experimental results are consistent with the analytical results of Bowden[30], who conducted an analytical study of MDOF spring-mass systems coupled by joints of varying stiffness and nonlinear behavior.

Plotted also in Figure 5-10 are the analytical results of Schaffer[31] for the frequency shift of a single DOF spring-mass system with deadband. The non-dimensional parameter used by Schaffer is the ratio of gap size to the linear sine wave amplitude of the displacement of the mass. The experimental results of this thesis would not necessarily be expected to agree closely with those of Schaffer because of the somewhat arbitrary choice of parameters to normalize the gap size by the joint rotation. However similar trends are observed and the good agreement of the two studies gives confidence that a reasonable normalization was chosen for this thesis work.

Figure 5-11 shows a plot of CMS error versus non-dimensional gap size for the cases in which forcing amplitude was varied for constant gap size. Figures 5-10 and 5-11 are plotted together in Figure 5-12 and

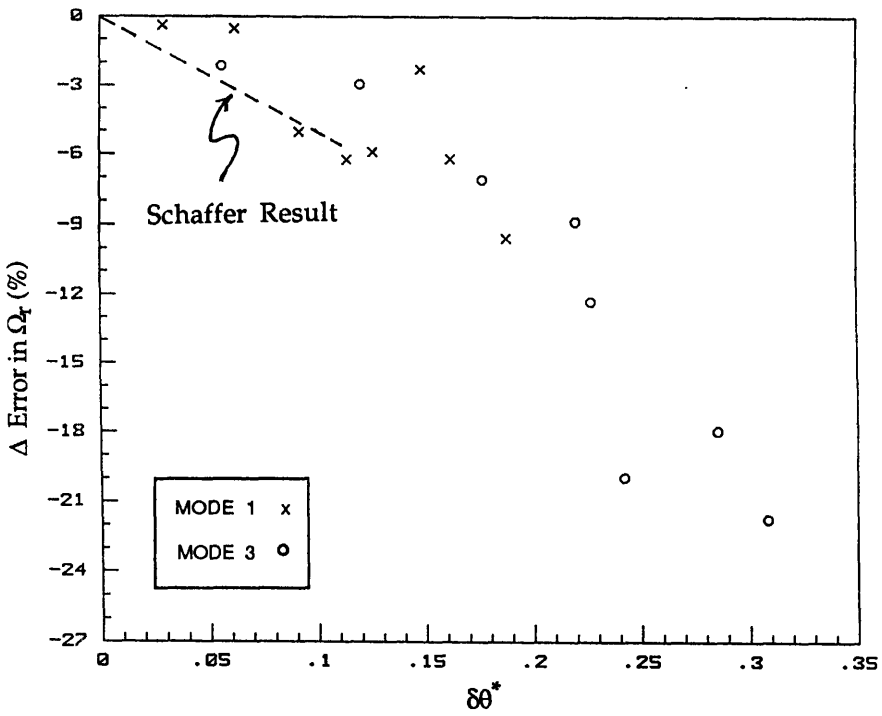

Figure 5-10: Error in CMS Modal Frequency Estimation Versus Normalized Gap Size--Constant Force Amplitude.

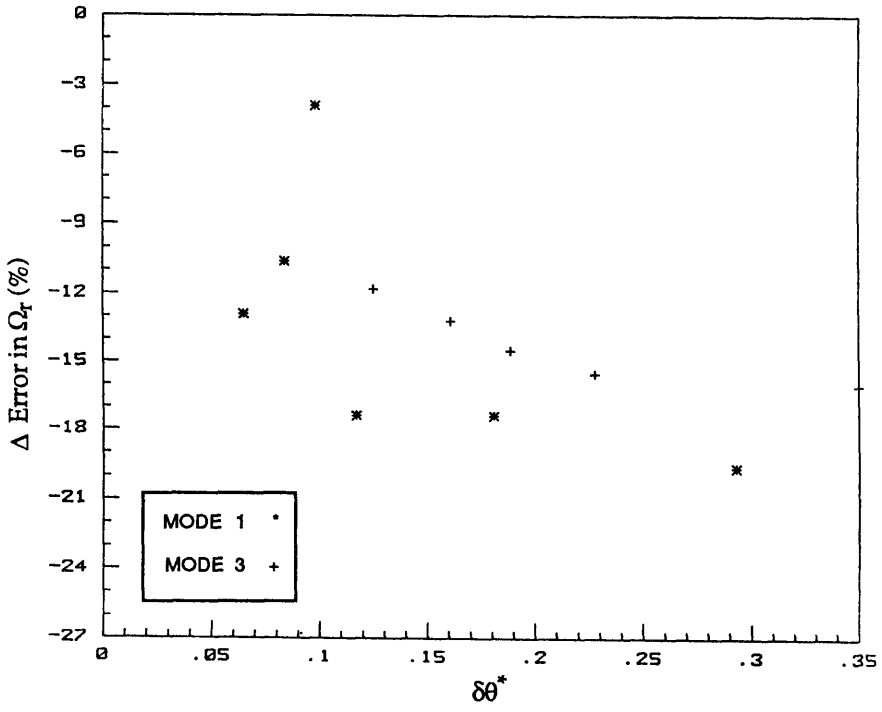

Figure 5-11: Error in CMS Modal Frequency Estimation Versus Normalized Gap Size--Variable Force Amplitude.

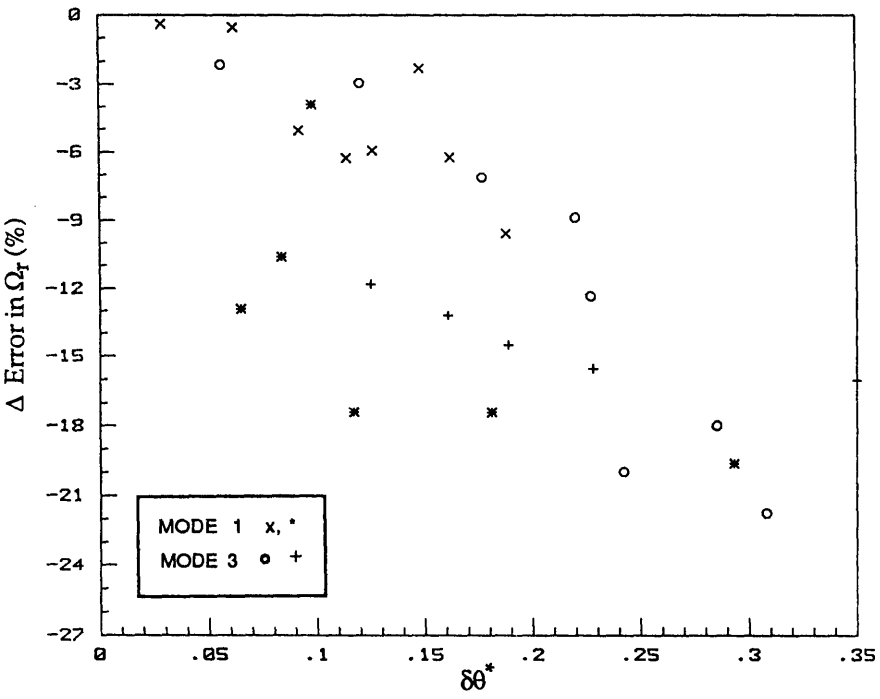

Figure 5-12: Composite Plot of CMS Modal Frequency Estimation Error Versus Normalized Deadband.
Figures 5-11 and 5-12 are plotted together.

unfortunately do not show good agreement. The data points should lie on a similar curve if the non-dimensionalization was chosen correctly. Points from the two curve are closest to one another at high values of $\delta\theta^*$; for low values of $\delta\theta^*$ the forcing amplitude was very high for some of the data points, allowing the possibility of other nonlinear effects or energy dissipation. Nonlinear systems are typically difficult to normalize; a "Reynolds Number" is unlikely to exist for this nonlinear system.

Data from mode 5 was not plotted in either Figure 5-10 or 5-11 because it did not agree at all with the other modes--it displayed a frequency shift comparable to that of mode three in most of the FRFs for much greater values of $\delta\theta^*$. Table 5-1 shows that the linear joint rotation for this mode is indeed small; given this value the value of $\delta\theta^*$ was usually greater than one, meaning that the gap size was larger than the maximum joint rotation for this mode. Perhaps the small frequency shift of mode 5 is due to some energy transfer from the extreme rattling of modes 1 and 3. The prospect of identifying effects on higher modes of a highly nonlinear structure may be unrealistic.

Chapter 6
Multi-Component Structures With Nonlinear Joints

In chapter 5 experimental frequency response measurements were presented showing what effect a joint with rotational freeplay had on the dynamics of a coupled structure consisting of two identical components. How "nonlinear" the structure was, or how much its behavior deviated from the linear case, depended on gap size, force amplitude and mode shape. The more interesting case, however, is how such a joint or several such joints affect the dynamics of a multi-component structure. While the complete treatment of this issue is beyond the scope of this thesis, it is worthwhile to present preliminary measurements for a three-component structure with one and two nonlinear joints.

An experimental FRF for a linear three-component structure has already been presented in Section 3.4.4, and is repeated for the sake of reference in Figure 6-1. A "moderate" amount of deadband (relative to the tests of Chapter 5) of .00095 radians was introduced into first only one joint, and then the second. The effects that the single and compound joint nonlinearity have on the coupled structure dynamics can be seen in Figures 6-1. Forcing amplitude was also moderate ($F/F_o = 1.7$).

Effects similar to those for the two-component structure are evident--corruption of the FRF especially at high frequency, shift in frequency of the natural modes, and attenuation of amplitude response. Unlike the two-component structure, all modes display these effects to

varying degrees, since each mode has some rotational coupling at the joint. Modes three and six are least affected since for these modes a point of inflection exists near the joint. Matters are worsened considerably when a deadband is added to the second joint in the structure. As the number of components and joints increase, the nonlinear effects would be expected to "average out" even further, since all mode shapes would excite a number of joints that exhibit deadband nonlinearity.

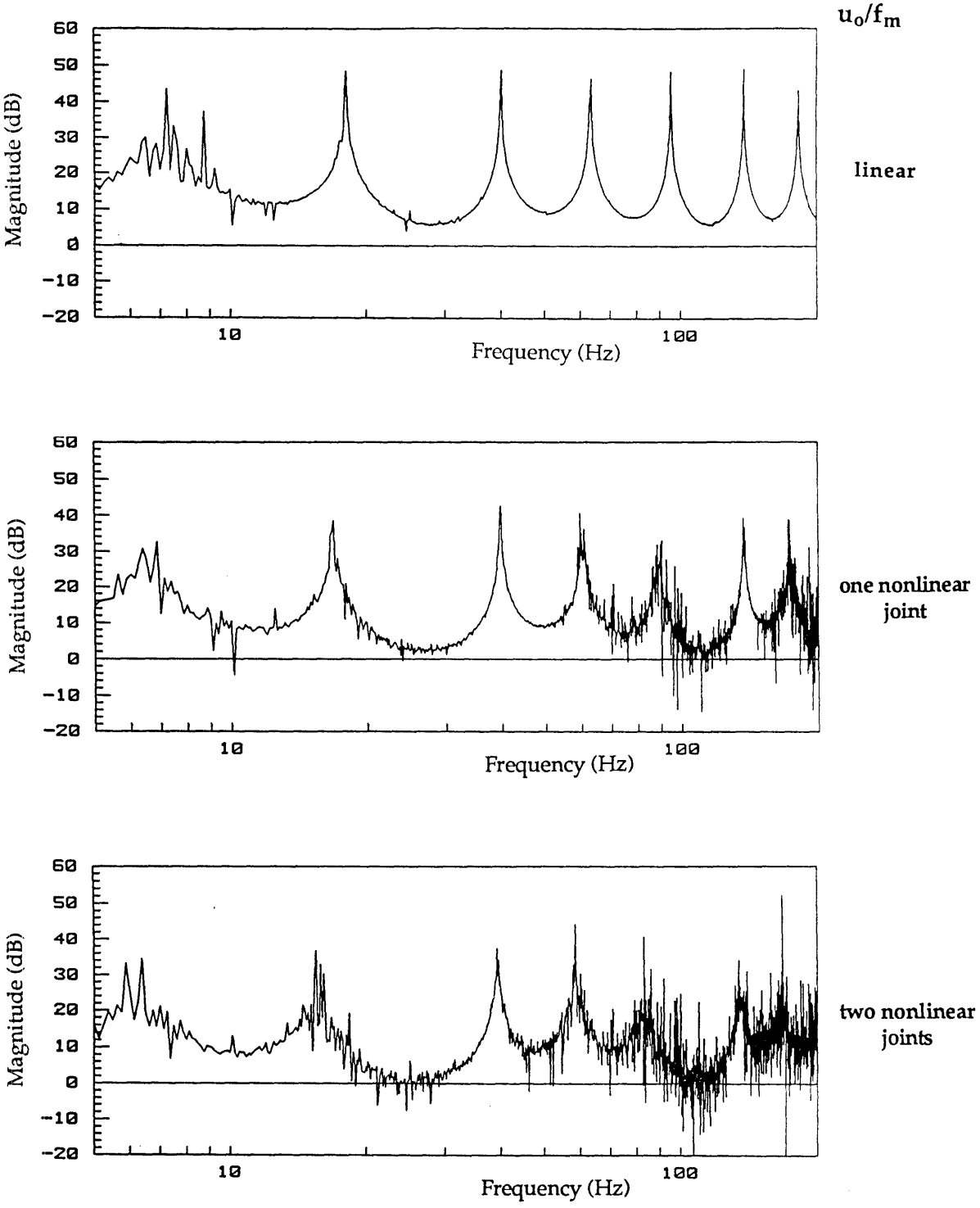

Figure 6-1: Effect of Joint Deadband on Multi-Component Structures.

A three-component structure is shown with one and two joints exhibiting rotational freeplay. Deadband size is .00095 rad and forcing level is $F/F_0 = 1.7$. First mode of the linear case is corrupted by stinger resonances.

Chapter 7
Important Issues in Experimental Component Mode Synthesis

This chapter summarizes the important issues that must be considered when undertaking component mode synthesis using experimentally derived modal parameters. Some of these concerns have been presented by previous authors[6,7,13]; these issues will now be discussed in terms of relevance to the present experiment and to the testing of more complicated structures, such as components of large space structures.

7.1 Linear Component Mode Synthesis

Choice of Coupling Components

The coupling coordinates are those degrees of freedom for which compatibility is enforced when analytically coupling the component frequency response functions. In this study both deflection and rotation were required for the coupling of the beam structures; coupling of only deflection at the interface (an equivalent pinned joint) produced a very different FRF as shown in Figure 4-7. Naturally these points and degrees of freedom occur along component interfaces--no measurement of interior degrees of freedom is required unless one is interested in response at some point other than the interface. The identification of coupling coordinates for the bay of a three-dimensional truss would be a more significant task, since joints may be coupled in six or more degrees of freedom. In addition, there would be many joints at the interface.

Rotational coupling is less important for structures that are coupled at many degrees of freedom, but it remains to be seen how important the rotational terms are for a truss-like structure. It may be that the rotational terms are unimportant, which would greatly simplify the measurement requirements. Clearly some experimental work is required in this area.

Measurement of the Necessary FRFs

Once the coupling coordinates have been identified, the "hard work" begins--the measurement of the frequency response functions at these points in order to determine the complete FRF matrix defined by these coordinates. In other words, the system modal frequencies and damping must be measured, along with the appropriate modal constants from (which the eigenvectors are determined) at each degree of freedom used in coupling. Theoretical CMS requires that the *exact* interface inertances (or mobilities or receptances) be measured, a very difficult task in practice. Approximate quantities can be measured, since there is usually a discrepancy in distance between sensor or load application and the true interface coordinate. The measured modal constants and calculated eigenvector estimates will thus be in error, a problem which increases with frequency as nodes and anti-nodes become more closely spaced and nearer to the interface.

While some simplifications can be made from the modal model to reduce the number of required measurements (see Chapter 3), it is typically necessary to measure a collocated force, linear deflection, and rotational quantity (moment or rotational deflection) at an interface coordinate. Rotational quantities are traditionally difficult to measure, as

special hardware may be required to exert a pure moment at the interface, and finite difference schemes are often required to calculate interface rotation based on linear displacement measurements. In addition, the identification of modal parameters based on modal analysis requires that each force is applied independently; that is, only one force or moment is to be applied to any degree of freedom during any one test. (Multi-shaker tests are possible, but each force excitation must be uncorrelated from the others). A stinger was used to meet this single-force requirement during the present study, although this requirement would be more difficult to enforce during modal testing of a truss bay. It would be feasible to measure the required inertances of a three-dimensional truss by conventional modal analysis techniques, but the measurement issues discussed here would have to be considered and addressed during the testing.

Residual Terms

The measured component dynamic modes must be augmented with the static contributions from out of range modes--both higher and lower--in order to accurately represent the component response. An experimental frequency response function already includes this information; during the development of the component modal model these terms must be correctly identified and included. If they are omitted, the resulting CMS prediction of superstructure frequency response will be in error. Higher frequency residual terms can be included by analyzing the component FRFs, or simply by measuring dynamic modes well beyond (1.5 or 2 times) the frequency range of interest for the CMS study. The latter technique was used with some success in the present study.

Analytical rigid body modes (actually low frequency suspension pendulum modes) were used to complete the component FRF models. These modes agreed well with the low frequency residual terms from the component FRFs. Unfortunately CMS prediction was poor in the low frequency range, but has been successful in other studies in the literature. The cause of this discrepancy has yet to be determined.

Necessity to Produce a Unified Modal Model

Both time domain and frequency domain CMS require a consistent set of component modal parameters from which to predict superstructure response. Discrepancies in the measured modal parameters--small but significant differences in the modal frequencies, damping, and modal constants--contribute to poor CMS prediction. The extension of CMS to more complicated truss structures which may exhibit internal resonances and very closely spaced modes may require the use of special software to identify the required modal model. Experimental CMS has not yet been applied to such structures; the accuracy of the procedure will need to be validated for such structures in future research.

Range of Linear CMS Accuracy

Experimental CMS is very accurate in the frequency range for which good component dynamic behavior is available. Near the "edges" of this region accuracy is sacrificed if the correct residual terms are not correctly included. The analytical low frequency residual corrections in the present study are somehow in error relative to the measured dynamic modes. Sensor calibration error may be a factor, or additional reaction forces from the stinger could have corrupted the true FRF measurements. It is

noteworthy that the "raw" CMS estimate for the first superstructure modal frequency was better than that using the unified modal model--apparently the correct residual terms were present in the measured data. This problem may yet be corrected by a more careful analysis of the measured data.

The most stringent constraint on CMS accuracy is the identification of correct eigenvector entries for the true interface degrees of freedom, a result of limitations on the placement of sensors and force application. Errors in this step place an upper limit on the frequency range of CMS accuracy, which may not be too much of a problem since lower frequency superstructure modes are usually of interest. Awareness of this source of error, and perhaps steps to correct for the error in the analysis stage, are definitely required in any experimental CMS study.

Choice of CMS Coupling Procedure

Both time domain (using measured residual flexibilities) and frequency domain CMS are satisfactory procedures for performing experimental component mode synthesis. The methods are very similar in that the same measurement information is used in both, although no formal comparison of the techniques has been conducted to assess relative accuracy given the same measurement base. Time domain CMS is somewhat easier to interface to analytical finite element models.

7.2 Consideration of Nonlinear Issues

This thesis will certainly not be the last word on experimental measurement of nonlinear structures, and it is recognized that each real-world system that displays nonlinear behavior such as joint deadband will have to be addressed individually and with new case-specific non-dimensionalizations. Some observations will now be made regarding CMS and modal analysis that will extend beyond the case study at hand.

Error in CMS Accuracy Due to Joint Deadband

Linear CMS has been demonstrated to accurately predict superstructure frequency response, though not without some problems. CMS accuracy is greatly reduced when deadband nonlinearity is present in the coupling between components, which has the effect of relaxing or violating the assumption of compatibility of deflection at the interface coordinates. Even small amounts of gap can alter the coupled structure modes (see Figures 5-4 and 5-9) which may at first inspection appear to behave linearly. Results from this and other studies indicate that the deviation of the actual structural response from the linear case depends on several things: the size of the gap relative to the local linear elastic deformations (a function of gap size, forcing amplitude and mode number) as well as whether the degree of freedom that exhibits the gap is important in the coupling of a particular mode (a function of mode shape). For instance, the "even" modes of the two-component structure did not display corruption due to the nonlinear joint because they were coupled only in shear at the joint interface.

These effects are evident once again in the three-component structure with nonlinear joints. A multi-component structure including many such joints would display a different behavior--the aforementioned effects would be more distributed or averaged out among all the structural modes, because a typical mode shape would likely excite several nonlinear joints. The deviation from the linear response would be more a function of gap size, number of joints, and forcing amplitude. Bowden[30] develops a "joint participation factor" which attempts to describe a nonlinear jointed structure in this fashion.

Forcing Amplitude

Wada[37] has warned of the dangers of extending models of coupled structural behavior to cases involving extremely low levels of force excitation--the "micro-g" level--since unusual or unmodelled effects may occur here. Indeed, unusual effects were observed when the structure with nonlinear joint was forced at extremely low force levels. In particular, the structure appeared to achieve a new linear equilibrium. While this observation is strictly case-specific, it should serve as a warning that unexpected and unmodelled effects may occur when testing "sloppy" joints at low amplitude.

Compensation for Nonlinear Joint Dynamics in CMS

Results from this study seem to encourage the application of averaging or describing function techniques to account for the deadband behavior in the joints directly in the component mode synthesis procedure. Bowden[30] has used describing functions to approximate the nonlinear behavior of joints in a state-space model. A proposal not

Chapter 8
Conclusions and Recommendations for Future Work

Linear component mode synthesis has been conducted for two- and three-component structures using experimentally determined component frequency response functions. Superstructure natural frequencies, damping values and response amplitudes were successfully predicted using a consistent modal model based on the measured component FRFs, validating work previously done in the literature. Incorporation of correct residual terms and difficulty in measuring exact interface inertances, resulting in incorrect eigenvector estimates, were identified as likely sources of error to be encountered in experimental component mode synthesis. Since joints are usually located at component interface, they may contribute to errors in CMS because their geometry can prohibit accurate measurement of the necessary interface dynamics. Rotational freeplay introduced in the joint between components resulted in significant shifts in coupled structure response and hence error in linear CMS prediction; these effects were discussed in terms of a non-dimensional gap size referenced to the local linear rotational deformation near the joint. The effect of deadband nonlinearity on the measured frequency response was also demonstrated. Modification of compatibility conditions by an appropriate describing function may be an avenue worth pursuing in order to account for nonlinear joint behavior directly in the component mode synthesis procedure.

Significant amounts of work can be done to extend the experimental component mode synthesis procedure from the analysis of "clean" laboratory structures to more realistic flight structures. Accordingly, it is appropriate to suggest several possible areas worthy of exploration in component mode synthesis:

1) extension of experimental CMS to truss-like structures characterized by closely spaced modes and multiple degree-of-freedom coupling.

2) further work is needed in the present study to address the low-frequency error in CMS prediction, and to determine the sensitivity of the predicted first modal frequency to changes in various parameters in the modal model.

3) the proposed "corrections" on the estimated eigenvectors should be carried out in order to assess the possible improvement in accuracy of the high-frequency mode predictions.

4) describing functions could be used to account for the nonlinear joint stiffness or compatibility conditions directly in the CMS procedure.

5) other types of nonlinearity--cubic stiffening, hysteresis--could be introduced into the coupling joint in order to assess CMS accuracy.

References

1. Ashley, H, "Some Considerations on Earthbound Dynamic Testing of Large Space Structures", AIAA Paper # 86-0908.

2. Card, M. F., Anderson, M. S., Walz, J. E., "Dynamic Response of a Flexible Space Beam", NASA Technical Memorandum 86441, May 1985.

3. Crawley, E. F., and O'Donnell, K. J., "A Procedure for Calculating the Damping in Multi-Element Space Structures", Acta Astronautica, Vol. 15, No. 12, 1987, pp. 987-996.

4. Ikegami, R., Church, S. M., Keinholz, D. A., and Fowler, B. L., "Experimental Characterization of Deployable Trusses and Joints", Structural Dynamics and Control Interaction of Flexible Structures, NASA Conference Publication 2467, April 1986, pp. 1271-1287.

5. Craig, R.R., "A Review of Time-Domain and Frequency-Domain Component Mode Synthesis Method", Combined Experimental Analytical Modeling of Dynamic Structural Systems, ASME, AMD-Vol. 67, June 1985, pp. 1-30.

6. Ewins, D. J., "Modal Test Requirements for Coupled Structure Analysis Using Experimentally-Derived Component Models", Combined Experimental Analytical Modeling of Dynamic Structural Systems, ASME, AMD-Vol.67, June 1985, pp. 31-47.

7. Martinez, D.R., Carne, T. G., and Miller, A. K., "Combined Experimental/Analytical Modeling Using Component Mode Synthesis", AIAA/ASME/ASCE/AHS 25th Structures, Structural Dynamics, & Materials Conference, May 1984, pp. 140-152.

8. Brassard, J., and Massoud, M., "Identification of a Complete Mobility Matrix of a Synthesized System From Component Mobility Measurements", Proceedings of 5th International Modal Analysis Conference, April 1987, pp. 319-323.

9. Ewins, D.J., and Sainsbury, M.G. "Mobility Measurements for the Vibration Analysis of Connected Structures." Shock and Vibration Bulletin 42, No. 1, January 1972, pp. 105-122.

10. Ewins, D. J., and Gleeson, P.T., "Experimental Determination of Multidirectional Mobility Data for Beams", Shock and Vibration Bulletin 45, #5, June 1975, pp.153-174.

11. MacNeal, R. H., "A Hybrid Method of Component Mode Synthesis." Computers and Structures, Vol. 1, No. 4, Dec. 1971, pp. 581-601.

12. Bathe, K-J. "Finite Element Procedures in Engineering Analysis." Englewood Cliffs: Prentice-Hall, Inc., 1982.

13. Ewins, D. J., Modal Testing: Theory and Practice. New York: Research Studies Press Ltd., 1984.

14. Hurty, W.P. "Dynamic Analysis of Structural Systems using Component Modes." AIAA Journal, Vol. 3, No. 4, April 1965, pp. 678-685.

15. Craig, R.R., and Bampton, M.C.C. "Coupling of Substructures for Dynamic Analysis." AIAA Journal, Vol. 6, No. 7, July 1968, pp. 1313-1319.

16. Rubin, S., "Improved Component-Mode Representation for Structural Dynamic Analysis." AIAA Journal, Vol. 13, No. 8, August 1975, pp. 995-1006.

17. Craig, R.R. Jr., and Chang, C-J., "On the Use of Attachment Modes in Substructure Coupling for Dynamic Analysis," Proceedings of the AIAA/ASME 18th Structures, Structural Dynamics and Materials Conference, Vol. B, 1977, pp. 89-99.

18. Benfield, W.A., and Hruda, R.F., "Vibration Analysis of Structures by Component Mode Substitution." AIAA Journal, Vol. 9, No.7, July 1971, pp. 1255-1261.

19. Kammer, D.C., and Baker, M., "A Comparison of the Craig-Bampton and Residual Flexibility Methods for Component Substructure Representation." AIAA/ASME/ASCE/AHS 26th Structures, Structural Dynamics and Materials Conference, April 1985, pp. 699-705.

20. Craig, R.R., Bachmeyer, R,C., and Howsman, T.G., "Some Approaches to Substructure Coupling with Damping." Proceedings of 4th International Conference on Applied Numerical Modeling, Vol. 63, December 1984, pp. 172-177.

21. Hasselman, T.K., and Kaplan, K., "Dynamic Analyis of Large Systems by Complex Mode Synthesis." Journal of Dynamic Systems, Measurement, and Control, Vol. 96, No. 3, September 1974, pp. 327-333.

22. Geering, H. P., "New Methods in Substructuring", AIAA/ASME/ASCE/AHS 21st Structures, Structural Dynamics, and Materials Conference, May 1980, pp. 801-808.

23. Imregun, M., Robb D.A. and Ewins, D.J., "Structural Modification and Coupling Dynamic Analysis Using Measured FRF Data." Proceedings fo the 5th International Modal Analysis Conference, Vol. 2, April 1987, pp. 1136-1141.

24. Bohlen, S., and Gaul, L., "Vibrations of Structures Coupled by Nonlinear Transfer Behaviour of Joints; A Combined Computational and Experimental Approach", Proceedings of 5th International Modal Analysis Conference, April 1987, pp. 86-91.

25. Chen, J.C., and Hunt D.L., "Application of Multiple Input Random and Polyreference Analysis Techniques to the Galileo Spacecraft Modal Test." AIAA/ASME/ASCE/AHS 25th Structures, Structural Dynamics and Materials Conference, May 1984, pp. 554-556.

26. Sarver, G., "Energy Transfer and Dissipation in Structures With Discrete Nonlinearities". Doctoral thesis dissertation, Massachusetts Institute of Technology, November 1987.

27. Rogers, L.C., and Richards, K.E., "Pacoss Program Overview and Status." NASA/DOD Control/Structures Interaction Technology, NASA Conference Publication 2447, Part 1, November 1986, pp. 85-109.

28. Crowley, S.M., Brown, D.L., and Allemeng, R.J., "The Extraction of Valid Residue Terms using the Polyreference Technique." 3rd International Modal Analysis Conference, 1985, pp. 80-85.

29. Goyder, H.G.D., "Foolproof Methods for Frequency Response Measurements", 2nd International Conference on Recent Advances in Structural Dynamics, University of Southhampton, England, 1984.

30. Bowden, M., and Dugundji, J., "Effects of Joint Damping and Joint Nonlinearity on the Dynamics of Space Structures." 29th AIAA/ASME/ASCE/AHS Structures, Structural Dynamics, and Materials Conference, April 1988, pp. 1764-1773.

31. Schaffer, S.E., and von Flotow, A. H., "Torturing Recursive Parameter Identification Algorithms with a Gap Nonlinearity." 29th AIAA/ASME/ASCE/AHS Structures, Structural Dynamics, and Materials Conference, April 1988, pp. 1711-1718.

32. Busby, H.R., Nopporn, C,. and Singh, R. "Experimental Modal Analysis of Non-Linear Systems: A Feasibility Study." Journal of Sound and Vibration, 1986, pp. 415-427.

33. Tomlinson, G.R., and Lam, J. "Frequency Response Characteristics of Structures with Single and Multiple Clearance-Type Non-Linearity." Journal of Sound and Vibration, 1984, pp. 111-125.

34. Hunter, N. F., "An Investigation of the Time History and Modal Responses of Some Simple Linear and Nonlinear Systems", Proceedings of 3rd International Modal Analysis Conference, Orlando, FL, 1985, pp. 410-418.

35. Mertens, M., et al., "Detection of Nonlinear Dynamic Behaviour of Mechanical Structures", Proceedings of 4th International Modal Analysis Conference, Los Angeles, CA, February 1986, pp.712-719.

36. Coyner, J. V., and Bachtell, E. E., "Box Truss Antenna Technology Status", NASA/DOD Control/ Structures Interaction Technology, Norfolk, VA, November 1986, pp. 717-736.

37. Wada, B. Panel discussion at the USAF/NASA Workshop on Model Determination for Large Space Structures, Pasadena CA, March 1988.

38. Gelb, A., and Vander Velde, W.E., Multiple-Input Describing Functions and Nonlinear System Design. New York: McGraw-Hill Inc., 1968, pp. 67-71.

Bibliography

Component Mode Synthesis

Allen, J.J. "Techniques for Implementing Statically Complete Component Mode Synthesis for Forced Response." Proceedings of 5th International Modal Analysis Conference, April 1987, pp. 42-48.

Baker, M. "Component Mode Synthesis Methods for Test-based, Rigidly Connected, Flexible Components." AIAA/ASME/ASCE/AHS 25th Structures, Structural Dynamics and Materials Conference, May 1984, pp. 153-163.

Benfield, W.A., and Hruda, R.F. "Vibration Analysis of Structures by Component Mode Substitution." AIAA Journal, Vol. 9, No.7, July 1971, pp. 1255-1261.

Blackwood, G. H. "Experimental Component Mode Synthesis of Structures with Sloppy Joints." AIAA/ASME/ASCE/AHS 29th Structures, Structural Dynamics and Materials Conference, April 1988, pp. 1565-1575.

Brassard, J., and Massoud, M. "Identification of a Complete Mobility Matrix of a Synthesized System from Component Mobility Measurements." Proceedings of 5th International Modal Analysis Conference, April 1987, pp. 319-323.

Charron, F., Lapierre, H., Jha, V.K., Sorocky, S.J., and Vigneron, F.R. "Demonstration of Modal Synthesis on an Experimental Structure and its Application to Large Spacecraft." Proceedings of Spacecraft Structures Conference, CNES, December 1983, pp. 185-190.

Craig, R.R. "A Review of Time-Domain and Frequency-Domain Component Mode Synthesis Method." ASCE/ASME Mechanics Conference, June 1985, Vol. 67, pp. 1-30.

Craig, R.R. "A Study of Modal Coupling Methods." Proceedings of Spacecraft Structures Conference, CNES, December 1985, pp. 75-80.

Craig, R.R., Bachmeyer, R,C., and Howsman, T.G. "Some Approaches to Substructure Coupling with Damping." Proceedings of 4th International Conference on Applied Numerical Modeling, Vol. 63, December 1984, pp. 172-177.

Craig, R.R., and Bampton, M.C.C. "Coupling of Substructures for Dynamic Analysis." AIAA Journal, Vol. 6, No. 7, July 1968, pp. 1313-1319.

Craig, R.R. Jr., and Chang, C-J., "On the Use of Attachment Modes in Substructure Coupling for Dynamic Analysis." Proceedings of the AIAA/ASME 18th Structures, Structural Dynamics and Materials Conference, Vol. B, 1977, pp. 89-99.

Craig, R.R., and Chung, Y. "Generalized Substructure Coupling Procedure for Damped Systems." AIAA Journal, Vol. 20, No. 3, March 1982, pp. 442-444.

Craig, R.R., and Zhenhua, N. "Component Mode Synthesis for Model Order Reduction of Non-Classically-Damped Systems." Proceedings of AIAA Guidance, Navigation, and Control Conference, August, 1987, pp. 1-10.

Crawley, E.F., and O'Donnell, W.J. "A Procedure for Calculating the Damping in Multi-Element Space Structures." Acta Astronautica, Vol. 15, No. 12, 1987, pp. 987-996.

Dowell, E.H. "On Some General Properties of Combined Dynamical Systems." Journal of Applied Mechanics, Vol. 46, No. 1, March 1979, pp. 206-209.

Dowell, E.H. "Component Mode Analysis of Nonlinear and Nonconservative Systems." Journal of Applied Mechanics, Vol. 47, No. 1, March 1980, pp. 172-175.

Dowell, E.H. "On the Modal Approach to Structural Modification." Journal of the American Helicopter Society, January 1984, pp. 75-77.

Ewins, D.J. "Modal Test Requirements for Coupled Structure Analysis using Experimentally-Derived Component Models." ASCE/ASME Mechanics Conference, June 1985, Vol. 67, pp. 31-47.

Ewins, D.J., and Gleeson, P.T. "Experimental Determination of Multidirectional Mobility Data for Beams." Shock and Vibration Bulletin 45, No. 5, June 1975, pp. 31-47.

Ewins, D.J., and Sainsbury, M.G. "Mobility Measurements for the Vibration Analysis of Connected Structures." Shock and Vibration Bulletin 42, No. 1, January 1972, pp. 105-122.

Geering, H.P. "New Methods in Substructuring." AIAA/ASME/ASCE/AHS 21st Structures, Structural Dynamics and Materials Conference, May 1980, pp. 801-808.

Hale, A.L. "Substructure Synthesis and its Iterative Improvement for Large Nonconservative Vibratory Systems." AIAA Journal, Vol. 22, No. 2, February 1984, pp. 265-272.

Hasselman, T.K., and Kaplan, K. "Dynamic Analyis of Large Systems by Complex Mode Synthesis." Journal of Dynamic Systems, Measurement, and Control, Vol. 96, No. 3, September 1974, pp. 327-333.

Hintz, R.M. "Analytical Methods in Component Modal Synthesis." AIAA Journal, Vol. 13, No. 8, August 1975, pp. 1007-1016.

Howsman, T.G., and Craig, R.R. "A Substructure Coupling Procedure Applicable to General Linear Time-Invariant Dynamic Systems." AIAA/ASME/ASCE/AHS 25th Structures, Structural Dynamics and Materials Conference, May 1984, pp. 164-171.

Hurty, W.P. "Dynamic Analysis of Structural Systems using Component Modes." AIAA Journal, Vol. 3, No. 4, April 1965, pp. 678-685.

Imregun, M. , Robb, D.A., and Ewins, D.J. "Structural Modification and Coupling Dynamic Analysis using Measured FRF Data." Proceedings of 5th International Modal Analysis Conference, April 1987, pp. 1136-1141.

Kammer, D.C., and Baker, M. "A Comparison of the Craig-Bampton and Residual Flexibility Methods for Component Substructure Representation." AIAA/ASME/ASCE/AHS 26th Structures, Structural Dynamics and Materials Conference, April 1985, pp. 699-705.

Klein, L.R., and Dowell, E.H. "Analysis of Modal Damping by Component Modes Method using Lagrange Multipliers." Journal of Applied Mechanics, Vol. 41, No. 2, June 1974, pp. 527-528.

Lu, Y., and Ma, Z. "A New Method of Component Modal Synthesis with High Accuracy Computational Efficiency Synthesis Flexibility and Adaptability." Proceedings of 3rd International Modal Conference, January 1985, pp. 291-298.

MacNeal, R. H., "A Hybrid Method of Component Mode Synthesis." Computers and Structures, Vol. 1, No. 4, Dec. 1971, pp. 581-601.

Martinez, D.R., Carne, T.G., and Miller, A.K. "Combined Experimental/Analytical Modeling Using Component Mode Synthesis." AIAA/ASME/ASCE/AHS 25th Structures, Structural Dynamics and Materials Conference, May 1984, pp. 140-151.

Meirovitch, L. "Substructure Synthesis." Computational Methods in Structural Dynamics , Maryland: Sijthoff and Noordhoff, 1980, pp. 385-409.

Meirovitch, L., and Hale, A.L. "A General Dynamic Synthesis for Structures with Discrete Substructures." AIAA/ASME/ASCE/AHS 21st Structures, Structural Dynamics and Materials Conference, May 1980, pp. 790-800.

Rubin, S. "Improved Component-Mode Representation for Structural Dynamic Analysis." AIAA Journal, Vol. 13, No. 8, August 1975, pp. 995-1006.

Song-Nian, G., Wen-Jie, Y., and Jie-Sheng, J. "An Experimental Mode Synthesis Technique." Proceedings of 5th International Modal Analysis Conference, April 1987, pp. 1198-1206.

Tongue, B.H., and Dowell, E.H. "Component Mode Analysis of Nonlinear, Nonconservative Systems." Journal of Applied Mechanics, Vol. 50, No. 1, March 1983, pp. 204-209.

Xiangjun, Q. "Reduction of DOF in Component Mode Synthesis by using Inter-Force Quasi-Compatability Constraint." Proceedings of 5th International Modal Analysis Conference, April 1987, pp. 307-314.

Zhu, S. "Modal Synthesis of Component with Gaps." Proceedings of 4th International Modal Analysis Conference, February 1986, pp. 264-269.

Modal Analysis

Allemang, R.J. "Modal Analysis: Twenty Years Back - Twenty Years Ahead." Sound and Vibration, January 1987, pp. 10-16.

Ashley, H. "Some Considerations on Earthbound Dynamic Testing of Large Space Structures." AIAA/ASME/ASCE/AHS 27th Structures, Structural Dynamics and Materials Conference, 1986, pp. 362-373.

Bathe, K-J. "Finite Element Procedures in Engineering Analysis." Englewood Cliffs: Prentice-Hall, Inc., 1982.

Beliveau, J.G., Massoud, M., Bourassa, P., Lauzier, C., Vigneron, F., and Soucy, Y. "Statistical Identification of the Dynamic Parameters of an Astromast from Finite Element and Test Results Using Bayesian Sensitivity Analysis." Proceedings of 2nd International Modal Analysis Conference, April 1984, pp. 85-95.

Berman, A., Wei, F.S., and Rao, K.V. "Improvement of Analytical Dynamic Models using Modal Test Data." AIAA/ASME/ASCE/AHS 21st Structures, Structural Dynamics and Materials Conference, May 1980, pp. 809-814.

Brown, D.L., Allemang, R.J., Zimmerman, R., and Mergeay, M. "Parameter Estimation Techniques for Modal Analysis." SAE Transactions, Vol. 88, 1980, pp. 828-846.

Card, M. F., Anderson, M. S., Walz, J. E., "Dynamic Response of a Flexible Space Beam", NASA Technical Memorandum 86441, May 1985.

Chen, J.C. "Evaluation of Modal Testing Methods." AIAA/ASME/ASCE/AHS 25th Structures, Structural Dynamics and Materials Conference, May 1984, pp. 561-572.

Chen, J.C., and Hunt D.L. "Application of Multiple Input Random and Polyreference Analysis Techniques to the Galileo Spacecraft Modal Test." AIAA/ASME/ASCE/AHS 25th Structures, Structural Dynamics and Materials Conference, May 1984, pp. 554-556.

Clark, M. "Multi Shaker Modal Testing using a Modified Random Excitation." Proceedings of 3rd International Modal Analysis Conference, January 1985, pp. 553-557.

Clifton, M.A., Hanna, D.S., and Keller, J.M. "A Multiple Shaker Stepped Sine Data Acquisition System." 3rd International Modal Analysis Conference, 1985, pp. 367-371.

Craig, R.R, and Blair, M.A. "A Generalized Multiple-Input,Multiple-Output Modal Parameter Estimation Algorithm." AIAA/ASME/ ASCE/AHS 25th Structures, Structural Dynamics and Materials Conference, May 1984, pp. 469-477.

Crowley, S.M., Brown, D.L., and Allemeng, R.J. "The Extraction of Valid Residue Terms using the Polyreference Technique." 3rd International Modal Analysis Conference, 1985, pp. 80-85.

Dossing, O. "Bruel and Kjaer: Structural Testing - Part 1-Mechanical Mobility Measurements." April 1987, pp. 1-47.

Ewins, D. J., Modal Testing: Theory and Practice. New York: Research Studies Press Ltd., 1984.

Ewins, D.J. "Uses and Abuses of Modal Testing." Sound and Vibration, January 1987, pp. 32-39.

Goyder, H.G., and Harwell U.K. "Foolproof Methods for Frequency Response Measurements." 2nd International Conference on Recent Advances in Structural Dynamics, 1984.

Gustaveson, D.K. "Direct Parameter Identification from Frequency Response Measurements." Proceedings of 5th International Modal Analysis Conference, April 1987, pp. 1352-1356.

Hamma, G.A., Smith, S., and Stroud, R.C. "An Evaluation of Excitation and Analysis Methods for Modal Testing." SAE Transactions, Vol. 85, 1976, pp. 2770-2783.

Hu, P.Y. "Response of Linear Systems to Magnitude Limited Random Excitation." SAE Transactions, No. 69, August 1969, pp. 1-8.

Hunt, D.L., Peterson, E.L., Vold, H., and Williams,R. "Optimal Selection of Excitation Methods for Enhanced Modal Testing." AIAA/ASME/ASCE/AHS 25th Structures, Structural Dynamics and Materials Conference, May 1984, pp. 549-553.

Hunt, D.L., Matthews, J., and Williams, R. "An Automated Tuning and Data Collection System for Sine Dwell Modal Testing." AIAA/ASME/ASCE/AHS 25th Structures, Structural Dynamics and Materials Conference, May 1984, pp. 507-509.

Ibrahim, S.R. "A Review of the Domain Modal Test Methods and Applications." Proceedings of Spacecraft Structures Conference, CNES, December 1985, pp. 205-207.

Kitagawa, M., and Kubomura, K. "Transient Load Analysis Method for Large Linear Structures with Local Nonlinearities and its Application to Space Shuttle Payload Analysis." AIAA/ASME/ASCE/AHS 26th Structures, Structural Dynamics and Materials Conference, April 1985, pp. 404-416.

Kuo, C.P., and Wada, B.K. "System Identification of a Truss Type Space Structure using the Multiple Boundary Condition Test (MBCT) Method." AIAA/ASME/ASCE/AHS 28th Structures, Structural Dynamics and Materials Conference, 1987, pp. 172-176.

Rao, D.K. "Electrodynamic Interaction Between a Resonating Structure and an Exciter." Proceedings of 5th International Modal Analysis Conference, April 1987, pp. 1142-1150.

Robson, J.D. "Researches in Random Viobration." 2nd International Conference on Recent Advances in Structural Dynamics, 1984.

Soni, M.L., and Agrawal, B.N. "Damping Synthesis for Flexible Space Structures using Combined Experimental and Analytical Models." AIAA/ASME/ASCE/AHS 26th Structures, Structural Dynamics and Materials Conference, April 1985, pp. 552-558.

Soucy, Y., and Vigneron, F.R. "Identification of Structural Properties of a Continuous Longeron Space Mast." AIAA/ASME/ASCE/ AHS 25th Structures, Structural Dynamics and Materials Conference, May 1984, pp. 130-139.

Vold, H., Kundrat, J., Rocklin, G.T., and Russell, R. "A Multi-Input Modal Estimation Algorithm for Mini-Computers." SAE Transactions, Vol. 91, 1982, pp. 815-821.

Weaver, H.J., and Pastrnak, J.W. "Multiple Shaker Excitation using Coherent Signals." Proceedings of 3rd International Modal Analysis Conference, 1985, pp. 117-123.

Nonlinear Systems

Bowden, M., and Dugundji, J., "Effects of Joint Damping and Joint Nonlinearity on the Dynamics of Space Structures." 29th AIAA/ASME/ASCE/AHS Structures, Structural Dynamics, and Materials Conference, April 1988, pp. 1764-1773.

Bohlen, S., and Gaul, S. "Vibrations of Structures Coupled by Nonlinear Transfer Behavior of Joints; A Combined Computational and Experimental Approach." Proceedings of 5th International Modal Analysis Conference, April 1987, pp. 86-91.

Busby, H.R., Nopporn, C., and Singh, R. "Experimental Modal Analysis of Non-Linear Systems: A Feasibility Study." Journal of Sound and Vibration, July 1986, pp. 415-426.

Chapman, J.M., Shaw, F.H., and Russell, W.C. "Dynamics of Trusses having Nonlinear Joints." NASA Conference Publication 2467, Structural Dynamics and Control Interaction of Flexible Structures, April 1986, pp. 540-565.

Crawley, E.F., and Aubert, A.C. "Identification of Nonlinear Structural Elements by Force-State Mapping." AIAA Journal, Vol. 24, No. 1, January 1986, pp. 155-162.

Crawley, E.F., and O'Donnell, K.J. "Force-State Mapping Identification of Nonlinear Joints." AIAA Journal, Vol. 25, No. 7, July 1987, pp. 1003-1010.

Fillod, R., Piranda , J., and Bonnecase, D. "Taking Non Linearities into Account in Modal Analysis by Curve Fitting of Transfer Functions." Proceedings of 3rd International Modal Analysis Conference, January 1985, pp. 88-95.

Gelb, A., and Vander Velde, W.E. Multiple-Input Describing Functions and Nonlinear Systems. New York: McGraw-Hill Inc., 1968.

He, J., and Ewins, D.J. "A Simple Method of Interpretation for the Modal Analysis of Nonlinear Systems." Proceedings of 5th International Modal Analysis Conference, April 1987, pp. 626-634.

Horta, L.G., and Juang, J.N. "Identifying Approximate LInear Models for Simple Nonlinear Sytems." J. Guidance, Vol. 9, No. 4, July-August 1986, pp.385-390.

Hunter, N.F. "An Investigation of the Time History and Modal Responses of some Simple Linear and Nonlinear Systems." Proceedings of 3rd International Modal Analysis Conference, 1985, pp. 410-418.

Idelsohn, S.G., and Cardona, A. "Recent Advances in Reduction Methods in Non Linear Structural Dynamics." 2nd International Conference on Recent Advances in Structural Dynamics, 1984.

Ikegami, R., Church, S.M., Keinholz, D.A., and Fowler, B.L. "Experimental Characterization of Deployable Trusses and Joints." NASA Conference Publication 2467, Structural Dynamics and Control Interaction of Flexible Structures, April 1986, pp. 1271-1287.

Mertens, M., Van der Auweraer, H., Vanherck, P., and Snoeys, R. "Detection of Nonlinear Dynamic Behavior of Mechanical Structures." Proceedings of 4th International Modal Analysis Conference, February 1986, pp. 712-719.

Sarver, G., "Energy Transfer and Dissipation in Structures With Discrete Nonlinearities". Doctoral thesis dissertation, Massachusetts Institute of Technology, November 1987.

Schaffer, S.E., and von Flotow, A. H., "Torturing Recursive Parameter Identification Algorithms with a Gap Nonlinearity." 29th AIAA/ASME/ASCE/AHS Structures, Structural Dynamics, and Materials Conference, April 1988, pp. 1711-1718.

Tomlinson, G.R., and Kirk, N.E. "Modal Analysis and Identification of Structural Non-Linearity." 2nd International Conference on Recent Advances in Structural Dynamics, 1984.

Tomlinson, G.R., and Lam, J. "Frequency Response Characteristics of Structures with Single and Multiple Clearance-Type Non-Linearity." Journal of Sound and Vibration, 1984, pp. 111-125.

Zavodney, L.D. "Can the Modal Analyst Afford to be Ignorant of Nonlinear Vibration Phenomena?" Proceedings of 5th International Modal Analysis Conference, April 1987, pp.154-159.

Appendix A
Equipment List

Item	Model/SN	Specifications
Bruel & Kjaer Vibration Exciter	Model 4809 SN368271	45N,10lbf, Sine Peak Frequency Range:10Hz- 20 kHz Max. Displacement: 8mm Max. Input Current: 5A
Crown D-150A Series II Professional Power Amplifier	Model 8176 SN063726	Dual Channel 20Hz-20kHz 80 watts per channel
Kistler Dual Mode Amplifier	Model 5004 SN242700	Output: Voltage +/- 10 V Current +/- 5 mA Impedance 100 +/- 5 Ohms Power Supply: 100-130 V Frequency: 60 Hz Power Consumption: 8VA
Kistler Load Cell pC/lbf	Model 9001 SN283030	Meas. Range: 1700 lbf Sensitivity: approx. -19 Threshold: .002 lbf Natural Frequency: 200 kHz CapacityL: 8 pf Weight: .1 oz.
PCB 3 Channel Structcel Conditioner	Model 433A03 SN183	115v 60 Hz
Structcel Accelerometer	Model 330A SN2350 1910 2375 2338	Nominal Sensitivity:200mv/g Range: 10 g Resolution: .001 g Frequency Range: +/- 5% sens. deviation 1-1000 Hz < 5% phase shift 1-500 Hz Resonant Frequency: 3000 Hz Transverse Sensitivity: < 2% Weight: 2 gm
PCB Petro Wax	Model 080A24	
Bently Nevada Proximeter	Series 7200	Range 5mm Sensitivity 200 Mv/mil

Signology Fourier Analyzer simultaneous	Model SP20	4 channel input 1 channel output Sample Rate: 51.2 kHz Bancwidth: DC to 20 kHz Antialising Filters 78% efficient Dynamic Range: 75 dB Resolution: 12 bits

Appendix B
Determination of Rigid Body Modes

Analytical rigid body modes are determined for the component in order to complete the modal model by providing the necessary low frequency residual terms. "Rigid body modes" are a misnomer in this study since no such modes actually exist; they are really low-frequency (0.4 Hertz) pendulum suspension modes. However, at frequencies well above the suspension modes, the high-frequency residual of the suspension modes is indistinguishable from the theoretical residual due to true rigid body modes. A simple pendulum example will demonstrate that the pendulum stiffness is negligible at high frequeny and that the inertia term is dominant. For a mass m suspended from a massless cable of length l, the linearized differential equation for the mass displacement takes the familiar form

$$m\ddot{x} + \frac{g}{l}mx = f \qquad \text{(B-1)}$$

The undamped inertance transfer function (or frequency response function) can be written as

$$\frac{\ddot{x}}{f} = -\frac{\frac{1}{m}\omega^2}{\frac{g}{l} - \omega^2} \qquad \text{(B-2)}$$

where g/l is the square of the natural frequency. For frequencies much greater then the natural frequency (a decade or more) the inertance is very close to the inertia term 1/m, which is the rigid body term for the mass.

Two rigid body modes exist for the component in the "free-free" test configuration of this study--one translational and one rotational mode. Figure B-1 illustrates the sign and notation conventions used to define deflections and forces on the component. Forces and moments are assumed to be applied at the beam interfaces for the purposes of derivation, although these forces were applied at a small distance from the very tip. Negligible increases in accuracy at low frequency are gained by considering this discrepancy and will therefor be omitted in the present derivation.

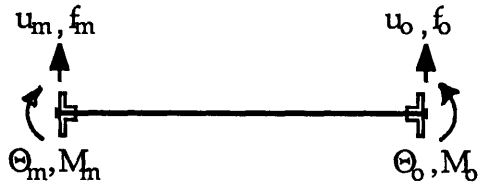

Length L
Mass m_b
Moment of Inertia J

Figure B-1: Sign Conventions for Single Component Deflections and Forces.

The quantities that are desired are the rigid body inertances, from which the rigid body modes can later be determined. The inertances are used directly in the CMS procedure to augment the dynamic response model.

Rigid body inertances are now determined using Newtonian mechanics. Linear acceleration of the interface points is due to both rigid body translation and rigid body rotation

$$\ddot{x}_m = \frac{1}{m_b} f_m + \left(\frac{L}{2}\right)\ddot{\theta}_m \tag{B-3}$$

$$= \frac{1}{m_b} f_m + \left(\frac{L}{2}\right)\left(\frac{L f_m}{2J}\right) \tag{B-4}$$

$$\frac{\ddot{x}_m}{f_m} = \left[\frac{1}{m} + \frac{L^2}{4J}\right] \tag{B-5}$$

Similarly

$$\frac{\ddot{x}_o}{f_m} = \left[\frac{1}{m} - \frac{L^2}{4J}\right] \tag{B-6}$$

Linear deflection due to moment at the interface is given by

$$\ddot{x}_m = \left(\frac{L}{2}\right)\frac{M_m}{J} \tag{B-7}$$

and the corresponding inertances terms are

$$\frac{\ddot{x}_m}{M_m} = \frac{L}{2J} \tag{B-8}$$

$$\frac{\ddot{x}_o}{M_m} = -\frac{L}{2J} \tag{B-9}$$

Interface rotation due to applied moment is given by

$$\frac{\ddot{\theta}_m}{M_m} = \frac{1}{J} \tag{B-10}$$

$$\frac{\ddot{\theta}_o}{M_m} = -\frac{1}{J} \tag{B-11}$$

These residual inertance terms can be used to adjust the four FRFs of the component modal model that are used to develop the "complete" FRF matrix of Section 3.4.1. A similar matrix representation can be made of the rigid body modes by enforcing reciprocity and structural symmetry (the latter dictates that the diagonal blocks of the FRF matrix are identical). This rigid body inertance matrix is shown in Eq. (B-12)

$$\begin{bmatrix} \ddot{x}_m \\ \ddot{\theta}_m \\ \ddot{x}_o \\ \ddot{\theta}_o \end{bmatrix} = \left[\begin{array}{cc:cc} \left(\frac{L^2}{4J} + \frac{1}{m_b}\right) & \frac{L}{2J} & & \\ \frac{L}{2J} & \frac{1}{J} & & \\ \hdashline & & \multicolumn{2}{c}{\text{sym.}} \\ \left(\frac{-L^2}{4J} + \frac{1}{m_b}\right) & -\frac{L}{2J} & & \\ -\frac{L}{2J} & -\frac{1}{J} & & \end{array}\right] \begin{bmatrix} f_m \\ M_m \\ f_o \\ M_o \end{bmatrix} \tag{B-12}$$

$$= \mathbf{H}^{RB}\mathbf{f} \tag{B-13}$$

This FRF matrix is constructed from the two rigid body mode shapes

$$H^{RB} = \Psi_{01}\Psi_{01}^{T} + \Psi_{02}\Psi_{02}^{T} \tag{B-14}$$

where the two rigid body modes of Table 4-2 are given by

$$\Psi_{01} = \begin{bmatrix} \frac{1}{\sqrt{m_b}} \\ 0 \\ \frac{1}{\sqrt{m_b}} \\ 0 \end{bmatrix} \tag{B-15}$$

$$\Psi_{02} = \begin{bmatrix} \frac{L}{2\sqrt{J}} \\ \frac{1}{\sqrt{J}} \\ -\frac{L}{2\sqrt{J}} \\ -\frac{1}{\sqrt{J}} \end{bmatrix} \tag{B-16}$$

Numerical entries are calculated from a measured beam mass of .835 kg, length of .645 m, and a moment of inertia J = .04316 kgm^2. The mass and moment of inertia take into account masses of bolts, joint assemblies, and sensors.

Appendix C
Unification of Modal Model

Curve-fitting was performed on each of the four measured transfer functions, one mode at a time, to produce estimates for natural frequency, damping, and modal constants. It is necessary to remove inconsistencies in this data to develop a "unified" modal model for the CMS analysis. The "unified" values of damping and natural frequencies for each mode were determined by taking the numerical average of the four estimates. Corrections on the order of only a few percent, or less, were required.

The determination of unified eigenvectors is now presented. Entries of the "complete" FRF matrix that were actually measured were presented previously as shaded regions in Eq. (3-16), and are presented again for reference. Note that diagonal blocks are identical and that elements within each 2x2 block display reciprocity in accordance with the assumptions of Chapters 3 and 4.

$$\begin{bmatrix} u_o \\ \Theta_o \\ \hline u_p \\ \Theta_p \end{bmatrix}^b = \left[\begin{array}{cc:cc} h_{11} & h_{12} & h_{13} & h_{14} \\ h_{21} & h_{22} & h_{23} & h_{24} \\ \hdashline h_{31} & h_{32} & h_{33} & h_{34} \\ h_{41} & h_{42} & h_{43} & h_{44} \end{array}\right]^b \begin{bmatrix} f_o \\ M_o \\ \hline f_p \\ M_p \end{bmatrix}^b \qquad \text{(C-1)}$$

As shown in Chapter 3, Eq. (C-1) can be rewritten in terms of the inertance model to reflect the modal constants A_{rij} in the matrix, with one denominator common to all modal constants.

$$\begin{bmatrix} \ddot{x}_m \\ \ddot{\theta}_m \\ \ddot{x}_o \\ \ddot{\theta}_o \end{bmatrix} = -\sum_{r=1}^{N} \frac{\omega^2}{\left(\Omega_r^2 + 2j\zeta_r\Omega_r\omega - \omega^2\right)} \begin{bmatrix} A_{r11} & A_{r12} & A_{r13} & A_{r14} \\ A_{r21} & A_{r22} & A_{r23} & A_{r24} \\ A_{r31} & A_{r32} & A_{r33} & A_{r34} \\ A_{r41} & A_{r42} & A_{r43} & A_{r44} \end{bmatrix} \begin{bmatrix} f_m \\ M_m \\ f_o \\ M_o \end{bmatrix} \quad \text{(C-2)}$$

The four measured modal constants can be written in terms of the modal vectors:

$$A_{r11} = \Psi_{r1}^2 \quad \text{(C-3a)}$$

$$A_{r21} = \Psi_{r2}\Psi_{r1} \quad \text{(C-3b)}$$

$$A_{r31} = \Psi_{r3}\Psi_{r1} \quad \text{(C-3c)}$$

$$A_{r32} = \Psi_{r3}\Psi_{r2} \quad \text{(C-3d)}$$

Given these four curve-fit modal constants for each mode, the eigenvector entries can be determined as

$$\Psi_{r1} = \sqrt{A_{r11}} \quad \text{(C-4)}$$

$$\Psi_{r2} = \frac{A_{r11}}{\Psi_{r1}} \quad \text{(C-5)}$$

Two estimates are available for third eigenvector entry; the arithmetic mean of these two estimates is used for the unified model.

$$\Psi_{r3} = \frac{A_{r31}}{\Psi_{r1}} \qquad \text{(C-6a)}$$

$$\Psi_{r3} = \frac{A_{r32}}{\Psi_{r2}} \qquad \text{(C-6b)}$$

Two estimates are available for the fourth eigenvector entry because reciprocity is assumed within each 2x2 block; once again the average of the two estimates is used in the unified model.

$$\Psi_{r4} = -\frac{A_{r32}}{\Psi_{r1}} \qquad \text{(C-7a)}$$

$$\Psi_{r4} = -\frac{A_{r12}}{\Psi_{r3}} \qquad \text{(C-7b)}$$